Dynamics of a Droplet that Assists III-V Nanowire Growth

Tornberg, Marcus

2020

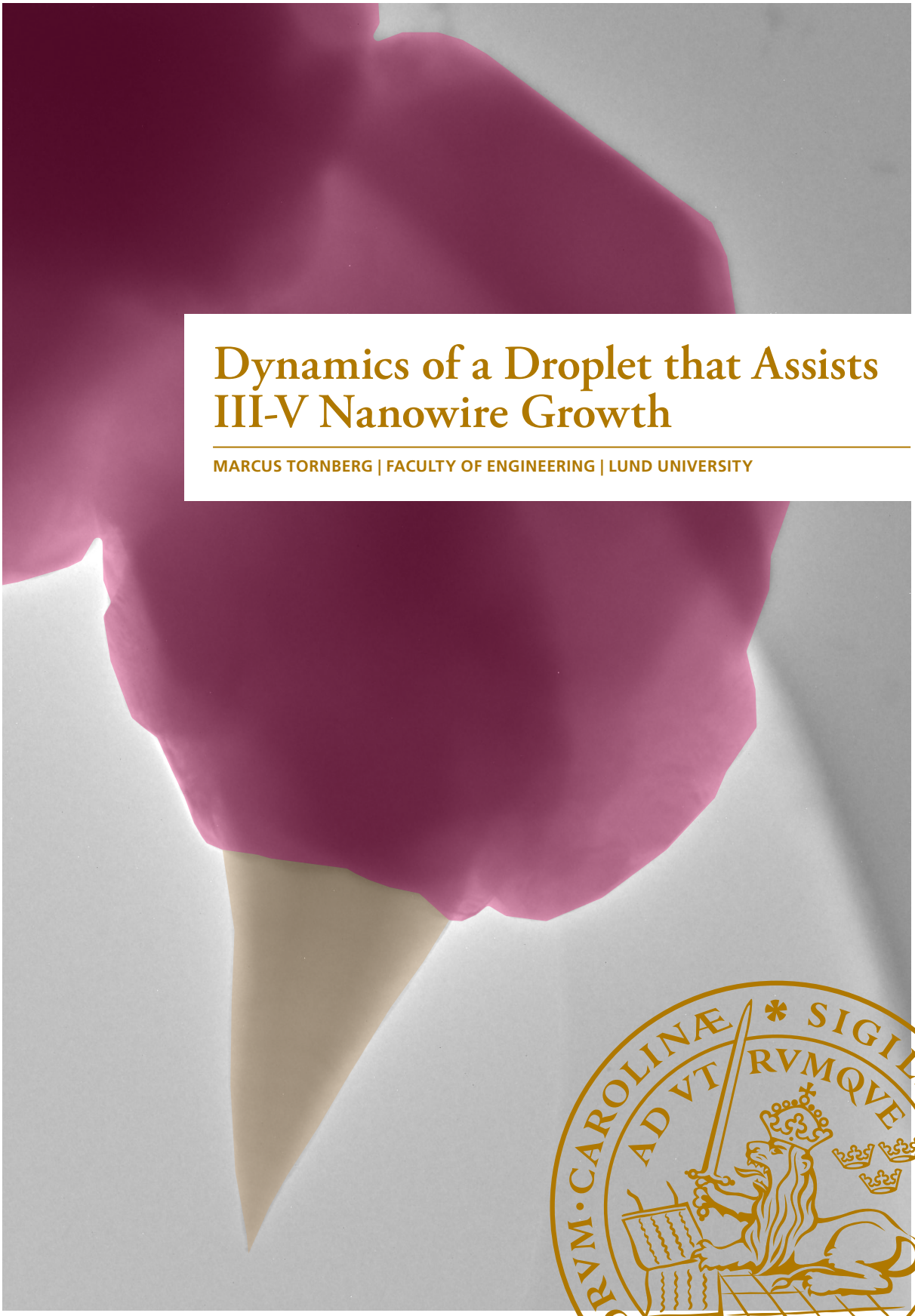

Dynamics of a Droplet that Assists III-V Nanowire Growth

MARCUS TORNBERG | FACULTY OF ENGINEERING | LUND UNIVERSITY

Printed by Media-Tryck, Lund 2020 NORDIC SWAN ECOLABEL 3041 0903

Lund University
Faculty of Engineering
Department of Physics

ISBN 978-91-7895-486-5

Dynamics of a Droplet that Assists III-V Nanowire Growth

Dynamics of a Droplet that Assists III-V Nanowire Growth

Marcus Tornberg

LUND
UNIVERSITY

DOCTORAL DISSERTATION

which, by due permission of the Faculty of Engineering of Lund University, Sweden, will be publicly defended on Monday, the 4th of May 2020 at 09:15 in Rydbergsalen at the Department of Physics, Sölvegatan 14, Lund, Sweden for the degree of Doctor of Philosophy in Engineering

Faculty opponent:
Assoc. Prof. Michael A. Filler
Georgia Institute of Technology, Georgia, U.S.A.

Thesis advisors:
Prof. Kimberly Thelander, Dr. Sebastian Lehmann & Prof. Reine Wallenberg

Organization
LUND UNIVERSITY

Department of Physics
Box 118
SE–221 00 LUND
Sweden

Document name
DOCTORAL DISSERTATION

Date of disputation
2020-05-04

Sponsoring organization

Author(s)
Marcus Tornberg

Title and subtitle
Dynamics of a Droplet that Assists III-V Nanowire Growth

Abstract
Control of the process of crystal growth has for decades been achieved by addressing the growth temperature and material supply of the growth species. Directional control of both crystal growth and etching has, for example, been achieved by utilizing a liquid droplet to assist the process. This is a common approach to achieve crystal growth of nanostructures, as in the case of Au-assisted III-V semiconductor nanowires. Although controlled droplet-assisted growth has been studied in depth, less attention has been given to the droplet composition and how it dynamically interacts with the nanowire.

This thesis explores the fundamental limits for one-directional droplet-assisted crystal growth. This is studied first by intentionally displacing the droplet from the facet at which it originally assisted the crystal growth. The process and cause for displacement is studied for Au-assisted GaAs and InAs nanowires by combining experimental observations and theoretical modeling of the droplet wetting. In addition, it is shown that the final position of the droplet can be controlled by tailoring the surfaces of the nanowire, which in turn is used for design of branched structures. Furthermore, this thesis focuses on the droplet dynamics and the formation of a truncation at the droplet-nanowire interface, as the geometry of the droplet wetting of the top facet approaches the fundamental limit.

The studies of this thesis are conducted using metal-organic chemical vapor deposition (MOCVD), both in- and outside an environmental transmission electron microscope (ETEM). Ex-situ analysis of droplet displacement allows us to investigate the statistics of the process, to understand trends of the droplet wetting. On the other hand, performing MOCVD inside an ETEM enables real-time studies of the dynamic processes during growth, such as observations of the droplet wetting angle or the facet truncation. Using a combination of theoretical modeling, high-temperature X-ray energy dispersive spectroscopy and direct imaging during growth, we measure and estimate the previously inaccessible gallium and arsenic concentration in the droplet, as well as the surface energies of the Au-Ga droplet and the GaAs nanowire sidewalls. These findings could in turn be used to further improve our understanding of the atomic arrangement at the crystal surfaces and interfaces during growth. Such an understanding could lead to improved control and design of crystal nanostructures.

Key words
Crystal Growth, III-V semiconductor nanowires, Environmental Transmission Electron Microscopy, MOCVD, X-ray Energy Dispersive Spectroscopy

Classification system and/or index terms (if any)

Supplementary bibliographical information

Language
English

ISSN and key title

ISBN
978-91-7895-486-5 (print)
978-91-7895-487-2 (pdf)

Recipient's notes

Number of pages
159

Price

Security classification

Dynamics of a Droplet that Assists III-V Nanowire Growth

Marcus Tornberg

LUND
UNIVERSITY

Cover illustration front: False-colored TEM image of a GaAs nanostructure after 3 hours of *in-situ* crystal growth.

Flipbook p.1-65 (odd): TEM image sequence of 15 s of steady-state Au-assisted GaAs nanowire growth (Nanowire diameter - 22 nm)

Flipbook p.2-64 (even): TEM image sequence of Au-assisted GaAs nanowire that increases its droplet volume (Nanowire diameter - 45 nm)

Funding information: These projects have been funded by Knut and Alice Wallenberg Foundation and NanoLund.

ISBN: 978-91-7895-486-5 (print)
ISBN: 978-91-7895-487-2 (pdf)

Division of Solid State Physics, Department of Physics
Faculty of Engineering, Lund University

Printed in Sweden by Media-Tryck, Lund University, Lund 2020

Media-Tryck is an Nordic Swan Ecolabel certified provider of printed material. Read more about our environmental work at www.mediatryck.lu.se

MADE IN SWEDEN

Contents

Summary

Control of the process of crystal growth has for decades been achieved by addressing the growth temperature and material supply of the growth species. Directional control of both crystal growth and etching has, for example, been achieved by utilizing a liquid droplet to assist the process. This is a common approach to achieve crystal growth of nanostructures, as in the case of Au-assisted III-V semiconductor nanowires. Although controlled droplet-assisted growth has been studied in depth, less attention has been given to the droplet composition and how it dynamically interacts with the nanowire.

This thesis explores the fundamental limits for one-directional droplet-assisted crystal growth. This is studied first by intentionally displacing the droplet from the facet at which it originally assisted the crystal growth. The process and cause for displacement is studied for Au-assisted GaAs and InAs nanowires by combining experimental observations and theoretical modeling of the droplet wetting. In addition, it is shown that the final position of the droplet can be controlled by tailoring the surfaces of the nanowire, which in turn is used for design of branched structures. Furthermore, this thesis focuses on the droplet dynamics and the formation of a truncation at the droplet-nanowire interface, as the geometry of the droplet wetting of the top facet approaches the fundamental limit.

The studies of this thesis are conducted using metal-organic chemical vapor deposition (MOCVD), both in- and outside an environmental transmission electron microscope (ETEM). Ex-situ analysis of droplet displacement allows us to investigate the statistics of the process, to understand trends of the droplet wetting. On the other hand, performing MOCVD inside an ETEM enables real-time studies of the dynamic processes during growth, such as observations of the droplet wetting angle or the facet truncation. Using a combination of theoretical modeling, high-temperature X-ray energy dispersive spectroscopy and direct imaging during growth, we measure and estimate the previously inaccessible gallium and arsenic concentration in the droplet, as well as the surface energies of the Au-Ga droplet and the GaAs nanowire sidewalls. These findings could in turn be used to further improve our understanding of the atomic arrangement at the crystal surfaces and interfaces during growth. Such an understanding could lead to improved control and design of crystal nanostructures.

Popular Science Summary (English & Svenska)

Atoms, the building blocks of nature, may be foreign to most of us in our daily life, but they ARE everything. They build up each and every material around us. And while we cannot see them with the naked eye, we can use microscopy to see and study how they order and why they form the materials they do. The booklet in your hand focuses on how atoms arranges themselves as they form a solid material and how the formation can be controlled. To study and understand the growth of a solid on atomic level we look at the growth as it happens using electron microscopy. In doing so, we can study what is needed for the atoms to arrange in a single pattern, a so called single crystal. Interestingly, atoms are fairly similar to humans in how they behave as a group.

Designing and making a single crystal can be a difficult and slow process. One common way is to build them from the bottom and up, atomically layer-by-layer. This is done by forming a small cluster of atoms, a nucleus, that is allowed to grow slowly so that each atom reaches its most favorable position. As a result, the newly formed atomic layer will most often adopt and continue the arrangement of the underlying layer, slowly building the single crystal.

The arrangement of atoms resembles the process of free seating at a dinner; it is most convenient if not all guests arrives at once, to allow everyone their time to find the seat and company they like the best. The chosen seat will be dependent on the friendliness of the environment, space and temperature. Sometimes, we change the seating arrangement to allow an additional friend at each of the tables. As in the case of finding a new seating arrangement, many solid materials, for example materials that combine elements of group III and V of the periodic table, have the ability to adopt more than one atomic arrangement. This means that the atoms can order themselves in different patterns, especially, when the size of the layer that is formed is smaller than a tenth of a micrometer.

To assist and control the crystal growth of small sizes, we use gold drops that help collect the atoms to the crystal. Each small drop, called droplet, forms crystal layers when they have collected enough atoms. This process continues layer after layer and sooner or later forms a crystal pillar under the droplet. Crystal growth from a droplet is a promising method for making tiny semiconducting components, which can be used as for example: light-sources, transistors (the brain-cell of your computer) or sensors for both proteins and light.

The fact that a small drop on the top of the pillar can assist the crystal growth, means that the growth direction can be changed by moving the droplet. For this reason, a major part of this thesis discusses the limits for having a droplet covering the top of a pillar. It also shows the consequences of going beyond that limit, by moving the droplet. As every process in nature strives towards reducing the energy of its components, we can tailor the environment to favor droplet movement.

It turns out that both droplet position and crystal growth are dependent on the atoms at the surface. In contrast to the atoms at the center of a material, the surface atoms interact with the material next to the solid as well. Like humans that attends the dinner without knowing anyone, it requires energy to interact with something/someone that we are unfamiliar with. If it's too hard to interact, we would simply leave the dinner early. If on the other hand, we bring some friends with us, it is easier to stick around even though the interactions with the rest of the group are difficult. With the same reasoning, the benefit for having atoms at the center of a material has to out-weigh the cost of the surface atoms in order for the solid to exist and grow. This energy cost at an interface is

called surface energy, and measures the energy needed for the surface interaction instead of being surrounded by solid atoms (friends) in the center.

However, it is difficult to measure the energy of an interface, and especially how the atoms at the surface would react in different environments. We can often predict how it would be in an ideal case, but when things get more complicated we need to test it in real life. This thesis has focused on increasing our understanding of the surfaces that is present during droplet-assisted crystal growth. We dive deep into how we can manipulate the crystal and its surfaces to control both the movement of the droplet on a pillar and the crystal growth. By enabling studies of the crystal growth inside a microscope, we can observe and measure things that are important for forming a crystal, such as composition of the droplet and how it interacts with the solid. Information which would help us understand what influences the formation and limits of a crystal using a droplet.

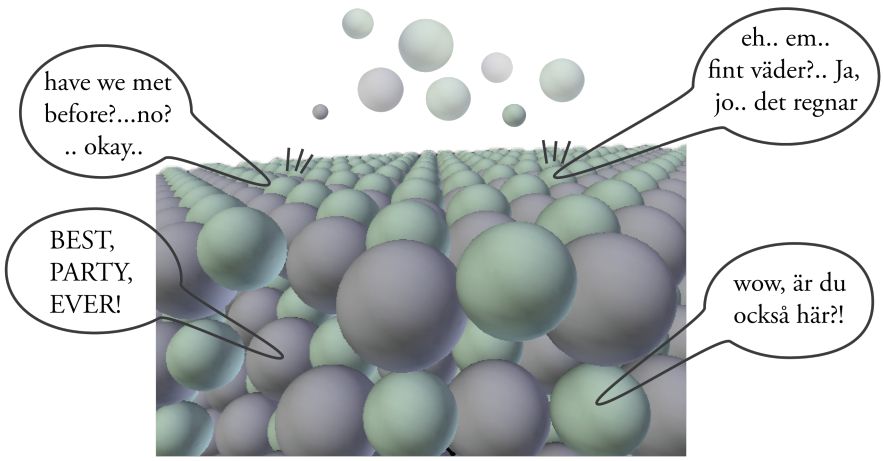

Figure : (eng.)Interactions at the surface can be awkward when compared to the interactions between friends.

(sv.) Småpratet vid ytan kan ibland vara stelt när man jämför det mer hur vi är med våra vänner.

Populärvetenskaplig Sammanfattning

Atomer, naturens byggstenar, är för många ganska främmande i vår vardag och kanske till och med till ordet. Dock är atomer ALLT; de bygger upp alla material du kan se omkring dig, även dig själv. Och även om vi inte kan se atomerna med ögat så kan vi ta hjälp av mikroskop. Med mikroskopi kan vi studera hur atomerna ordnar sig själva och hur de skapar de material som de gör. Avhandlingen du håller i handen behandlar hur atomer kan arrangera sig själva för att bilda ett fast material. Men den undersöker också hur vi kan kontrollera processen som bygger upp det fasta materialet av atomer. För att kunna undersöka och förstå hur atomerna staplas och 'växer´ det fasta materialet, så tittar vi på när atomerna staplas. Detta gör att vi kan ta reda på vad som krävs för att atomer ska ordna sig i samma mönster, och bygga en singelkristall. Vad som kanske inte är helt väntat är att atomer ibland beter sig mycket likt oss människor.

Att skapa och bygga en singelkristall kan vara en långsam och stundtals svår process. Det vanligaste sättet att bygga dessa helt ordnade material är att börja från botten och bygga lager för lager av atomer. Detta görs genom att ett antal atomer går ihop till ett kluster, en kärna, som sedan växer långsamt så att alla atomer har tid att hitta sin 'bästa' plats. Eftersom atomerna anpassar sig till hur atomerna i lagret under och runt om sitter, så får ofta atomerna i det nya lagret samma ordning som lagret under.

Atomernas arrangemang påminner om hur bordsplacering fungerar på en middag. Om det är fri bordsplacering så är det ofta smidigast om inte alla gäster kommer samtidigt. Detta ger då alla gäster tid att hitta den plats och bekantskap som de gillar bäst. Vilken plats vi väljer beror på vilket sällskap som sitter vid bordet, hur mycket plats som finns och hur varmt det är. Ibland hämtar vi till och med en extra stol för att få plats med en extra vän vid varje bord för att det ska bli så bra för oss som möjligt, och därmed ändrar vi det ursprungliga arrangemanget. På samma sätt kan många material, bland annat de som består av grundämnen från grupp III och V i periodiska systemet, arrangera sina atomer på fler än ett sätt. För dessa typer av material så har det visat sig lättast att arrangera atomer på fler än ett sätt om atomlagren är mindre än en tiondels mikrometer i diameter.

För att hjälpa och kontrollera uppbyggnaden av små kristaller så använder vi oss av guld-baserade droppar. Dessa droppar bidrar till att samla upp atomer som kan användas för att bygga kristallen, atomlager för atomlager. Eftersom varje nytt atomlager bildas under droppen så kommer kristallen till slut att forma en kristallpelare av ordnade atomer under droppen. Detta sätt att skapa kristallpelare, så kallade nanotrådar, har visat sig vara bra för att skapa små (jättesmå) halvledarkomponenter som kan användas som ljuskällor, transistorer (hjärncellerna i din datorn) eller som sensorer för proteiner och ljus.

Om en gulddroppe kan hjälpa atombyggnaden så mycket att det skapas en pelare under den, så betyder det också att vi kan ändra hur atomerna staplas genom att flytta droppen. För att få mer förståelse för hur det påverkar kristalltillväxten, så fokuserar denna avhandlingen på vad som begränsar droppen att vara på toppen av pelaren. Inte bara det, utan avhandlingen behandlar även hur pelaren, kristalltillväxten och droppen påverkas när vi flyttar droppen. Eftersom allting i naturen försöker minska sin energi, så kan vi skräddarsy en miljö för att droppen ska vilja röra sig från toppen.

Både droppens rörelse och kristalltillväxten är beroende av atomerna på ytan. Till skillnad från atomerna i mitten av kristallpelaren måste atomerna på ytan interagera med vad som finns utanför kristallen. Detta är precis som när vi människor ska gå på en middag där vi inte känner någon alls. Det kräver kraft och energi att interagera eller prata med någon vi inte känner. Om det är för svårt att interagera, så lämnar vi hellre middagen. Har vi däremot gått till middagen med vänner så är det lättare att stanna kvar även om interaktionen med de andra på middagen är stel. På samma sätt så måste fördelen för alla atomer i mitten av pelaren vara större än energin det kostar för atomerna på ytan, annars kan inte kristallen finnas eller bli större. Energikostnaden för ytatomer kallas för ytenergi och beskriver energin som krävs för att interagera med något som inte är kristallens atomer.

Det har visat sig vara svårt att mäta energin för en yta och framförallt hur atomerna reagerar i andra miljöer. Vi kan ofta förutspå vad som händer i ideala fall genom att räkna, men för ytor som ständigt förändras, så som när en kristall växter, behöver vi försöka mäta när det händer. Denna avhandling har fokuserat på att öka vår förståelse av de ytor som är närvarande under kristalltillväxt med hjälp av en droppe. Studien dyker ner i hur vi kan manipulera kristallen och dess ytor för att kontrollera både kristalltillväxten och en droppes rörelse på en pelare. Genom att titta på atombyggandet i ett elektron mikroskop kan vi mäta egenskaper som är viktiga för kristalltillväxten, så som droppens beståndsdelar och hur den interagerar med pelaren. Information som kommer att hjälpa oss förstå vad som påverkar skapandet av en kristall och dess begränsningar med hjälp av en droppe.

List of Publications and Contributions

This thesis is based on the following publications, referred to by their Roman numerals:

I *Kinetics of Au-Ga Droplet Mediated Decomposition of GaAs Nanowires*

M. Tornberg, D. Jacobsson, A. R. Persson, R. Wallenberg, K. A. Dick & S. Kodambaka
Nano Letters, 19 (6), 3498, (2019)

II *In-situ Analysis of Catalyst Composition during Gold Catalyzed GaAs Nanowire Growth*

C.B. Maliakkal, D. Jacobsson, **M.Tornberg**, A.R. Persson, J. Johansson, R. Wallenberg & K.A. Dick
Nature Communications, 10, 4577, (2019)

III *Thermodynamic Stability of Gold-Assisted InAs Nanowire Growth*

M. Tornberg, K. A. Dick & S. Lehmann
Journal of Physical Chemistry, 121, 39 (2017)

IV *Limits of III-V Nanowire Growth Based on Droplet Dynamics*

M.Tornberg, C.B. Maliakkal, D. Jacobsson, K.A. Dick, J. Johansson
Submitted to Journal of Physical Chemistry Letters

V *Branched InAs Nanowire Growth by Droplet Confinement*

M. Tornberg, K. A. Dick & S. Lehmann
Applied Physics Letters, 113, 123104 (2018)

My contributions

I *Kinetics of Au-Ga Droplet Mediated Decomposition of GaAs Nanowires*

I had the main role in designing the experiment and the analysis of the droplet composition and droplet-assisted etching. The experiments were conducted together with DJ and SK. The manuscript was drafted by me and refined by all authors.

II *In-situ Analysis of Catalyst Composition during Gold Catalyzed GaAs Nanowire Growth*

I was part of the project initiation for using the gallium concentration to estimate the arsenic concentration in the droplet using thermodynamic phase diagram. I had one of the main roles in developing the growth and experimental design, together with DJ and CBM. In addition, I was involved in the quantification and analysis for the X-ray EDS measurement. The manuscript was written by CBM and refined by all authors.

III *Thermodynamic Stability of Gold-Assisted InAs Nanowire Growth*

I did the experimental design, growth, microscopy and analysis and had the main role in drafting the manuscript. The manuscript was refined by all authors.

IV *Limits of III-V Nanowire Growth Based on Droplet Dynamics*

I had the main role in setting up the collaboration for theoretical modeling. I designed the in-situ experiment to specifically target the droplet dynamics and had the main role in analyzing the data and draft the letter. The growth was conducted together with DJ and CBM. The letter was refined by all authors.

V *Branched InAs Nanowire Growth by Droplet Confinement*

I initiated the project of using barriers to control the droplet and designed the experiment based on the results of paper III. I was leading the growth and microscopy analysis and the main role of drafting the letter, and the letter which was later refined by all authors

Acknowledgement

Even though there is only one name on the cover page, this thesis is far from the work of one person. I have been fortunate to have had so many people that, in one way or another, have contributed to either the science presented within this thesis or my personal development. You are not forgotten, I promise. With that said, there are certain persons that have contributed greatly to this thesis.

First, I would like to express my greatest gratitude towards Kimberly, for the opportunity to join this incredibly talented group of people for 5+ years. I am genuinely impressed by your endless curiosity, and the fact that no matter what, you always seem to find time and solutions for most things. From the struggles of working with a custom instrument, to my effort of getting you to be more at the microscope. I could not have asked for a better adviser and guide into the world of science and research. Speaking of curiosity, Sebastian, your eager to understand details and endless streams of Why? How? and What if? have been some of the perks of asking you for advice and collaborating with you. I would also like to thank Reine, for any data you have found with the follow-up question, 'what did you do here?'. These questions have kept me on edge as an experimentalist, as it thought and advised me on how to keep track of scientific data.

The *in-situ* studies that are included in this thesis would not have been possible without the talented people, which I have had the opportunity to work alongside at the microscope. I would like to thank Carina, Robin, Axel and Suneel for the many, and at times long, hours of in-situ experiments, as well as the discussions that sometimes led to scientific investigations and reports and sometimes just improved our mood. In addition, I also need to emphasize the pleasure it has been to work alongside Daniel in the development of the crystal growth in a microscope.

The presented scientific work would not have been the same without the scientific and casual interaction originating from the collaborations. I would like to share my gratitude towards Jonas, for sharing your competence and enthusiasm of the theory of crystal growth. To Reza, who apart from being a talented microscopist, seems to know everyone at a conference. And Sepideh, for being one of the persons that introduced me to not only science, research, and academia, but also the mentality that when you have had your Friday afternoon coffee: the week is supposed to be over.

Thank you to all who are, or has been, part of the research group led by Kimberly, who every week have met and shared news, insights, data, vacation pictures and/or an occasional cake. I have realized that surrounding myself with talented and clever people and sharing experiences is a great way learn more things about the world. A great thanks to all of you for sharing your knowledge and experiences to advance your own science but also to contribute to the science made by your colleagues.

I would like to express my gratitude to the colleagues that made the work place the second home it has been, from odd discussions to scientific, graphical and administrative support. Among those are Martin, Laura, Calle and Mårten who have had a great impact on both my working environment and the way I approach science.

Last, but not least, to the ones who have endured, supported and shared my ups and downs: my friends, my family and my soon-to-be wife. For your endless support, encouragement and energy, I am truly grateful.

THANK YOU! yes, you. For opening this thesis to find something of interest or use. If this something is of scientific value, that is even better! If you find this thesis out of your scope or interest, and you do not know anyone that might find it of interest. Don't be afraid to find other creative uses for this printed thesis, whether it being as a door-stopper, present-wrapping, or to elevate your computer screen. Just make sure this piece of tree gets a purpose even as a booklet

Abbreviations in Text

Chemicals

As	Aresnic
AsH_3	Arsine
Au	Gold
Ga	Gallium
In	Indium
DMGa	Di-Methyl-Gallium
MMGa	Mono-Methyl-Gallium
Si	Silicon
SiH_4	Silane
TMGa	Tri-Methyl-Gallium $Ga(CH_3)_3$
TMIn	Tri-Methyl-Indium $In(CH_3)_3$

Instrumentation and Techniques

CVD	Chemical Vapor Deposition
EDS	Energy Dispersive Spectroscopy
ETEM	Environmental TEM
FEG	Field Emission Gun
MEMS	Micro-Electro-Mechanical-System
MFC	Mass Flow Controller
MOCVD	Metal-Organic CVD
SEM	Scanning Electron Microscope
TEM	Transmission Electron Microscope

Symbols

at.%	Atomic Percent
μ	Chemical Potential
γ	Surface Tension / Surface Energy
l	Liquid
μ m	Micrometer (10^{-6} m)
nm	Nanometer (10^{-9} m)
s	Solid
v	Vapor
Å	Ångström ($10^{-10}m$)

Introduction

Learning from Nature
- to be able to trick it

Crystal growth can lead to spectacular sights and attractions in nature, ranging from naturally occurring gemstones, to the limestone landscapes in Yellowstone (Wyoming, USA). To be considered a crystal, a material has to have its atoms ordered in all three directions. While the large limestone formations consist of more than one atomic ordering, it is a cluster of crystals that creates these formations. Depending on the climate, the source of the material and process of solidification, the cluster of crystals can form a wide range of shapes from large terraces to stalagmites. Each crystal is formed from a small nucleus, and the crystal grows larger as material gets deposited or solidified. To avoid several crystals forming, and only have one atomic arrangement, the growth is controlled so that the incoming atoms adopt the arrangement of atoms in the crystal. This process of single crystal growth is called epitaxy, a term adopted from Greek which was introduced as upon (epi-) arrangment (-taxis) in 1928[1,2]. The concept of crystal growth is simple; provide the 'right' environment for a crystal to form, including temperature, pressure and growth material, and the system will strive towards growing the crystal. This process would proceed as long as the environmental conditions allow.

The resulting crystal shape is an effect of the atomic arrangement (the so-called crystal structure), the environment surrounding the crystal and external driving forces. By studying how the crystals are formed from a small nucleus in nature, scientists gain inspiration for how to grow other types of material which are not naturally occurring such as crystalline semiconductors. As crystals can grow in several crystal structures and shapes, it is important to understand what causes these atomic arrangements in order to be able to control crystal growth, a control which would lead to the ability to design the crystal of interest. However, as the resulting growth is dependent on the thermodynamic properties of the surrounding environment (*e.g.* temperature, pressure, composition), the crystal control becomes a collaboration with nature, figuring out which environment supports which crystal structure and shape.

The resulting shape of the single crystal growth is primarily determined by the atomic arrangement of the crystal. Which surfaces that are terminating the crystal depends on the specific atoms at the surface and how they interact with their neighboring atoms. In contrast to the atoms enclosed in the crystal, the atoms of the surface not only interact with the crystal atoms but also with the atoms of the surrounding environment. Depending on how many crystal neighbors the atom loses by being

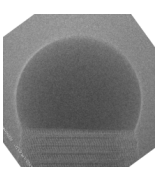

part of the surface, the interaction with the surrounding environment will be of differing strength. A surface with higher atom density (few missing neighbors) will therefore require less energy to maintain in comparison to a surface with low atom density. For this reason, low index crystal facets (*e.g.* (1 0 0) or (1 1 1)) that have dense packing of atoms in the plane, are generally more favorable crystal surfaces than those of a higher index. The interaction between the surface atoms and the surrounding environment is referred to as surface energy. This is a parameter which we will see is important for the growth and its limits in chapters 3 and 4.

If two surfaces with different surface energies are exposed to the growth material, the supplied atoms will favor covering of the surface with the highest energy. As a result, the facet of higher energy grows smaller and smaller, eventually disappearing[3,4]. The final crystal will therefore be enclosed by the surfaces of lowest energies, a shape which is referred to as the equilibrium shape according to Wulff's theorem[3,4]. Wulff also stated that the surface energies of a facet were proportional to its distance from the center of the crystal[4], a statement that indicates that if the crystal is allowed to reach its minimum energy, the distance to the facets or their sizes would represent the surface energies. This has been utilized experimentally to estimate the ratios between different facets' surface energy[5].

Materials that can adopt more than one crystal structure, so-called polymorphic materials, can adopt different equilibrium shapes. As each crystal structure has different atomic positions and symmetries, the atomic arrangement of the different crystal facets will be changed. In turn, the surface energies and the crystal shape will be changed accordingly. Polymorphism is common for binary oxides (*e.g.* Al_2O_3) but also for semiconductor materials (*e.g.* ZnS or GaAs), and is the compound equivalent to the allotropes of the chemical elements. One of the most common allotropes is carbon, which can crystallize in both graphite and diamond structures, two materials with completely different properties.

To reduce the energy cost of having the interaction at the surface, the atoms either bind to other atoms of the crystal surface or attract atoms from the surrounding environment[2]. These processes are referred to as reconstruction or passivation. In the case of reconstruction, the surface atoms rearrange their positions to reduce the interaction with the surrounding environment, forming patterns on the surface itself. How the surface atoms reconstruct depends on the atoms of the surface and what type of environment they are exposed to[6]. The alternative for the surface atoms to lower the surface energy, is by binding to an atom of the surrounding environment. Hydrogen passivation of surfaces has, for example, been shown to lower the surface energy of III-V semiconductors[7]. In addition, hydrogen and chlorine passivation of surfaces have been shown to affect the resulting shape of the crystal growth[8–10]. In general, reconstruction and/or passivation of the surfaces occurs to lower the surface energies, therefore affecting the equilibrium shape[4].

Taking Advantage of Nature - Shaping a Crystal

This thesis focuses on how to control the shape of a crystal by the addition of a liquid alloy particle, *i.e.* a droplet. Instead of crystal growth occurring homogeneously over a planar substrate, the addition of a droplet is intended to promote solidification at its interface to the solid. If the crystal growth rates are higher at the substrate-droplet interface in comparison to the vapor-solid interface, the droplet-assisted growth will lead to a pillar-shaped crystal[11–14]. This droplet-assisted growth of pillars has been shown to be a promising approach when growing semiconductor crystals for

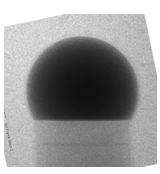

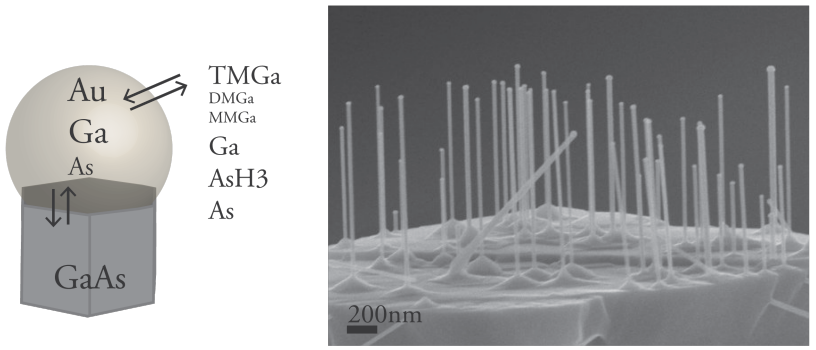

Figure 1.2: An illustration of a Au-assisted GaAs nanowire surrounded by vapor-phase precursors for gallium and arsenic. Here, the vapor consists of tri-methyl-gallium (TMGa) and its derivatives containing only two, one or no methyl groups along with arsine (AsH3). The growth is then determined based on the material supply to the droplet and the crystal. It is partly determined by the competing processes of condensation and evaporation at the droplet-vapor interface, but also the competition of dissolution (melting) and solidification (freezing) at the droplet-crystal interface. This material flow ideally results in growth of a nanowire per droplet, as seen from the scanning electron micrograph. The nanowires exhibit different lengths and widths as a result of variations in droplet sizes and how close they are positioned.

photoelectrical devices[15,16], electron transport[17] or sensors[18]. To enable the continuous growth of these pillars we rely on the fact that the droplet remains at the top of the pillar. My contribution, and the core of this thesis, has been to study the limit for having a droplet in contact with, *i.e.* wetting, the top facet of the pillar. This has been investigated by studying the consequences for going beyond that limit.

The pillar-shaped semiconductor crystal growth was first reported for silicon crystals with diameters from tens of nanometers to 0.3 mm[11,19]. These structures, known as micro- or nanowires, were grown using a liquid Au−Si alloy to assist the growth of silicon at 950 °C from decomposed silane (SiH_4). Similarly, it was later observed how Au-alloy particles on a planar semiconductor material, such as GaAs, promote crystal growth beneath the droplet to form a semiconducting nanowire[14,20,21]. In these reported cases, the metal-organic compound tri-methyl-gallium (TMGa/$Ga(CH_3)_3$) and the hydride, Arsine (AsH_3), were supplied to a substrate at 400-500 °C with pre-deposited gold particles. At these temperatures, the precursors TMGa and AsH_3 pyrolyse into their derivates of mono/di-methyl-gallium*, gallium, AsH_2 and arsenic[22–24]. The gallium and arsenic can then be incorporated into the droplet and contribute to crystal growth.

Crystal Growth

Crystal growth of semiconductors using metal-organics and hydrides as precursors, referred to as Metal-Organic Chemical Vapor Deposition (MOCVD), is mainly controlled by the temperature of the sample, the partial pressures of the growth species and the precursor flows and ratios. Controlling temperature and precursors is therefore an approach to study crystal growth by creating

*MMGa/$Ga(CH_3)$ and DMGa/$Ga(CH_3)_2$

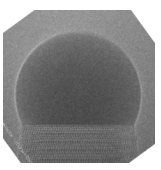

a growth-stimulating artificial environment. The temperature of the sample largely influences the individual chemical potentials of the vapor, liquid and solid phase. In other words, it affects the interaction energy between atoms in the same phase. Consequently, it influences the net flux of material across the liquid-vapor interface, accounting for diffusion, evaporation and condensation. Similarly, the ratio between solidification and dissolution at the solid-liquid interface is also affected by temperature. The reaction of crystal growth or dissolution is illustrated in figure 1.2, and will depend on which phase is the most energetically favorable. In the case of crystal growth, the crystal (solid phase) has the lowest free energy and chemical potential of all present phases.

Furthermore, the temperature also influences the pyrolysis of the precursors, with an increasing effectiveness of molecule decomposition as the temperature increases [25–27]. The fact that the temperature does affect all phase transformations and the amount of growth species, means that its effect can be hard to interpret. For this reason, temperature is often used as a parameter for achieving successful growth, but seldom varied during fundamental studies of growth as it affects several parameters at the same time. The influence of temperature on growth and especially on the droplet composition has been studied in papers I and II of this thesis and will be addressed in detail in chapter 2.

The supply of growth species, *e.g.* gallium and arsenic, depends on the pyrolysis of the precursors. The decomposition of the precursors has been shown to depend on the composition vapor, and was reported for mixtures of TMGa and AsH_3 [25,27]. This means that that changing the precursor flux to the sample does not necessarily change the amount of gallium and arsenic that reaches the growth front linearly. Nevertheless, the ratio between the precursors reflects the proportions of growth species that reach the droplet and can thus affect its volume. As an example, lowering the AsH_3/TMGa ratio has been reported to relatively increase the Au-based droplet size, a finding which has been correlated with increased gallium content [28,29]. The method of increasing the droplet volume by controlling the precursor flows was utilized in the droplet-wetting studies of papers III and IV.

Changing the precursor flux has also been shown to affect the atomic arrangement of the grown III-V semiconductor nanowire [30,31]. It has been shown that most III-V semiconductors are polymorphic materials, with the ability to adopt both cubic zincblende and hexagonal wurtzite crystal structures [32,33]. These studies have shown that the different crystal structures can be achieved by controlling the ratio of supplied precursors for the group III and V elements (V/III ratio). Changing the precursors gradually from higher to lower V/III ratios altered the growth from forming zincblende to wurtzite at intermediate ratios [28,31]. This trend was shown for several material systems when changing the supply of group V precursor. In addition, reducing the precursor ratio further during growth of GaAs showed a transition back to zincblende crystal. This zincblende transition was later observed to occur in conjunction with expansion of the droplet [29,34]. However, if the volume or shape of the droplet is the critical parameter for forming wurtzite or zincblende still remains unknown as the conditions for forming the crystals are different in more than just the droplet volume, *e.g.* precursor supply and droplet composition.

In addition to the crystal structure switching, scientists have managed to engineer and tailor the growth of complex structures such as nano-trees [35], flags [36], branches [35,37–39], zig-zag wires [40,41] and crosses [42,43]. All these structures have been enabled and discussed from the perspective of droplet or surface engineering. In practice, this was achieved by affecting the droplet composition and/or

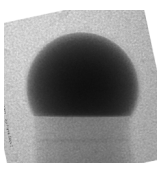

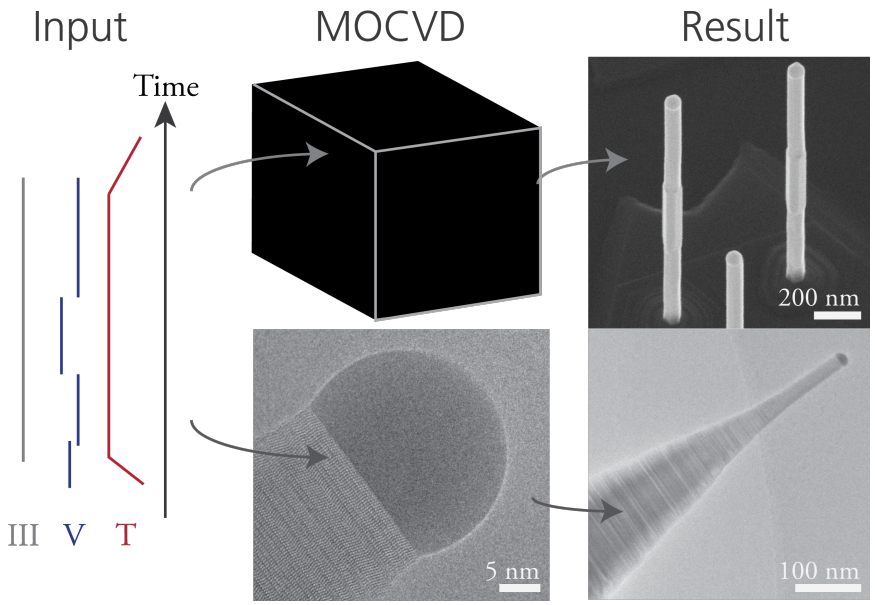

Figure 1.3: Investigation of the growth can be performed either by post-growth (*ex-situ* studies) or as the crystal is growing (*in-situ* studies). Both use precursor flow (group III or V) and temperature (T) over time as input parameter to control the growth. However, for *ex-situ* experiments the MOCVD is taking place within a black box with little transparency whereas the *in-situ* experiments (*e.g.* using an ETEM) allow observation of growth and dynamics in real-time using electron microscopy. Once the nanowires have been grown it is possible to observe them in both cases.

volume either by pulsing the precursor fluxes or annealing. To understand the droplet-assisted (or particle-assisted for a solid-catalyst) crystal growth, and all its possibilities, we would need to investigate the droplet composition and how it influences the crystal growth.

Observing Crystal Growth

To date, with only a few exceptions, studies of crystal growth have been conducted by performing material deposition, using for example MOCVD, followed by cooling to room temperature. When the process is finished, the final sample is imaged and/or analyzed in vacuum. In principle, a growth experiment is designed by a flow scheme for the precursors and a temperature profile which sets the condition for crystal growth. The crystal growth is then conducted within a growth chamber followed by cooling to room temperature. After transfer from the growth chamber to the analytical tool (*e.g.* electron microscope), it is possible to study the success of the crystal growth. What this means is that the resulting image or data, which we base our analysis on, can be a result of both the growth and the cooling conditions[30,33,44]. The conceptual process is illustrated in figure 1.3 starting from the input parameters, through the black box of the growth chamber and then imaging the result. One major drawback with this type of 'archeology' studies is the fact that it is hard to study unsuccessful growth or its limits. If nothing grows, there is nothing to study. But as long as something grows, it could be studied and evaluated after cooling. For over 50 years, the investigation of nanowires using post-growth analysis has been successfully developed and has

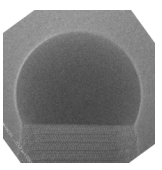

driven our understanding of crystal growth. It has enabled us to produce crystals with few stacking faults and complex morphologies such as branched structures, crosses, heterostructures and so on. However, if we want to study the limits of growth or the detailed dynamics of growth we would need to observe it as it happens; to look inside the 'black box'. The number of studies of the crystal growth and dynamics in real-time has been gradually increasing, using techniques such as spectroscopy[8], diffraction[45,46], reflectivity measurements[47] and imaging[48,49].

To remove the 'black box' in of MOCVD in thesis, both imaging and spectroscopy have be enabled during growth by performing the crystal growth within an electron microscope. In an effort to understand the role of the droplet, I engaged in developing the growth of III-V semiconductor nanowires inside a transmission electron microscope (TEM). The instrument, described in greater depth in chapter 2, allows metal-organic compounds and hydrides to be delivered to a heated sample region. The instrument was designed with the intention of replicating an MOCVD system with the ability to study the dynamics of the droplet and crystal growth. Instead of observing the result after cooling, the TEM enables observation of the crystal growth as it happens (illustrated in figure 1.3). Utilizing the knowledge from earlier post-growth studies of crystal growth using MOCVD, we developed the crystal growth of, primarily, Au-assisted GaAs inside the microscope at temperatures of 420-550 °C for various partial pressures of the precursor gases[50,51]. This development was essential for the studies of crystal growth and droplet of GaAs nanowires in papers II and IV.

Successful crystal growth of nanowires inside a microscope allows us to study the dynamics of a droplet that assist growth. More precisely, it allows us to conduct studies in an environment similar to the crystal growth in a commercial MOCVD reactor. This enables us and other scientists to take advantage of the experiments and conclusions from our *in-situ* experiments when later designing crystal growth on a larger scale. In particular, we can use it for predicting and designing growth without being able, or needing, to observe the crystal growth.

The main scientific topic of this thesis is the role of the droplet and its dynamics on the nanowire in a growth environment and in vacuum. As part of the process for understanding the droplet, we investigated how the droplet composition changes with temperature. The composition of the droplet (liquid phase) is an essential parameter for understanding and predicting growth, as it partly determines the chemical potential of the droplet. Temporary changes to the liquid chemical potential, away from the equilibrium, affect the rate and probability for solidification and crystal growth. The composition of the droplet is commonly addressed by estimations after growth[30,31,44] or by theoretical predictions[52]. These experimental post-growth, or *ex-situ*, measurements have provided insight into the droplet composition prior to cooling by evaluating the growth during cooling[30]. However, this only works for successful growth experiments when the droplet has been able to assist growth. And even in those cases, we analyze the final product rather than the process of growth. Ideally, we would like observe and study the droplet that assists the growth of single nanowires using *in-situ* experiments and transfer the knowledge to the *ex-situ* experiments.

As a result of the uncertainty of the droplet composition and the lack of existing data during growth, part of this thesis includes the development of chemical analysis during crystal growth. The development included the experimental design, testing and analysis of X-ray energy dispersive spectroscopy of both nanowire and droplet at temperatures between 300 and 600 °C. The method was later used to evaluate the assumption that the projected volume can be used as a way of estimating the change in composition of the Au-Ga droplet during nanowire growth. This enabled observations of the

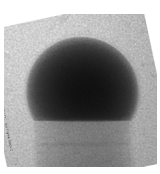

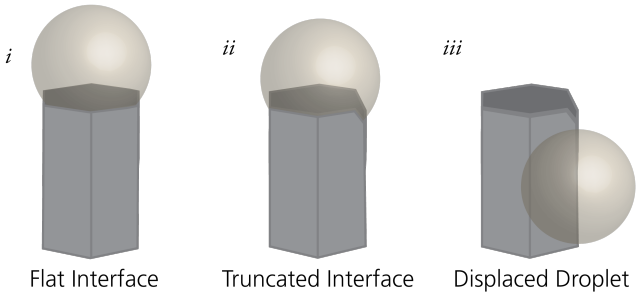

Figure 1.4: Illustrations of a droplet on a nanowire with a flat (i) or truncated (ii) growth interface. For the nanowires whose droplets have been displaced from the top facet, the droplets are found at the nanowire sidewall (iii).

droplet projection to be related to composition without continuous spectroscopy measurements during *in-situ* experiments, an approach which benefits studies of dynamic events during crystal growth, *e.g.* droplet movement.

The Limit of Droplet-Assisted Nanowire Growth

One of the limits of droplet-assisted nanowire growth is the location of the droplet. It has to remain on the same crystal facet to continue the growth in the same direction[37,53,54], a limit which has been utillized for growing nano-flags[36] and L-shaped[39] nanowires. Displacement of the droplet from the top facet has been previously reported for InAs[43,55], InP[36] and InAsSb[39] using *ex-situ* analysis and imaging. These studies attributed the droplet displacement to the expansion of the droplet volume by comparing it to calculations[56]. In addition, Kelrich *et al.* then suggested that droplet displacement was a possible result of the formation of a truncated top facet during growth[36]. Since the studies were conducted post-growth it introduces the question, what came first, the displacement or the facet?. Figure 1.4 illustrates the droplet-nanowire interfaces for a flat and truncated interface along with the situation for a nanowire with a displaced droplet. While the mechanism was suggested from the observations of the cooled system, it was compared to the observations made by studies of Au-assisted nanowire growth inside a microscope[29,57,58]. These *in-situ* studies of semiconductor nanowires of different compounds observed an oscillating truncation of the interface between the droplet and the nanowire. For the studies of GaAs nanowires, the truncated facet was only observed for droplets assisting zincblende crystal growth with a large droplet[29]. The origin and implications of the truncation have been discussed as a source of material for nanowire growth and nucleation[57,58]. However, its origins have not been investigated aside from this.

The core of this thesis demonstrates how the droplet dynamics take part in the formation of the truncation, and eventually the displacement of the droplet. Displacement of the droplet highlights the fundamental limit of droplet-assisted nanowire growth, as the droplet is no longer in contact with the facet that was previously grown. The investigation connects *ex-situ* MOCVD studies of droplet displacement and control, with the *in-situ* result of truncation formation. In addition, it shows the connection between displacement and truncation. This thesis relies heavily on surface energies, parameters which are used rather liberally in theoretical works or model fittings but rarely

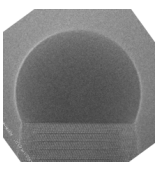

so in experimental works. This is understandable, as the surface and its surface energy can vary with pressure, neighboring environment and temperature[6,59]. In addition, the surface energies are not necessarily measurable but, as yet, rely on secondary measurements such as evaporation rate or, as in the case of chapter 4, droplet wetting and displacement. My studies and contributions are aimed to showcase the influence of surface energies on the droplet wetting of a nanowire.

Dynamics of a Droplet that Assists III-V Nanowire Growth

The following chapters introduce MOCVD and *in-situ* studies of nanowire growth for understanding the droplet composition and wetting during crystal growth. Chapter 2 introduces the practical aspects of microscopy and crystal growth. In addition, it introduces the technique for chemical analysis at growth temperature (above 300 °C) and how an MOCVD system connected to the TEM has been used to control the crystal growth.

The methodology presented in chapter 2 is used for studying the assisting properties of the droplet for nanowire growth and decomposition. These are processes which are both assisted with atomic layer control (papers I and II). This is presented in chapter 3, which introduces the principle of crystal growth, the effect of having a droplet and the importance of its composition.

Chapter 4 demonstrates how the droplet can be displaced from the top of the nanowire during crystal growth. It introduces the concept of wetting and surface energies to explore the limits of one-directional droplet-assisted growth. The chapter discusses how to control the droplet wetting the sidewall by alternating crystal structure of the nanowire. It is discussed from the perspective of surface energies and highlights the current gap between experiments and theoretical estimation, a gap that primarily stems from the lack of experimental investigations on surface energies of III-V semiconductors.

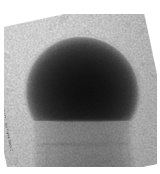

Observing Crystal Growth - (E)Transmission Electron Microscopy

MOCVD + TEM = TRUE

The investigations of the crystal growth presented within the framework of this thesis have been partially conducted using an environmental transmission electron microscope (ETEM), allowing real-time observations in chemically reactive environments. Its environmental attribute stems from the ability to have a large pressure difference between the sample and high-vacuum region where the electrons beam is generated. For this reason, it has been used in our research to recreate a small MOCVD reactor inside the microscope to observe the crystal growth as it proceeds layer by layer. While direct observations of a crystal growing one atomic layer at a time can be fascinating in themselves, correlating the observations with analysis of the crystal structure and composition provides further insights into how the crystals are formed[29,34]. Both crystal structure and composition are crucial parameters for understanding the fundamentals of crystal growth at the nanoscale and can be investigated with a TEM. This chapter introduces the instrumentation of environmental transmission electron microscopy for crystal growth using MOCVD. This is a setup that has enabled studies of the droplet composition and dynamics during droplet-assisted crystal growth, as well as its influence on the process.

There are several methods to 'observe' crystal growth and decomposition including; measuring the pressure and vapor composition around the sample[60,61], reflectometry measurements[47,62], X-ray topography[63–65] and diffraction[45,66], neutron scattering[67], or electron microscopy[68–71]. The benefit of electron imaging, as well as X-ray topography, is the fact that they enable direct observation of the reaction and its dynamics. Such direct observations have been reported and shown to be useful when studying phase transformations[64,68,70,72]. While both techniques are able to study formation for crystals, they excel at different length scales. X-ray topography is commonly used for studies of the microstructures[73,74] whereas (transmission) electron imaging is used for studies of nanostructures[20,70]. The combined improvements of the electron source brightness[75,76], mechanical stability of the instrument, and correction of the lens aberrations[77], have enabled reproducible atomic resolution with medium electron energies (100-400 keV). In addition, improvements of the electron detection allow high resolution (4096^2 pixels and beyond) and acquisition rate (>25 frames/seconds). These advancements make (transmission) electron microscopy a great technique for time-resolved studies of nucleation and growth of crystal with atomic resolution[51,78].

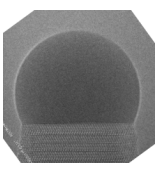

Growth of a crystal from precursors or liquids requires environments (partial pressures) which can be far from the low pressure ($< 10^{-4}$ Pa) at which a normal transmission electron microscope (TEM) operates[79]. The microscope requirement of low pressure is primarily to avoid deposition onto the electron gun which would limit, or even hinder, the electron emission. In addition, the low pressure of the microscope limits electron collisions with the vapor and thus allows more of the electrons that are generated to reach the sample. As the electron path is open between the generation at the electron gun and the sample region, an increased pressure at the sample will result in an elevated pressure at the electron source. The difference between an environmental microscope and a normal microscope is the ability to keep the electron gun at low pressure even though the sample region is not. Two alternatives to achieve high pressure difference were suggested in 1935[80,81], both of which are used in today's instrumentation for environmental microscopy. One of the suggested approaches was to encapsulate and contain the reactive environment between two electron transparent windows, forming a **closed reaction cell**[82–84]. The two windows separate the sample and reactive species from the microscope itself. It is therefore possible to have a high pressure within the cell without affecting the rest of the microscope. As a result, it is possible to study both liquid[84,85] and gas phase[86–88] reactions.

The alternative to a closed reaction cell for environmental microscopy studies is to improve the pumping efficiency of the vapor. Increasing the pumping capacity around the sample region and the pathway leading to the electron gun lowers the effect of a locally high sample pressure. This can be achieved by introducing additional apertures above and below the sample, which creates an **open environmental cell** within the microscope[89]. The introduction of apertures enables additional differential pumping in the microscope. And as a result, it is possible to maintain a larger pressure difference between the sample region (the objective pole-piece) and the rest of the microscope[68,69]. This means that a majority of the gas can be contained within the objective pole-piece keeping a pressure as high as 5 kPa[89]. Of specific interest for crystal growth of semiconductor nanowires, this pressure range is sufficient to mimic the partial pressures of MOCVD of III-V semiconductor material (<20 Pa*).

The environmental TEM (ETEM) used in this thesis is, in its simplest form, an MOCVD system connected to a TEM that has been modified with additional apertures. Here, the microscope and the CVD system can be connected through either the sample holder, the microscope side-ports or needle injectors which deliver gases close to the sample. As optimal condition for the electron gun and TEM imaging favors low pressure and room temperature, this concept of crystal growth in a TEM has its practical challenges. Crystal growth using MOCVD is performed at pressures four to five magnitudes higher than the microscope base-pressure and at temperatures above 200 °C. The following chapter will cover the methods for conventional electron imaging and chemical analysis. In addition, it introduces the factors which make the microscope an environmental TEM and how these factors affect the analysis.

*Based on precursor flows presented in Paper III

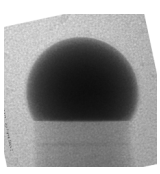

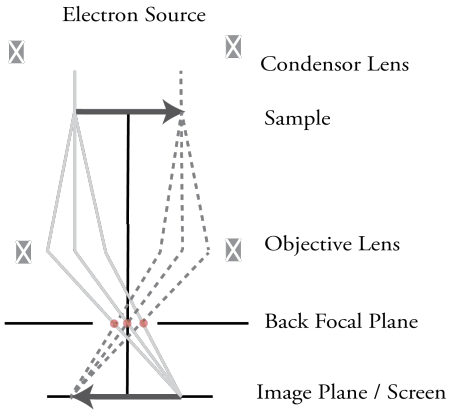

Figure 2.1: A simplified ray diagram of a microscope including an electron source and a set of magnetic coils that creates a parallel beam onto the sample. The information from the sample is condensed by the objective lens (magnetic coils) which focuses the electrons in the back focal plane (BFP). The electrons spread after passing the back focal plane and project an image onto the image plane. The red dots in at the back focal plane represent the resulting diffraction spots.

Transmission Electron Imaging

Observations of crystal growth from a droplet and the resulting structure at the atomic level are, in this thesis, performed using a TEM. This technique, similar to an optical microscope, uses a 'light source' to illuminate the sample and create a projection of the sample onto a viewing screen, or camera, which is schematically shown in figure 2.1. Instead of light, electrons are generated by extracting the surface electrons of an **electron gun**, electrons which are commonly accelerated to 30-300 keV[*] by an electric field. Following the acceleration, the electrons are selected by apertures to form an electron beam aimed at the sample. The beam of electrons is then deflected and focused by magnetic lenses along the microscope column such that the electrons reaching the sample are traveling in parallel. If the sample is electron transparent, *i.e.* less than the mean free path of an electron in the sample[† 79], the transmitted electrons can be collected by an electron-sensitive camera to create an image. Imaging by illuminating a large area of the sample with parallel electrons is referred to as **conventional TEM** imaging. This has been the main technique to observe and image both the growing and the final crystals presented within this thesis.

Imaging and Diffraction

Imaging using the transmitted electrons from a parallel beam of electrons, using conventional TEM, provides the combined information of the amplitude and phase of the electron signal. This is a result of the thickness, density, scattering, atomic arrangement and orientation of the sample. This imaging mode provides an overview of the sample and can indicate where changes occur within the

[*] For some instruments up to several MeV

[†] The average distance an electron travels without scattering

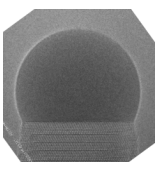

crystal. If you, for example, know that the sample contains two separate phases, contrast changes could help select regions of interest. In the case of figure 2.2a, the contrast shows stripes along the sample (indicated by the added lines) which in this case is a result of a change in the crystal structure.

To confirm that the observed striped contrast is caused by changes of the crystal structure, we utilize the electrons diffracted by the sample and the symmetry of their scattering. If the crystals do not have the same symmetry from the viewing direction it is possible to separate one crystal structure from another. In the case of III-V semiconductor nanowires, viewing the crystal along a $\langle 1\,\bar{1}\,0\rangle$-axis makes it easier to distinguish between the common crystal structures (wurtzite and zincblende).

The diffracted electrons can be imaged by moving the back focal plane of the objective lens onto the image plane. This **electron diffraction** pattern, as seen in figure 2.2b, is a Fourier transform of the information which the electron carries and contains information about the projected periodicity of the sample. Each dot of the pattern represents constructive interference of the electrons diffracted by the atomic planes parallel to the viewing direction of the crystal. The distance between the diffraction spot and the center of the pattern is inversely related to the real-space distance between the planes that caused the diffraction. This means that the closer the atomic planes are to each other in real-space, the further away they will appear in the diffraction pattern. As a result of representing symmetry and inter-planar distances, the diffraction pattern is specific for each crystal structure, material and crystal orientation.

If multiple crystals are illuminated by the parallel beam, the patterns from all crystals will be superimposed onto each other. Figure 2.2b shows the diffraction pattern of the image in figure 2.2a, containing at least two crystals. The majority of the sample is represented by the rectangular pattern of strong reflections. However, not all diffraction spots can be described by the rectangular pattern, as the dot marked by blue indicates a second crystal structure or orientation. Figure 2.2b illustrates the symmetry difference between the atomic arrangement of the present crystal structures: wurtzite (red rectangle) and zincblende (blue hexagon).

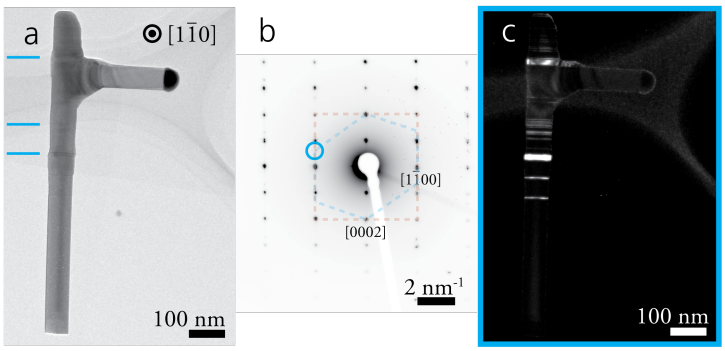

Figure 2.2: A conventional TEM image of an InAs nano-structure (a) with its corresponding (b) electron diffraction pattern that shows the frequency map of the crystal. This can be used to directly evaluate the structure by knowing what direction we are looking from. Here the nanowire is viewed along a $\langle 1\,\bar{1}\,0\rangle$-direction and the two superimposed diffraction patterns are outlined in red (wurtzite) and blue (zincblende). Each spot in the diffraction pattern carries information and can be selected to image which part of the crystal contributed to this electron deflection. In this case, a diffraction spot (blue circle) of the minority component is selected to image the small segments and stacking faults in (c). Note that the diffraction pattern has been color-inverted. This image series is part of the reported studies of branched nanowire structures in paper V.

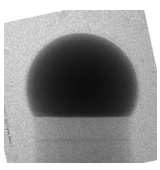

Knowing how the electrons have been diffracted by the crystal allows for specific imaging techniques to separate the information from each individual type of crystal. As all electrons passing through the same spot in the diffraction pattern are in phase, we can use them to create an image containing the information from only those electrons. By inserting an aperture in the back focal plane, to block out every electron except those passing through that aperture (as illustrated by the blue ring of figure 2.2b), it is possible to get a diffraction contrast image. Such an image shows the regions that have had electrons contributing to that diffraction spot as bright regions (figure 2.2c). Due to limited scattering of the vacuum around the sample, the image appears with a dark background, which is a reason it is referred to as dark-field imaging. The dark-field image of figure 2.2c shows the zincblende crystals which have contributed to the electrons diffracted through the 'blue' aperture. Diffraction imaging is therefore a great way to visualize and analyze stacking faults and the location of different crystal or chemical phases within the sample.

Chemical Analysis - X-ray EDS

The chemical composition of the sample can be investigated by studying how the electrons interact in-elastically with the sample, *i.e.* electrons that have lost energy to the sample. This can be investigated either by measuring the energy which the electrons have lost while passing the sample, or, as in this thesis, by studying the secondary X-ray photons generated by the sample. These X-rays are emitted as a result of an incoming electron from the electron beam, knocking out a core electron of the sample. When a higher energy electron of the atom reduces its energy to fill the temporarily empty electron state, its reduced energy is emitted as an X-ray photon. Using X-ray energy dispersive spectroscopy (EDS*), we can visualize the emitted photons for a set range of energies, as seen in figure 2.3. The collection and energy quantification of the photons is performed using a stationary photon energy detector. X-rays that are generated by an electron reoccupying an empty state in the K-shell will result in peak energies which are referred to as K-lines. This principle is the foundation for the terminology of K-, L- and M-lines, which relate the X-ray energy to the electron state which was reoccupied.

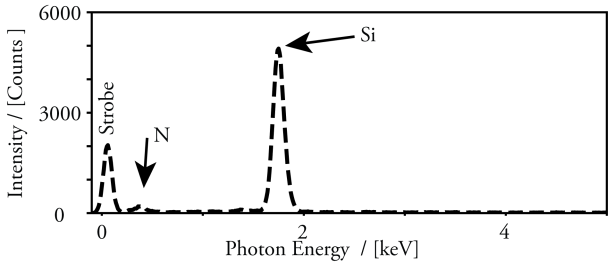

Figure 2.3: A typical spectrum acquired by X-ray energy dispersive spectroscopy (EDS) showing the intensity of the photons emitted with energies lower than 5 keV from the SiN_x sample. Both the strobe (noise) peak and the intensity peaks related to silicon and nitrogen are labeled.

*Alternatively: XEDS or EDXS

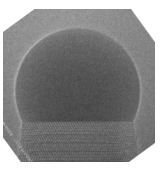

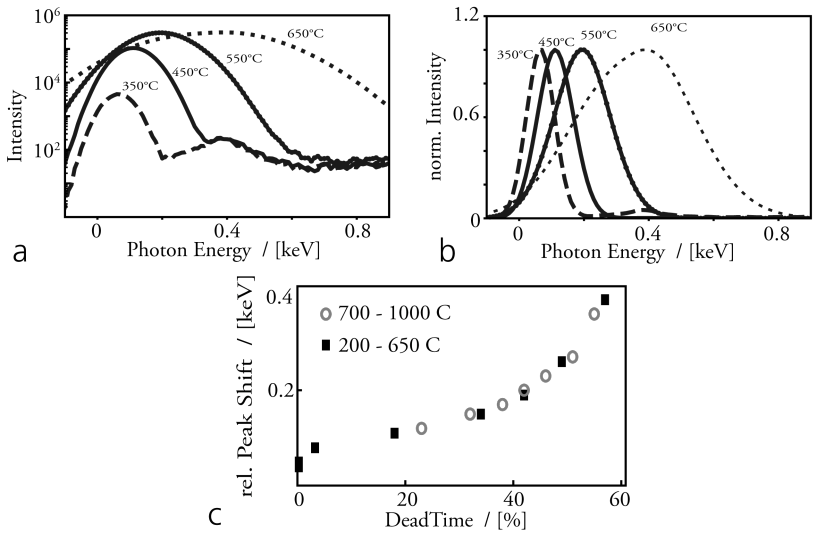

Figure 2.4: X-ray EDS spectra for temperatures from 350 °C to 650 °C shown on both a logarithmic scale (a) and with normalized intensity (b). The peak is observed to increase in intensity (a) and shift to higher energies (b) with temperature. The spectra have been acquired over 45 s excluding dead-time of the detector and are individually normalized based on the peak height of interest. The relative shift of the peak maximum to higher energies is shown as function of dead-time rather than temperature (c).

Each element of the periodic table has a distinct set of energy levels and will therefore emit X-rays that are characteristic for the element. Depending on how many different characteristic X-ray photons can be emitted from an element and their individual energies, the collected spectrum can be used to identify the elements of the sample. This is shown in the spectrum of figure 2.3, where silicon (Si) and nitrogen (N) have been identified due to the presence of one energy peak per element, at 1.74 and 0.32 keV, respectively. The intensity of the peaks is dependent on: the size and density of the material, the ionization crossection (the area which can be ionized), flourescence and X-ray absorption, but also the collection angle and efficiency of the detector[79,90,91].

As a result, the spectrum allows relative quantification of the species by comparing the intensity of a full family of X-ray photon lines (*e.g.* K- or L-lines) with the intensity measurement for another element. In this thesis, the Cliff-Lorimer approach has been used for evaluating the composition which relates the relative peak intensities and composition by a factor k (Cliff-Lorimer k-factor)[90]. This k-factor is individual for each element and can either be experimentally determined by investigating a sample with known stoichiometry or calculated from the ionization crossection, X-ray absorption and yield of florescence[90,91].

X-ray energy dispersive spectroscopy in TEM is relatively straightforward for solid materials at room temperature and vacuum. However, in order to observe crystal growth of III-V semiconductors under MOCVD-like conditions, room temperature does not suffice. One of the stepping stones for this thesis is the chemical characterization during crystal growth and its dependence on the temperature. For chemical analysis of the droplet that assists crystal growth, the droplet constantly moves at the speed of the nanowire growth rate. This means that we need to track the droplet in real-time to avoid illumination of the crystal. To study a moving or growing crystal, we condensed the

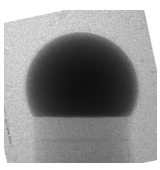

electron beam to illuminate a circular spot of 20-30 nm in diameter. This allowed us as operators to observe the object in real-time and adjust the position of the illumination as we were collecting the spectrum. As part of my contribution to papers I and II, I evaluated the measurement error during chemical quantification using EDS. The evaluation was based on the experimental reproducibility of a spectrum at elevated temperatures and the quantification error. In addition, I evaluated the limit for when the EDS acquisition and quantification at high temperature would result in a misleading result for our instrumental setup. Heating of a sample means more atomic vibrations and larger deviations of the emitted photon energies, which would result in the broadening of the spectrum peaks[92,93]. An energy broadening of the spectrum peaks could influence the chemical quantification significantly if it causes the peaks to overlap. Accordingly, it would be most beneficial for our quantification to limit the energy broadening of the spectrum peaks.

In addition, temperature has in some cases been shown to result in a shift of the spectrum peaks to higher energies[92,94]. In our case, we see a significant increase in strobe-peak* intensity and average energy with temperatures above 350 °C. Figure 2.4a and b show the detected photon energies that correspond to the strobe-peak for temperatures between 350 °C and 650 °C. The additional photons detected at elevated temperatures have energies below 1 keV, which is shown in figure 2.4a on a logarithmic scale. The strobe peaks are not only stronger at elevated temperatures but are also shown to be shifted to a higher energy. This is shown more clearly for the spectra that have been normalized using their maximum peak intensity as in figure 2.4b.

As a result of the increased photon signal, the time when the detector is not registering new photons but instead processes and analyzes the previously incoming photon is increased. The more time spent on processing in comparison to collecting photons, *i.e.* higher dead-time, the longer the period before the detector resets and can analyze a new incoming photon. We can observe an increased peak shift to higher energies as a result of the dead-time in figure 2.4c, for temperatures between 200 °C and 1000 °C. For temperatures above 650 °C the detector was retracted to reduce its solid collection angle. This resulted in a reduction of the number of incoming photons to the detector and in turn the dead-time, which was shown to limit the peak-shift to higher energies.

Our hypothesis of the peak-shift to higher energy is based on the collection of photons. As the dead-time (intensity) increases, it increases the possibility for having more than one photon reaching the detector during each collection interval for the photons. The detector only measures the energy that has been transferred to the detector from the X-ray; by measuring the amount of ionized material, the detector does not keep track of the number of photons it corresponds to[95]. This leads to a common artifact when performing EDS analysis using high signal, called pile-up, *i.e.* peaks that are not related to individual X-rays but rather to combinations of them. Our hypothesis is that this pile-up of X-rays results in the peak-shift to higher energies. Reducing the intensity that reaches the detector would therefore limit the peak-shift artifact of the spectrum and possibly enable EDS measurements at even higher temperatures.

In comparison to the strobe-peak observations, we observe that the peaks of higher energy are less affected by the event that causes the artifact. Figure 2.5a (next page) shows the silicon K_α peak at 1.74 keV for the same spectra as the strobe peaks were extracted. In contrast to the strobe-peak, the Si-peak does not exhibit a strong shift until above 550 °C. In fact, for quantification using the maximum peak height as a measure of the peak intensity; the temperatures below 550 °C provide the

*noise peak

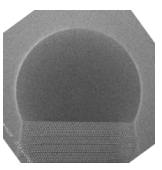

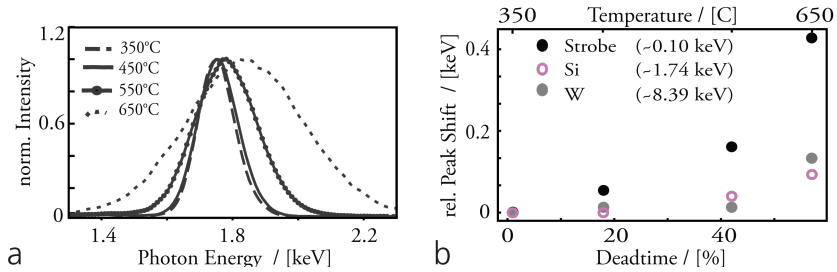

Figure 2.5: X-ray EDS spectra presented for the elemental peak for silicon (1.74 keV) with varying temperatures from 350 °C and 650 °C (a). The normalized spectra show the shift of the Si-peak with increased temperature. Comparing the energy shift of the peak maximum for the strobe (●), silicon (○) and tungsten (●) peaks shows that the temperature, or dead-time, is influencing the strobe peak more than the elemental peaks (b).

same result. The graph of figure 2.5b illustrates the peak shifts as a function of dead-time, illustrating that the intensity peaks of the characteristic X-rays of silicon and tungsten (W) are not exhibiting a significant shift in energy for dead-times below 50%.

Observing a peak shift at elevated temperatures which is dependent on X-ray energy implies a few important aspects for the *in-situ* experiments. First, it indicates that the higher energy peaks are preferred for quantification, not only because the background signal is lower for higher energies but also because the peak-shift has been observed to be less significant. As a consequence, the EDS quantification in papers I, II, and IV are carried out using the highest possible energy for each element (below 20 keV), which means using the L-lines for gold and K-lines for gallium, indium and arsenic.

Secondly, I observed that for the temperatures used in growth of III-V semiconductor nanowires (400-500 °C) the peak shift is not sufficiently significant to influence the quantification. This analysis shows that X-ray quantification at temperatures below 450 and possibly even 550 °C is reliable with respect to the peak-shifts for the acquisition parameters used here.

Third and finally, the fact that the strobe-peak position is related to temperature and intensity indicates that it could be used as an internal reference of temperature. In this case, we have utilized the strobe-peak position to investigate if the set temperature in the beginning of an experiment is similar to the same set temperature at the end of the experiment. Since we are growing material onto our sample and that the intensity seems to be dependent on the temperature rather than the sample, the strobe-peak position could act as a temperature sensor. If, the dead-time, strobe-peak shift and set temperature are the same for the measurements it is likely that we have similar real temperature conditions. As the peak shift is most likely an artifact from photon pile-up, we have restricted ourselves to using it as an temperature confirmation within the experiments and not between experiments.

The Design of our ETEM

The *in-situ* investigations of crystal growth using an environmental TEM of this thesis are designed to mimic MOCVD conditions, including elevated pressures and temperatures. To mimic CVD,

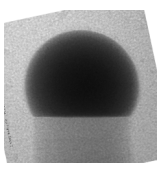

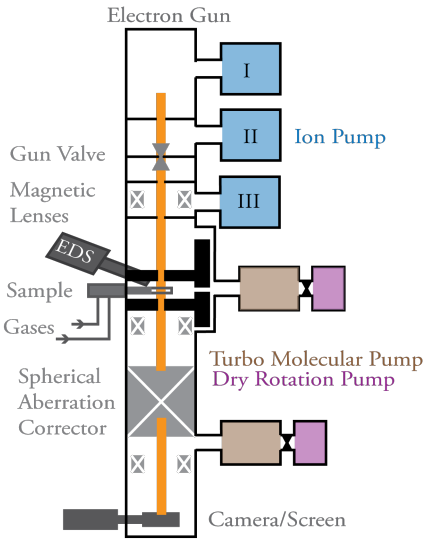

Figure 2.6: A schematic of the environmental TEM (Hitachi HF3300S) showing the principal magnetic coils and apertures which the electron beam passes on its way from the electron gun, through the sample and to the camera. In contrast to the other TEM used in the studies of this thesis (Jeol 3000F) it includes an additional ion pump (III) and a spherical aberration corrector for imaging. Apart from the imaging, the setups both include X-ray spectrometers (marked: EDS) to evaluate the chemical composition of the sample. Note that several magnetic coils and the proper electron influence from the coils are omitted from the schematic for simplistic reasons.

gases have to be supplied to the sample and the instrument has to be able to operate at pressures above 10^{-4} Pa, which requires additional pumping techniques. The microscope used in this thesis is illustrated in figure 2.6 where electrons generated at the electron gun in the top are passing through the gun valve before entering the microscope column. In the microscope column the electrons get selected by the condenser aperture and focused by the condenser lens to a beam which illuminates the sample. As the electron beam passes the sample it is focused by the objective lens and aperture to form an image of the sample onto the camera or screen.

In the environmental TEM setup, an image corrector is inserted after the objective lens to correct the spherical aberrations introduced by the objective lens. This corrector is a set of multipole (*e.g.* hexa- or octapoles) magnetic coils that is optimized to create a spherical aberration which negates the aberration created by the objective lens[77]. As a result, the final image will have a higher point-to-point resolution than without the correction.

Conducting a gas experiment inside the microscope inevitably increases the pressure in the entire microscope. The main pathway for removing gas is by pumping the sample region (pole-piece gap) using turbo molecular pumps. In the case of having III-V semiconductor precursors in an ETEM, this pumping is supported by a scrubber that filters the gas before releasing its harmless components out in the room.

As briefly mentioned in the beginning of this chapter, an open reaction cell can be obtained by introducing a set of additional apertures above and below the sample holder[89] . The additional apertures create an intermediate chamber which acts as an additional volume buffer between the

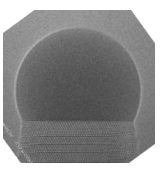

volume where gas is injected and the electron gun. As a result of additional differential pumping enabled by these apertures, this intermediate chamber partially protects the pressure-sensitive parts of the microscope from the majority of the gas. To further limit the gas reaching the electron gun, the column is supported by a third ion pump (III) just below the gun valve, as illustrated in figure 2.6. This removes a large fraction of the gas that has leaked upwards from the sample region, and is crucial to limit material deposition on our cold field emission electron gun (FEG).

The fact that cold FEGs emit electrons at room temperature, as a result of an initial electric pulse (a so-called flash current), increases the likelihood of material deposition onto its surface when compared to a hot filament. The initial flash generates surface electrons that are extracted by an anode, causing a cascade effect generating new surface electrons[*]. This is a process which maintains the electron emission as long as the tip of the electron gun is clean. As material deposits onto the FEG the current starts to decrease, a process which is slower at lower pressures[79]. Despite the intermediate chamber and additional pumping, working at elevated sample pressures containing small molecules or atoms, *e.g.* H_2, increases the gas reaching the electron gun and thus the rate at which the emission of electrons from the cold FEG decreases. As a result, the FEG needs to be cleaned during gas experiments by re-applying an electric pulse (flash), thus resetting the electron beam current to its target value. During experiments using high gas-flows, this is performed as often as every ten minutes, in comparison to every four hours at proper vacuum conditions (10^{-5} Pa).

Gas Handling System - MOCVD

As part of this thesis I have been involved in the development and transfer of the knowledge from *ex-situ* MOCVD of III-V semiconductor nanowires into nucleation and crystal growth inside the TEM. Using knowledge of the temperature windows and partial pressures which have previously yielded successful growths, we were able to find good starting points for *in-situ* growth. This information allowed us to nucleate crystal growth of GaP, InP, GaAs and InAs using gold as a promoter. As of now, we have also reached the point where we can tune the process to enable growth of both crystal structures of GaAs, from zincblende via mixed into wurtzite structure.

In striving to make as controlled crystal growth studies as possible and for them to be as applicable to growth outside a TEM as possible, there is a great benefit in being able to control the flow of material and the concentrations at the sample tip. This is, in particular, since the material supply is strongly affecting the resulting crystal structure[28,30,96], morphology[36,97,98] and the composition[99] of the resulting structure. In addition, increased control of the gas supply would benefit the understanding and analysis of our observations, as the amount of supplied material is essential for crystal growth. This type of control is in part dependent on how the material supply is handled but also how fast the material can be transported away from the sample.

[*] A cold cathode

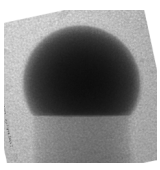

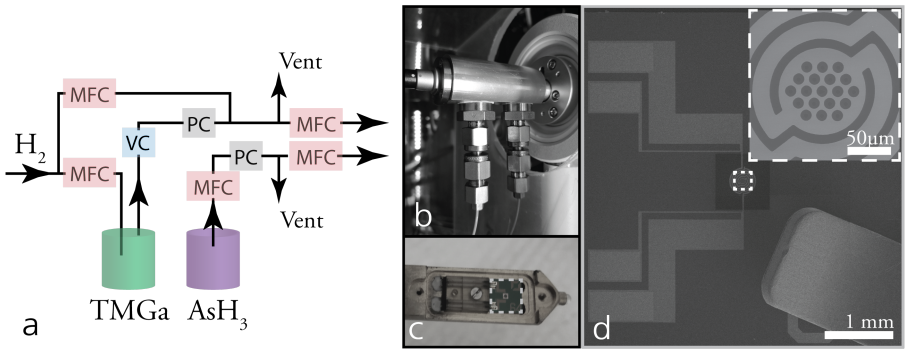

Figure 2.7: Overview of the gas handling system and its connection to the microscope. The extracted precursors for group III and V elements (or oxygen, hydrogen or nitrogen) are controlled using a standalone gas handling system. A simplistic schematic shows the gas flow and control for GaAs and AsH_3 (a). The gas flows are controlled separately by mass flow and pressure controllers (MFC and PC) and excess gas can be bypassed to the ventilation (vent) without having to force it into the microscope. When the gas composition in both lines is set, which can be monitored by vapor concentration measurements (VC), the gases are led in two separate gas lines to the TEM holder (b). This feature is used to separate group III and V elements until it reaches the sample loaded onto a MEMS-device at the holder tip (c). The SEM image of the MEMS-device (d) shows the four contacts pads (to the left) needed for the Joule-heating of the sample region in the center. The panel inset shows the 19 electron transparent SiN_x windows for electron imaging at the center of the device.

Providing Material to the Microscope

There are several ways of providing materials for crystal growth within a microscope. For the simplest case, material could be deposited on the holder and then evaporated inside the microscope using the electron beam to provide material for growth[100,101]. This is a method which provides a pulsed experiment where the components for growth are created, followed by the observation until the components have been consumed or diffused away. Another common technique which increases the control of the growth conditions is to connect gas tubes or effusion cells directly to the microscope side-ports[49,89,102] or through the holder itself[83]. Using an external supply of material to the microscope allows for more sensitive control of the gas flow, as growth species can be provided by continuously leaking a steady flow of gas into the microscope. In this case, the constant material flow could be evaluated from the pressure inside the microscope.

More advanced ways of supplying gas can increase the control of the gas flow and its content to the sample region, commonly by mixing the gases before transporting them to the microscope[88,103]. In our case, an MOCVD system has been connected to the microscope which allows for full control over the gas composition and partial pressures during the experiment. With the ability to tune the composition and the flow of vapor, we are able to achieve and study crystal growth using droplets (as in the case of nanowires) over a large parameter window. In addition to the composition control of the gas, we want to be able to rapidly alter the gas flow in order to study the atomically sharp crystal and material heterostructures. Systematic and fast gas control would provide insights into mechanisms such as crystal formation, the droplet-assisted growth and the cause of failure during directional crystal growth.

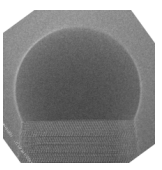

With an MOCVD system, it is possible to combine and control the flows of metal-organic compounds (*e.g.* tri-methyl-gallium [TMGa]), hydrides (*e.g.* Arsine [AsH_3]) and process gases such as H_2, O_2 or N_2. The control is achieved by flowing a set amount of H_2 through the metal-organic source, as shown for TMGa in figure 2.7a, which evaporates the metal-organic precursor into the gas-stream. How much of the precursor is evaporated is determined by the ratio between the vapor pressure of the source material, the flow of H_2 and the pressure in the gas line. Experimentally, the amount of metal-organic species in the gas line is monitored using a vapor concentration measurement that correlates absorption of infrared light with the gas concentration. The mixture of H_2 and precursor is then diluted further if needed by additional H_2 before being led to the microscope.

The gas pressure, composition and flows are controlled within our gas-handling system by pressure (PC), mass flow (MFC) controllers. These controllers, and the dilution, allow us to vary the flow of the growth species over 3 orders of magnitude within the same growth experiment. As a result, we can tailor the flow and partial pressures to the microscope by controlling the flow through the metal-organic source, the dilution flow and the amount of the gas that is led to the microscope. The wide range of partial pressures is needed to reach the conditions for crystal growth of both wurtzite and zincblende GaAs based on *ex-situ* growth studies[28]. In addition, being able to access a large parameter window for precursor flows can also enable tailored growth of other III-V semiconductor materials (*e.g.* InAs and GaP)[30,33]. Figure 2.7a schematically shows the design of the gas-handling system and the nodes where we can control or monitor pressure, concentration or flows of the precursors.

As for regular MOCVD, the gas-handling system connected to the ETEM keeps the material supply of group III and V precursors separated through the holder until it reaches the sample. To keep the flows separated we therefore need two inlets into the holder, as shown in figure 2.7b. This individual control of group III and V supply in the gas-stream allows us to tune and optimize crystal growth without directly affecting both flows. The full control of the MOCVD system together with knowledge from *ex-situ* MOCVD studies enables us to realize pure crystal growth (with few defects) and eventually complex structures, such as heterostructures or branching.

Enable Rapid Switching of Gasses

The open cell design of the microscope allows the gas at the sample to respond rapidly to changes in the gas flow. With an open cell design as in figure 2.7c-d, there is nothing that keeps the gas at the sample and the gas can therefore be continuously replaced as a result of the pumping of the microscope. This would in principle allow the replacement of the gases to be as fast as the material flow from the last MFC before the holder to the sample region. The material flow will be dependent on how the material is supplied to the sample region. In our case it could either be supplied via capillary tubing through the holder or directly to the microscope through a side-port. The time needed to adjust to changes of the gas flow would be reduced if the gas were to be supplied from the side-port of the microscope rather than through the holder. This is because the holder generally requires the tubes to be thinner than the 1/4″ steel tubing from which the rest of the gas-handling system is constructed. Having a narrow diameter of the tubing would result in a reduced flow[104] and a dead-volume of material collected at the position where the tube diameter narrows. The environment at the sample will therefore not be fully stable until this dead-volume of gas has been completely replaced. The studies performed in this thesis have supplied gases through

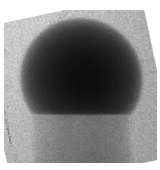

the holder, but have not been limited by the slower adjustment rate of the gas-flows, as they have mostly focused on the steady-state of the droplet-nanowire system. This would be a experimental limitation for studies of abrupt changes in the growth, as in growth of heterostructures.

The open cell ETEM design comes with a practical limitation; the fact that we are releasing the gases into the microscope limits the total pressure to a few Pa before potentially overloading the electron gun. Still, this is a sufficiently high pressure to reach the molar flows needed for semiconductor crystal growth, an estimation based on the partial pressures of paper III. Higher sample pressures of up to 400 Pa can be reached by covering the sample holder tip with a steel lid. This lid contains an orifice just above the sample region which allows imaging. In addition, the orifice keeps the microscope pressure relatively low in comparison to the sample pressure as the orifice provides an additional step of differential pumping of the microscope. The drawback of this semi-closed cell is the slow replacement of the volume under the lid due to the additional differential pumping. The environment under the lid can take several tens of minutes to re-stabilize at a new pressure, a long time period for crystal growth at growth rates of nm/s. In addition to the slow response time of the gas environment, the lid blocks the X-ray signal from the sample, which hinders chemical analysis using X-ray EDS.

In contrast to letting the gas out in the microscope, is the more commercially common[105–107] closed cell, where the sample region is enclosed between electron transparent windows. In this closed system, the gases are supplied and pumped out through the holder. The benefit of the closed cell is that it protects your microscope chamber, column and electron gun from high pressures and harsh gases, thus making it possible to perform ETEM-like experiments in a regular microscope that operates at high vacuum[105]. The closed cell holders provide controlled gas flow into the holder and return the bi-products and non-reacted material out from the microscope through the holder again. This provides an easy way of analyzing all bi-products of the reaction. Experiments using these gas reactors inside a microscope include oxidation or hydrogen studies and have shown the ability to alter the pressure in as little as 20 seconds[105]. While 20 seconds are rapid changes for a closed cell experiment, the crystal growth of III-V nanowires using MOCVD-like conditions would have grown tens of atomic layers in that time (approximately 1 nm/s for a 40 nm wide pillar). A gas replacement rate of 20 s would limit the ability to study abrupt changes of the gas environment and in turn sharp phase transitions.

The closed cell does have some practical challenges, which is why the instrument presented within this thesis is using an open environmental cell. First, removing the necessity of leading gases out from the holder, by using an open cell, makes it practically easier to supply two gases into the microscope at the same time. Not by mixing the gases and carrying them together to the sample, but to have two parallel gas inlets reaching the sample through the holder. This increases the individual control of the separate gases, at the same time as it mimics the regular MOCVD by having two lines for the precursors. In fact, since we can release the gases into the microscope, we could supply them through the microscope instead, which removes the criterion of leading them in through the holder. This opens up for more practical solutions for the holder design such as double-tilt holders. Being able to tilt, or rotate, the sample in two directions makes it easier to reliably reach atomic resolution. As a result, crystals that have nucleated inside the microscope can be rotated to align the crystal with the viewing direction such that it is possible to see crystal growth with atomic resolution.

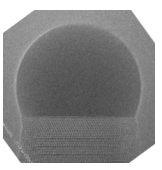

Being able to rotate crystals that have been formed such that we can achieve atomic resolution allows for detailed studies of crystal growth. Together with the ability to control the conditions at the sample, by separately controlling the precursors for group III and V elements, this has enabled crystal growth studies over a large parameter space. This is sufficient to enable crystal growth of both crystal structures of III-V semiconductor nanowires. In addition, chemical analysis using EDS was shown to be reliable at the temperatures generally used for crystal growth (<550 °C). Above that temperature, the spectrum peaks started to shift to higher energies dependent on peak energy. Experiments at higher temperatures could most likely be conducted by reducing the intensity reaching the detector, either through reducing the solid angle of the detector or perhaps reducing the heated area at the sample holder. With the combined possibilities of *in-situ* imaging and analysis of crystal growth, I have been able to investigate the droplet that assists nanowire growth and how it dynamically changes at conditions that favors growth.

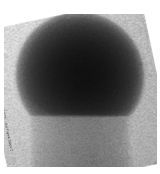

Crystal Growth and the Droplet that Assists

If we want to study the droplet and its influence on nanowire growth, it is important to understand and reach steady crystal growth. The first step is to know the factors which control the crystal growth. The second step would be to target these factors using the input parameters for MOCVD in an ETEM. To further understand the thermodynamic role of the droplet, this chapter introduces the concepts of crystal nucleation[108,109] and reaction rates[110]. In addition, it covers how the droplet influences these processes and how these can be evaluated using the droplet composition.

Crystal growth is, at its core, a phase transformation from one phase into a solid phase with a periodic arrangement of the atoms. As introduced in the first chapter, this thesis focuses on the phase transformation of vapor phase (v) group III and V precursor material into a crystalline solid phase (s) III-V semiconductors, using MOCVD.

$$\mathrm{III}(v) + \mathrm{V}(v) \xrightleftharpoons{(droplet)} \mathrm{III{-}V}(s) \tag{3.1}$$

The solidification process can either be achieved through direct deposition or through an intermediate phase, such as a droplet. Based on the available material and the environmental condition, such as temperature and pressure, the thermodynamics determine which phase that will be formed based on the minimization of Gibbs free energy[108]. As a result, chemical reactions are driven to minimize the energy of the systems and eventually reach an equilibrium state where all present phases have the same chemical potential. The rate at which the system reaches the equilibrium depends on the energy gradient of the involved phases[108,109,111]. In the case of deposition, the rate of crystal growth depends on the evaporation and the impingement of atoms, processes which depend on the chemical potential (and Gibbs free energy) of the solid and the vapor phase, respectively.

With that in mind, a thermodynamic equilibrium can only be reached for an isolated system* with constant pressure and temperature[112]. For continuous crystal growth, we prevent the system from reaching an equilibrium by constantly supplying growth species. Resupplying growth species ensures a continued difference in chemical potential between the vapor and the solid phase, which results in continuous crystal growth. When a system with constant material supply is stabilized, *i.e.* when the reaction rates are constant, it is commonly referred to as a stationary or steady state rather

*No in- or outflux of material to the reaction

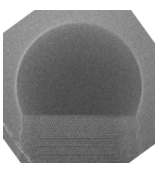

than an equilibrium state. Crystal growth under steady-state conditions can be limited either by the driving force to reach the thermodynamic equilibrium, or by the rate at which the growth species are supplied to the reaction.

We can manipulate the growth by stabilizing an additional phase, *e.g.* a liquid. If both the liquid and the solid are stable phases we can grow a crystal from solidification of the liquid but also through direct deposition from the vapor. Depending on which pathway is the most favorable for deposition, the growth will be favored away from, or under, the droplet. One way of forming a stable liquid and solid is to change the temperature, pressure and composition of the system to allow both phases to exist. Alternatively, we can introduce an additional component to enable the stability of two phases, as in the case for Au-assisted semiconductor growth. In this case, gold is introduced to form liquid alloys (droplets) with group III or IV elements on top of a surface. These Au-based droplets have been shown to increase the activity of the semiconductor surface in contact with the droplet. Depending on the gas environment and the temperature, the Au-based droplets have been shown to assist for instance the crystal growth of Si, GaAs and InAs[11,12,14] but also the dissolution of GaAs[113]. When assisting growth, Au-based alloys were shown to increase the growth rate at the droplet-semiconductor interface which in turn resulted in the formation of semiconductor nanowires rather than a thin film[14].

Similar to nanowire growth, assisted dissolution has been observed from both annealing and MOCVD studies, where nanowires have been shown to shorten with time[114–119]. From a thermodynamic perspective this process would be similar to reversed growth if the difference in chemical potential could be reversed, making the vapor the lowest energy phase of the system. In the case of the Au-GaAs system, gold has been shown to assist pit-formation on GaAs substrates[113,120] below 420 °C. In addition, gold contacts have been shown to assist in the etching of GaAs at temperatures between 200 and 350 °C. These observations have been observed well below the temperature for congruent evaporation of GaAs, which occurs at around 623 °C[60]. Since the etching occurs at lower temperatures this indicates that the gold activates the decomposition of GaAs. In paper I, I showed that a Au-Ga alloy can assist the etching of a GaAs nanowire in vacuum at temperatures between 300 and 400 °C. In this range the etching was observed to be occurring layer by layer at a temperature-dependent rate. In a way, this study suggests that the growth can be reversed with control.

In order to study and increase our understanding of droplet-assisted nanowire growth, we start by considering the simpler case without a droplet. The influence and purpose of the droplet are then evaluated based on its interface to the solid[121]. Reports have shown the droplet to dictate the phase, rate and even direction of crystal growth, based on the droplet shape[34,122], size[28,123] and composition[124]. Up until the studies of this thesis, the composition of the droplet has not previously been measured at conditions for crystal growth by MOCVD. This chapter introduces the measurements of the droplet composition as it assists crystal growth and dissolution of GaAs nanowires (papers I and II). In addition, the relation between volume, shape and composition of the droplet is presented to connect to previous *in-situ* experiments.

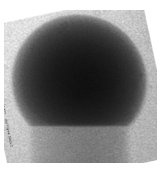

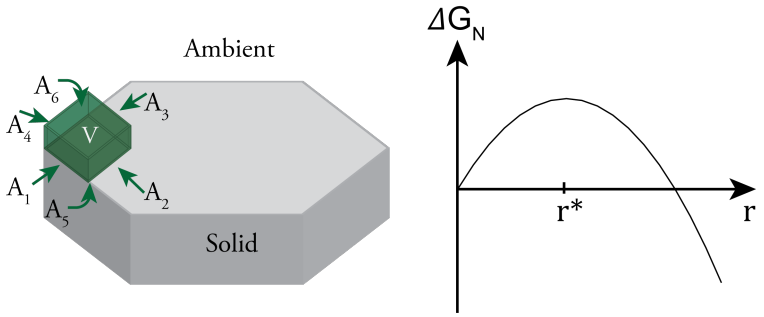

Figure 3.1: An illustration of a nucleus (green) on a flat interface which has the volume (V) and the individual surface areas A_j. The change in Gibbs free energy (ΔG) described in equation 3.2 is then depicted for the cluster as a function of its size (r). From size zero, we observe a positive energy change to add atoms to the cluster, until the point of reaching the critical size (r*). From there on it is favorable to add atoms and thus grow the crystal.

Chemical Potential and Nucleation

The basic concept of crystal growth is to enable phase transformation into a solid crystal by controlling the in- and/or outflux of material to the steady-state system. For a cluster of atoms to nucleate, as illustrated in figure 3.1a, the system has to gain energy by the phase transformation into a solid crystal. Nucleation of a crystal is partly controlled by the difference in chemical potentials between the phases involved, *e.g.* solid crystal (s) and ambient phase (a) ($\mu^s - \mu^a$ [eV/atompair])*. This relates to how much energy each atom would gain by being incorporated into the center of a crystal rather than being in the vapor. The total energy contribution from forming the crystal phase depends on the number of atoms that are part of the nucleus, which is usually quantified as the nucleus volume (V) and is normalized to the unit volume of an atom (Ω) [2,108,125]. As long as the chemical potential of the solid is the lowest among the involved phases in the steady-state system, it will be possible to form a crystal [12,108].

In reality, atoms that are incorporated into a solid phase create new surfaces. Formation of these surfaces introduces an energy barrier due to the fact that the atoms at the surface interact with the phase in contact with the nucleus. The surface energy (γ [eV/Å^2]) of each surface depends on the material, atomic arrangement of the surface and the ambient phase. The total energy required to maintain the surfaces is therefore related to the areas (A) of the facets that enclose the nucleus. Further discussion of the surface energies will be given in chapter 4. Combining the energy reduction of forming a crystal with the cost for creating j number of surfaces yields the change of Gibbs free energy of nucleation (ΔG_N) [108,126]

$$\Delta G_N = (\mu^s - \mu^a)\frac{V}{\Omega} + \sum_j \gamma_j A_j, \tag{3.2}$$

This relation describes the change in free energy from the perspective of classical nucleation theory [125] and the energy change is illustrated graphically in figure 3.1b. The figure showcases the formation

*Also known as supersaturation ($\Delta\mu$) in crystal growth

energy of a solid material depending on the size of the cluster in figure 3.1a. For the cluster to change size and remain stable, the state of the system has to have reached a lower Gibbs free energy[108]. In the case of clusters smaller than a critical size (r*), the surface energy will be dominating and make each added atom less favorable. Any formed cluster will be more likely to dissolve instead of growing. If a cluster of the size (r*) were to be formed, the energy of the system will be lower by either reducing the cluster size or increasing its size. Beyond the critical size, it is more likely to continue the growth of the crystal instead of dissolving it (negative slope of the $\Delta G(r)$).

The rate at which crystal growth occurs is based on the difference is in chemical potential between the crystal and the ambient[109]. In the simplest case, the rate of crystal growth can be determined by the nucleation rate (J_N). By defining the activation energy as the maximum change in Gibbs free energy ($\Delta G_N(r^*)$), the nucleation rate can be determined by the following Arrhenius dependence:[108,110]

$$J_N \propto e^{-\Delta G_N(r^*)/k_b T} \tag{3.3}$$

where k_b and T represent the Boltzmann constant and the temperature of the system. However, for the nucleation to be the rate-limiting step, it means that the diffusion and/or impingement of the growth species to the growth front must be faster than the nucleation rate[111].

Crystal Growth Assisted by a Droplet

The benefit of the presented nucleation theory is that it is not specific to crystal growth from a liquid or a vapor phase[109,125], as long as the surface energies and difference in chemical potential are adjusted accordingly. As a result, the theory also applies to crystal growth from a liquid where the ambient phase (a) is a liquid (l) rather than vapor (v)[127]. Due to the general nature of the model, it has also been adopted for the crystal growth of droplet-assisted nanowires[123,128,129].

Steady-state droplet-assisted nanowire growth implies that the most favorable pathway for the growth species is from the vapor through the liquid to eventually reach the solid phase. In other words, there has to be a gradient of the chemical potentials from the vapor to the crystal with the liquid chemical potential as an intermediate step according to:

$$\sum_{i=\mathrm{III,V}} \mu_i^v > \sum_{i=\mathrm{III,V}} \mu_i^l > \mu_{\mathrm{III-V}}^s \tag{3.4}$$

where μ_i indicates the partial chemical potentials of the components i, *e.g.* gallium, arsenic and gold for Au-assisted GaAs growth, for each phase[110,126]. The intermediate liquid phase is in some sense the link between material supply and the crystal growth. This means that the liquid chemical potential is one of the controlling factors for the growth rate. First it controls the phase transformation at the vapor-liquid interface by controlling the evaporation and condensation. This is because the rates of these controlling processes are determined by the difference between the chemical potential of the liquid and the vapor phase. Secondly, it controls the competing processes of crystallization and dissolution at the liquid-solid interface, as both processes are influenced by the chemical potentials of the liquid and the solid. As a result, it is important to understand what determines the liquid chemical potential in order to study the limits and advantages of droplet-assisted nanowire growth.

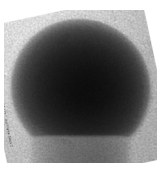

The chemical potential of a liquid can be expressed by the regular solution model for a given temperature (T), and combines the chemical potential of all i species involved in the reaction. The liquid chemical potential depends on the standard chemical potential of the pure species ($\mu^l_{0,i}$), the enthalpy of mixing based on the molar fraction (χ^l_i), and the excess enthalpy of mixing that includes the interaction terms ($\mu^l_{int,i}$) between all elements of the liquid[121,130]. As a result, we can calculate the liquid chemical potential for the Au-based droplet that assists GaAs nanowire growth as follows:

$$\mu^l(T) = \sum_{i=Ga,As} \mu^l_{0,i}(T) + k_b T \ln(\chi^l_i) + \mu^l_{int,i}(\chi_{Ga}, \chi_{As}, \chi_{Au}, T) \tag{3.5}$$

The relation shows that the chemical potential of the liquid, and therefore the Gibbs free energy of nucleation (equation (3.2)), is dependent on both of the liquid components, their respective molar fractions and the temperature. The growth will therefore be, to some extent, controlled by the amount of growth species in the liquid, which in this case will depend on the arsenic and gallium solubility in gold. More specifically, the composition of the droplet will be directly influencing the growth rate as it affects the difference in chemical potential between the vapor and the liquid phase, but also between the liquid and the solid phase.

Controlling and Observing the Droplet

As the liquid state is a deciding factor for the droplet-assisted crystal growth, being able to control the droplet properties would in turn influence the growth. This could be as simple as adjusting the temperature or, more intricately, by addressing the composition of the droplet. In practice, the composition of the droplet, *i.e.* the liquid chemical potential, is indirectly controlled by the growth parameters (precursor flow and temperature). For MOCVD, partial pressures and temperature can be controlled, where the latter will affect all three phases simultaneously as the chemical potentials of the solid, liquid and vapor all depend on temperature[112]. On the other hand, it is possible to control and increase the vapor to liquid phase transformation by increasing the partial pressures of the growth species in the vapor. Supplying more precursor material, *e.g.* TMGa, will result in a higher partial pressure of gallium in the vapor. A higher partial pressure of gallium would result in an increased incorporation of gallium into the liquid due to a larger difference in chemical potential between the vapor and the liquid. In the case where the gallium supply is not the rate-limiting step for the nanowire growth, the droplet would accumulate gallium[29,34]. This has been observed from *ex-situ* MOCVD studies of droplet-assisted nanowire growth, where the droplet volume has been observed to increase with group III element[131–133].

Measurements of the droplet composition have so far been made by chemical analysis at room temperature and vacuum. The droplet composition has been evaluated at room temperature either by direct X-ray EDS of the droplet[33,44,116], or by additional evaluation of the parasitic growth which occurred during sample cooling[30,31]. In the latter case, the parasitic growth was used to extrapolate the measured composition to the composition at growth conditions. Reported measurements have stated gallium concentrations ranging from 1 to 50 atomic percent (at.%) in the droplet, depending on the cooling environment after controlled Au-assisted GaAs growth[33,44,116]. Cooling in an AsH_3-free atmosphere has been reported to maintain larger portions of gallium in the alloy when measured at room temperature. These reports have observed concentrations from 22 at.% up to 50 at.% gallium in the droplet,[28,44] which depends on the cooling rate[52]. In contrast, cooling the nanowires in an

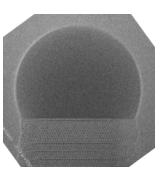

AsH_3/H_2 environment results in gallium concentrations below 10 at.% in the droplet[31,44]. Notably, the composition of the Au-Ga alloy was observed to correspond to stable solid phases at room temperature according to the equilibrium phase diagram of Au-Ga[44,134]. This observations indicate that the composition during growth may be different from the reported measurements.

For *in-situ* growth studies, the chemical composition has instead been estimated by correlating changes in droplet size to the change of gallium content[29]. It has been used under the assumption that the volume changes of gold and arsenic are minor. While not resulting in an absolute value, this approach allows for relative studies *during growth*, comparing higher and lower concentrations of gallium in the droplet. The approach has been used for *in-situ* studies on crystal structure formation[29] and the process of nanowire kinking (a change in growth direction)[53]. Importantly, assessing the droplet composition from its volume assumes that the droplet volume is controlled directly by one of the growth species. The approach has been validated and used as part of the studies presented in papers II and IV. Further, considering the significance of the liquid composition for the crystal growth of nanowires, this thesis includes the X-ray EDS investigation of the droplet composition during Au-assisted dissolution (etching) and crystal growth of GaAs nanowires.

Droplet-assisted Etching - Reversed Growth

While most of studies presented in this thesis have been addressing the droplet during conditions for crystal growth, the investigation of the reversed process (etching) of paper I showed the similarities between etching and growth. We enabled Au-assisted etching of GaAs nanowires by keeping a low partial pressure of gallium and arsenic in the vapor during annealing of the sample. In practice, the experiment was conducted inside an ETEM, where the vapor was pumped away from the nanowires, with the intention of reversing the chemical potentials of relation (3.4). We investigated how the droplet composition in vacuum is affected by temperature, and how the Au-assisted etching could be controlled by the temperature. The observations included layer-by-layer etching of GaAs, which resembles the *in-situ* TEM observations of layer-by-layer growth of Au-assisted GaAs nanowires[29,78,135]. As a result of the temperature-dependent etch rate, we could determine the rate-limiting step for the thermally activated etching.

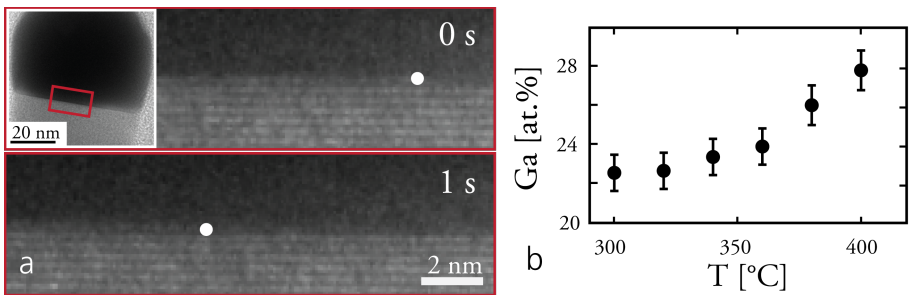

Figure 3.2: Heating a GaAs nanowire in contact with an Au-Ga-alloy in vacuum etches the crystal layer by layer, here at 360 °C (a). Each horizontal line corresponds to a layer of zincblende GaAs. The white markers indicate the front of the etching for TEM images taken one second apart; to the right of the dot is the dark contrast of the liquid and ahead is still the contrast of a crystal. The steady-state gallium (Ga) concentration in the Au-Ga droplet on a GaAs nanowire increases with temperature (T) from 22 to 28 at.% over the temperature interval between 300 °C and 400 °C (b).

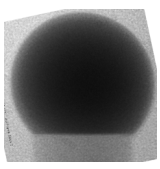

This annealing experiment was investigating Au-assisted GaAs nanowires, which were pre-grown in an MOCVD reactor separate from the TEM at 550 °C . The growth was enabled by supplying TMGa and AsH3, before the sample was cooled in an AsH3 and H2 environment in an MOCVD reactor. More details on the growth can be found in paper I. The nanowires were then mechanically transferred, in air, onto a silicon-based micro electro-mechanical system (MEMS) device with electron transparent SiN_x windows that could be restively heated (figure 2.7). Prior to heating, the Au-Ga alloy contained less than 3 at.% gallium, which is in agreement with previous *ex-situ* studies of alloys cooled in AsH_3 [44,116]. As the sample was heated, the alloy melted just below 350 °C with a gallium composition of 22.7 at.%. This composition was retained after cooling below the solidification temperature, which would correspond to an alloy that has been cooled in an AsH_3-free environment.

Steady-state Etching

For set temperatures above 300 °C we observed that the GaAs nanowire started to dissolve at the interface to the Au-based alloy. This etching occurred one layer at a time at an increasing rate as we increased the temperature. The layer-by-layer etching was observed to reach a steady-state rate at each temperature, at which the etching rate of GaAs and composition of the droplet remained steady. This type of assisted etching has been observed for Au-assisted GaAs[116], InAs[118], SnO[119] and Ge[136]. However, the droplets of these previous reports have been shown not to retain their spherical/elliptical shape during the experiment. Instead it appears as if they have been pinned to the film or an oxide, similar to the image of figure S4 in paper I (page 81).

Increasing the set temperature above 340 °C resulted in an increased gallium concentration of the droplet. This onset of gallium incorporation is connected to the melting of the alloy, which according to the Au-Ga-As phase diagram occurs at 345 °C[134]. Above this onset temperature, the gallium concentration further increased with temperature to a maximum of 28 at.% at 400 °C as shown in figure 3.2b. The steady-state compositions shown in figure 3.2b were evaluated using *in-situ* X-ray EDS measurements of the droplet, as presented earlier in chapter 2.

The observation that GaAs etching occurs below 420 °C at its $\{\bar{1}\,\bar{1}\,\bar{1}\}$-interface to the Au-based droplet, without observation of etching of the sidewall, indicates that the gold assists the etching process. The assisting effect of gold has previously been observed for temperatures below 400 °C when investigating GaAs nanowires in contact with large gold contact pads[115], Au-assisted evaporation on GaAs[120], or gold particles in contact with large GaAs surfaces[113]. However, the interplay between the droplet and the nanowire that is discussed in paper I, would provide information about how stable the nanowire system is with respect to temperature. This information would be useful for studies that requires further processing of the nanowires, as for example when designing electrical devices[137].

The time needed to etch a layer of GaAs at steady-state conditions was observed to decrease as the temperature increased, ranging from 30 s to 1.5 s for the interval between 300 °C and 400 °C. With the assumption that the dissolution of GaAs into the droplet is a thermally activated process, *i.e.* an Arrhenius dependence, we were able to extract the activation energy of the droplet-assisted etching process as 1.21 eV.

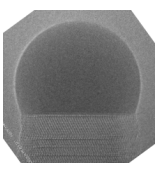

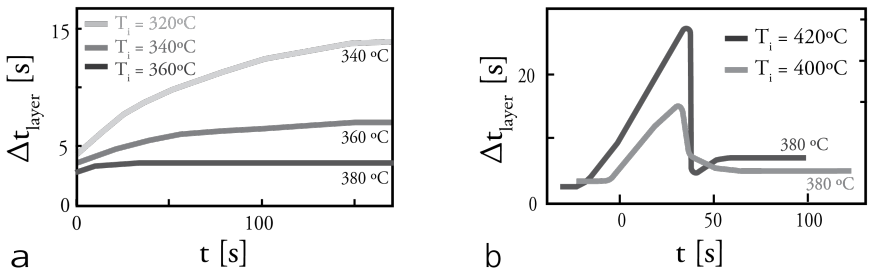

Figure 3.3: Graphs illustrating the effect of heating (a) and cooling (b) the zincblende GaAs nanowire with respect to the time needed to remove a layer (Δt_{layer}) of GaAs. The temperature written along the graphs is the final temperature which was reached at time (t) 0. In addition, the initial temperature (T_i) is specified for each graph indicating the previous steady-state temperature. We observe that 100 s is not sufficient to reach a steady state after heating to 340 °C but heating from 360 to 380 °C results in a stabilization within 30 s. However, cooling to 380 °C (b) requires 45 s for the etching rate to reach a steady state. This figure illustrates trends rather than the raw data for simplicity; the raw data can be found in paper I.

Rate-Limiting Step of Etching

In addition to the activation energy, we could determine the rate-limiting step for etching by studies of how the system responded to a change in temperature (paper I). By increasing the temperature the droplet required a higher concentration of gallium in order to reach its steady-state condition, which could be provided by a temporarily increased etching rate of GaAs, as shown in figure 3.3a. For the opposite case, the droplet reduces its steady-state gallium concentration as a result of a decrease in temperature. During gallium depletion of the droplet, the etching process temporarily slowed down as a result of the gallium concentration being too high. This time, the droplet needs a significantly longer time to reach a steady-state condition, as can be seen in figure 3.3b. Longer times needed for depletion in comparison to the accumulation suggest that it is a slower process to remove gallium from the droplet than to supply it.

Gallium can be removed from the droplet in two ways, either through evaporation or through out-diffusion to the supporting membrane or substrate[60,138]. For a Au-assisted GaAs nanowire with a diameter of 50 nm to reach a steady state, approximately 12 000 atoms of gallium and arsenic need to be transported from droplet during the time it takes for a layer of GaAs to be etched. If evaporation were to be the main pathway for material transport, the ratio of gallium atoms should be proportional to the evaporation rate (J_{ev}), described by Knudsen in 1909[111], which depends on the vapor pressure (p_v), the area of evaporation (A), and the molecular mass (m):

$$J_{ev} = \frac{p_v A}{\sqrt{2\pi m k_b T}} \tag{3.6}$$

When considering the vapor pressure of gallium at 360 °C (5e-12 Pa)[139], and, the area of a hemispherical droplet, less than one gallium atom per second would be expected to evaporate from the droplet. This is a much lower rate when compared to the etch rates observed (400 to 8 000 atoms per second). As such, this excludes evaporation as the main pathway for removing gallium from the droplet. It should be noted at this point that arsenic has a vapor pressure that exceeds the background pressure of the microscope where the heating is conducted, resulting in a very high evaporation rate. Instead, gallium out-diffusion to the underlying substrate is considered the dominating mechanism for gallium removal, and, therefore the rate-limiting step connected to the activation energy of etch-

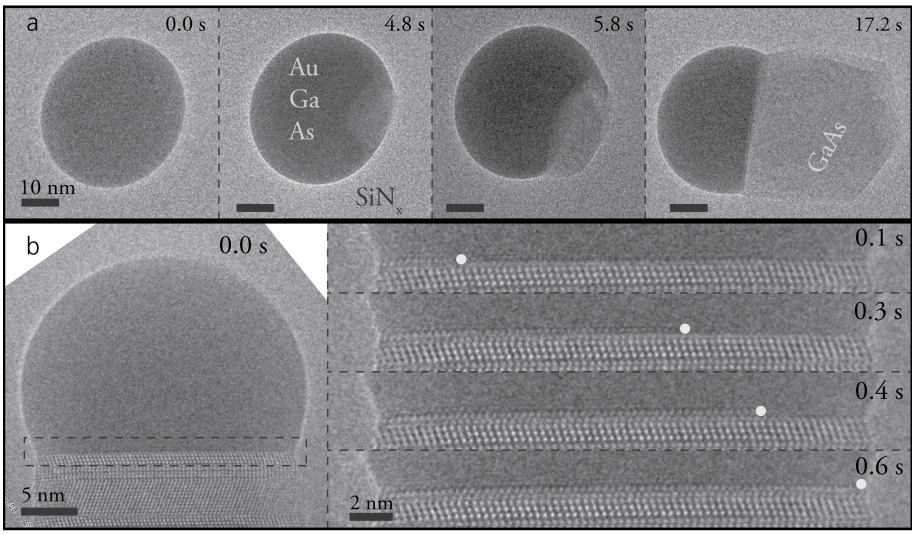

Figure 3.4: The nucleation of a GaAs crystal from a Au-Ga droplet in a SiN_x membrane (a). The image sequence shows how the droplet solidifies crystal GaAs at 4.8 s, a nucleus which grows as the droplet adjusts its position to find the most energetically favorable interface. As the growth proceeds we can follow the step propagation of each grown layer at the interface between the droplet and the nanowire (b). The white dot in each of the frames indicate the propagating atomic step of the new GaAs layer under the Au-Ga droplet. A longer sequence of the one in (b) is presented as a flip-book on the odd-numbered pages of this thesis, showing the continuous process of growth.

ing. These results show how knowledge of the droplet composition and reaction rate can be used to evaluate the rate-limiting step of the etching process.

Droplet-assisting Growth

To determine the chemical composition of the droplet at growth conditions, as in paper II, we need to supply precursors for the growth species to promote growth in the first place, *e.g.* TMGa and AsH_3. Using an ETEM for the studies, we were supplying gallium and arsenic at sufficiently high partial pressures to nucleate GaAs nanowires from gold particles at a set temperature of 420°C. The particles were deposited onto the similar MEMS devices with SiN_x-windows as were used for the etching experiment.

The growth process was initiated by first introducing gallium to alloy with the gold at 420 °C, causing the alloy to melt and eventually become saturated with gallium. From there, the droplet was supersaturated with gallium and arsenic until nucleation and growth of GaAs occurred. In the beginning, there is no directional growth as the droplet moves around to find the most favorable facet as it continues to grow the crystal. As it finds a local energy minimum for its wetting and position, it starts to assist the one-directional nanowire growth. This nucleation process is shown in figure 3.4a for a Au-Ga droplet nucleating GaAs. The droplet-assisted nanowire growth reached a steady state and grew in the $[\bar{1}\,\bar{1}\,\bar{1}]/[0\,0\,0\,\bar{1}]$ direction at this temperature and flows (4.4e-5 mmol/min AsH_3 and 2.33e-10 mol/min TMGa). The growth an atomic layer is shown for a Au-assisted GaAs nanowire in figure 3.4b. The figure shows how the interface between the droplet and the nanowire slowly

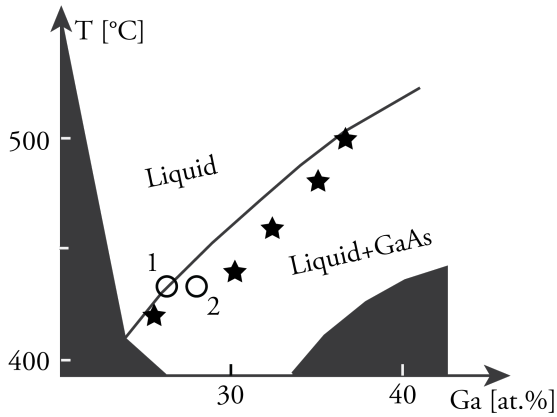

Figure 3.5: A schematic section of the Au-Ga phase diagram for a fixed amount of arsenic (0.01 atomic %). The circle marking the liquidus line (1) corresponds to an equilibrium between GaAs precipitations and the liquid. Increasing the gallium content of the droplet, as indicated by the circle (2), favors formation of more solid GaAs. As presented in paper II, we utilized the fact that growth proceeds for gallium (Ga) concentrations and temperatures (T) within the two-phase region. We were able to estimate the lower limit of the arsenic concentration in the droplet as 0.01 at.%, on the condition that all the experimentally measured compositions (★) should be supersaturating the liquid.

builds a new layer, and the step front can be followed using the white dot as a guide. The details of the layer nucleation and growth has been previously reported for Au-assisted GaAs[29,51,78], and even though the layer growth is not the focus of this thesis, it is an underlying requirement to study the droplet composition as it assist nanowire formation.

The droplet composition was determined from X-ray EDS measurements when the droplet-assisted nanowire growth had reached a steady state. For the analysis of the steady-state condition, we allowed the observed droplet size, microscope pressure and growth rate to stabilize. We measured the composition of the droplet by illuminating it using a ∼10-20 nm diameter beam and measuring the emitted X-rays (EDS). Collecting the EDS spectra for 60 s while tracking the part of the droplet furthest away from the nanowire interface allowed us to limit the scattering from the nanowire itself. For each temperature between 420 and 500 °C, we evaluated the steady-state composition of the droplet. While not being able to resolve the arsenic concentration above the noise level (<1%), we could observe an increasing gallium concentration of the droplet with temperature. Starting from 26 at.% at 420 °C, the gallium concentration increased up to 36 at.% at 500 °C, which is illustrated with stars in figure 3.5. Aside from the temperature dependence, we observed an increased gallium content in the droplet as we decreased the V/III-ratio of the precursor supply. Further discussion on the precursor effect on droplet composition is presented in paper II.

To evaluate the arsenic concentration of the droplet, we utilized thermodynamic calculations to generate phase diagrams between gold and gallium for several concentrations of arsenic. The calculations, presented in paper II, showed that increased arsenic concentration shifted the phase border between pure liquid (Au+Ga+As), and the mixture of a liquid and solid GaAs. An illustration of the region of interest is presented in figure 3.5 showing the liquid and GaAs phase for a fixed arsenic concentration of 0.01 at.%. Knowing that the liquid assists growth, we know that the liquid is supersaturated (2) during growth and therefore has a higher gallium concentration than at equilibrium (1). As a result we were able to estimate the lower limit of the arsenic concentration in the droplet

as 0.01%, with the condition that all the experimentally measured compositions (marked with stars in figure 3.5) should be supersaturating the liquid.

Droplet Volume: a Tool to Determine its Composition

While X-ray EDS is a practical tool for analyzing the chemical composition of the sample, it can be time consuming and potentially damaging to the sample. During EDS analysis, the sample is temporarily exposed to a higher electron dose in comparison to the conventional TEM imaging mode (20 000 compared to 1 000 electrons/$Å^2$s) due to illuminating a smaller area with a similar amount of electrons. To investigate the influence of the beam on the Au-GaAs system, we used the melting point of the Au-Ga-alloy (345 °C) to investigate if imaging conditions of the electron beam influenced the temperature significantly. During the experiments presented, the melting of the alloy was observed to occur just below 350 °C during imaging. However, what we could observe, was that strong illumination conditions during X-ray EDS acquisitions could result in a shape deformation of the droplet. As a result, we generally reduced the intensity of the beam during spectroscopy, by using a smaller condenser aperture.

Performing spectroscopy on the droplet or the nanowire temporarily limits the possibility of observing the dynamic processes at the growth interface as the X-ray analysis focuses on either the droplet or the nanowire. X-ray EDS acquisition provides an average composition of the part of interest, which can be correlated with imaging before or/and after the spectroscopy. Each X-ray spectrum was acquired for at least 30 s of photon collection to allow a good signal-to-noise ratio, and such that the majority of the signal comes from the sample. This means that we trade a minute of imaging of the crystal growth and interfaces to obtain the chemical information. For reactions that have reached a steady state, the X-ray EDS enables chemical analysis that can be compared to what happens the minute after, or before. As such we could measure the growth rate of the nanowire and then conduct X-ray EDS, and they can be correlated even though they were not acquired simultaneously. However, this method would not be appropriate when studying transient effects or processes that have not reached a steady state, as the system then changes from minute to minute.

To analyze transient effects of crystal growth, when we either go from one steady state to another or when no steady state is achievable, we have investigated the relation between the droplet volume and its composition. In this case, we studied the Au-based droplet that assists GaAs nanowire growth at several steady-state conditions. Since we have the ability to measure a steady-state composition, and to observe a projection of the droplet volume in the TEM, we could validate if changes in gallium concentration can be related to the change of droplet volume. This volume to composition comparison requires three assumptions.

First, the arsenic concentration is assumed to be low and possible changes are small in comparison to those of gallium. From the estimate of paper II and the previously reported estimations[52,134] the arsenic concentration in the droplet is likely to be between 0.01 and 1 at.%. Considering that these predictions are the extreme values for the arsenic concentration, it is unlikely that fluctuations within an experiment span the full range of concentrations. The change in volume which could be attributed to changes of arsenic concentration would therefore be small in comparison to the effect of changed gallium concentration. Paper II showed that the gallium concentration of the droplet

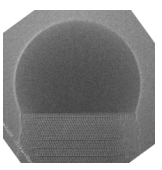

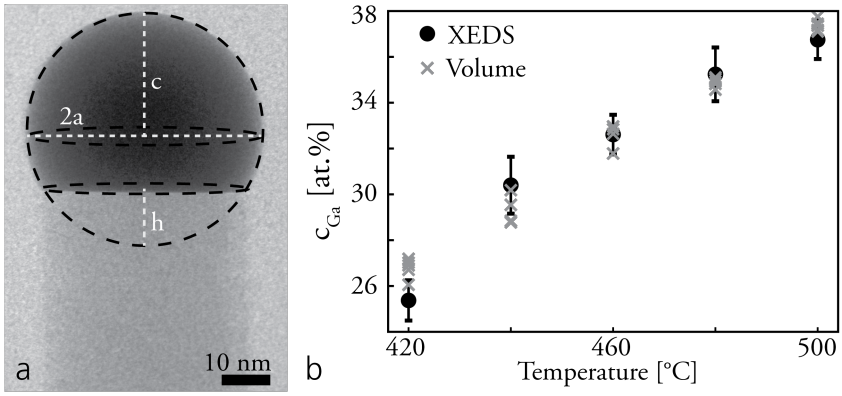

Figure 3.6: The droplet volume was estimated based on its projected volume from the TEM images taking into account the asymmetry of the droplet (a and c) as well as the missing cap of the volume (a). A plot of the gallium concentration of the droplet during GaAs nanowire growth for temperatures between 420 and 500 °C (b). The droplet composition was measured during steady-state growth using X-ray EDS (•), and the margin of error is presented as the combined error, σ, of the measurement (M) and quantification (Q) $[(\sigma_M^2+\sigma_Q^2)^{1/2}]$. Using the volume at 460 °C correlated with the X-ray EDS measurement, the change in volume was used to estimate the composition at the other temperatures. This is presented for five individual measurements of the volume (×) for each temperature.

could increase by up to 10 at.% for temperature between 400 to 500 °C, and as much as 40 at.% during studies of V/III-ratio at 420°C.

Secondly, using the droplet volume to probe its composition requires the gold content of the droplet to remain constant, otherwise we would need to know the rate of gold depletion. This is, for example, not the case for Au-assisted Si nanowires where the droplets have been reported to be incorporated into[140], or diffuse away along the sidewalls of the nanowire[141]. As part of the annealing and etching studies of papers I and II, we compared the droplet composition and shape over time. And while fluctuation at a steady-state condition is observed, we found that the shape and composition were stable for intervals smaller than 20 minutes. We have so far not observed a reduction in droplet size for steady-state growth of GaAs during hours of experiments.

Third and finally, we assume that the two-dimensional projection of the droplet onto the image plane represents a spheroidal cap on top of the nanowire. We have found that more often than not, the projection of the droplet on top of a nanowire is not spherical but instead elliptical. So long as the droplet shape is symmetric around the growth direction, the projection of the droplet would be representative for the volume of a spheroidal cap. This requires that the symmetry of the droplet-nanowire interface is more than twofold symmetric, as the droplet shape can be strongly affected by the symmetry of its interface[122]. In the case of droplet-nanowire interface for nanowires with hexagonal crossections, it has been considered to differ slightly from the hexagonal symmetry[142]. It was suggested that it can be more favorable for the droplet to smoothen its corners, making them rounder instead of adopting the sharp hexagonal shape. However, even if the droplet is not covering the full nanowire top-facet, its interface will likely have a similar symmetry as the nanowire crossection. In principle, as long as the nanowire would not have an elongated top facet projection, *e.g.* a rectangular crossection, the droplet projection would be representative of the volume.

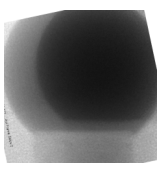

With these assumptions in mind, we measured the droplet composition of a Au-alloy assisting GaAs nanowire growth at 460 °C using X-ray EDS. The chemical quantification was then compared with the droplet-projection measurement including height ($2c - h$), width ($2a$) and the elongation (a/c) of the spheroid as shown in figure 3.6a. The projection was converted to a volume by subtracting the missing cap (V_{cap}) of the spheroid ($V_{spheroid}$).

$$V = V_{spheroid} - V_{cap} = \frac{4\pi}{3}a^2c - \frac{\pi}{3}\frac{a^2}{c^2}h^2(3c - h) \tag{3.7}$$

The gallium concentration measurements were performed at steady-state conditions for temperatures between 420 °C and 500 °C using X-ray EDS, as part of paper II. The gallium quantification at each temperature is plotted in black in figure 3.6b. Measuring the droplet projection at each of the temperatures, we calculated the volume change and converted it to the change of gallium atoms it would correspond to. As a result, we got an estimation of the gallium concentration in the droplet, which is presented as crosses in figure 3.6b. The largest estimation error for the gallium composition using the droplet projection was observed at 420 °C (1.5 at.%). This error corresponds to an actual error of less than 6% [*]. It is worth noting that this estimation error of the gallium composition is comparable to the measurement error of the EDS quantification of paper I ($\pm 0.8 - 1$ at.%).

This means that it is possible to estimate the changes in droplet composition by a rather simple measurement of the droplet projection and a reference composition. The benefit of this approach is that we are able to estimate the droplet composition while simultaneously observing the dynamic changes of the crystal growth.

A Solid Reference Point for Growth

Nucleation theory and crystal growth are centered around minimizing the energy of the system, forming the most energetically favored phase(s). While the chemical potentials of the included phases are important, their absolute values are not as important as their potential relative to each other. For crystal growth, the chemical potential of the solid is commonly used as a reference potential for the other involved phases. The solid chemical potential, also known as the cohesive energy of the solid, depends on the temperature and crystal structure. So for material systems that can form more than one crystal structure, the chemical potentials of each crystal structure can be used to predict the resulting growth. Thus, the solid acts as a reference point for the system. In contrast to the bulk formation of III-V semiconductor zincblende crystals, crystal growth of nanowires has been shown to enable formation of the otherwise metastable wurtzite phase[32,98]. For most of III-V semiconductors, the chemical potential of a wurtzite crystal is slightly higher than the zincblende counterpart (10-20 meV/atompair)[143–145]. On the other hand, the surface energies of the wurtzite crystal are usually lower than those of the zincblende crystal[7,146,147]. In other words, the atoms are less benefited by forming a solid wurtzite in comparison to zincblende. However, the surface of a wurtzite crystal is easier to stabilize than that of the zincblende counterpart.

The polymorphic behavior of nanowires can be observed when crystal growth occurs along a $\langle 1\,1\,1 \rangle$-direction, as the atoms in a zincblende $\{1\,1\,1\}$-plane are identical to the arrangement of a wurtzite

[*] (27/25.5)

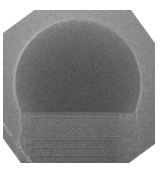

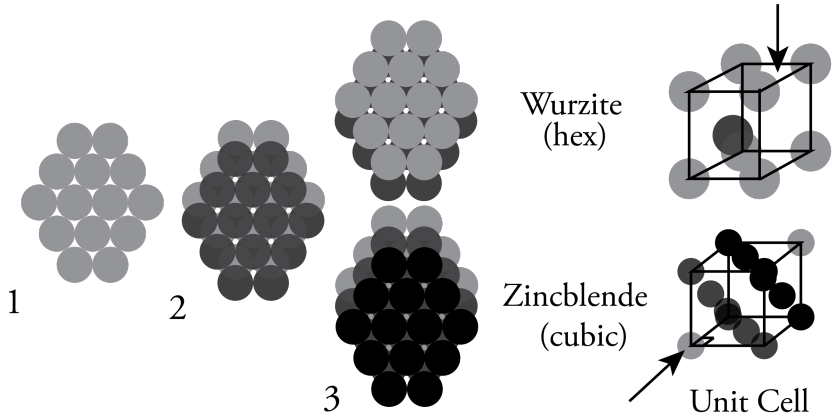

Figure 3.7: Illustration of the stacking of close-packed atomic layers, and how the two types of crystal (cubic and hexagonal) are considered identical for one (1) and two (2) stacked layers. The addition of the third (3) layer dictates which structure is formed based on whether the third layer is placed on top of the first (leaving 'holes' through the structure) or if it is placed above the openings created in (2). These cases, with two and three uniquely stacked layers are referred to as wurtzite and zincblende, respectively. The unit cells of both crystals are illustrated, along with the viewing direction (arrows) of the pattern in shown for 1,2 and 3 layers. For simplification, each circle in the illustration represent a III-V pair.

{0 0 0 1}-plane*. As the crystals share an identical atomic plane it is possible to alternate between the crystal structures by stacking the atomic planes slightly different, as illustrated in figure 3.7. The illustration in figure 3.7 introduces the stacking of one and two atomic layers, before the position of the third layer determines which crystal has been formed. If the third layer is identical to the first, this would correspond to a hexagonal wurtzite stacking (sometimes referred to ABA stacking). On the other hand, if that layer were to be a third unique layer before repeating the stacking sequence, the crystal adopts a cubic zincblende structure (ABCA stacking). The illustration also shows the different unit cells with respect to the stacking, displaying the [1 1 1]-direction of the cubic crystal as the space diagonal of the cube (arrow). This schematic visualizes the III-V pair as a single object for simplicity, in practice this is represented by a cation(III)-anion(V) pair.[148–150]. Experimentally, the resulting crystal structure has been successfully controlled by the partial pressures and ratio between group III and V precursors[30,33,98,151,152]. By increasing the V/III ratio of the metal-organic precursors, III-V semiconductor nanowires have shown the ability to switch from zincblende to wurtzite and back to zincblende again[30,33]. These transitions have been shown to be gradual such that the crystal structure is mixed at intermediate conditions[153], conditions between pure structures.

Our current understanding of nucleation of the two crystal structures is that formation of wurtzite requires a higher supersaturation of the liquid with respect to the solid ($\mu^s - \mu^l$)[123,145,154]. A higher supersaturation implies a smaller critical nucleus based an the Gibbs free energy of nucleation [equation (3.2)]. Reducing the size of the formed nucleus increases its surface area to volume ratio, which makes the surfaces of the nucleus more influential on the total change in Gibbs free energy. As the wurtzite crystal generally has lower surface energies than the zincblende counterpart,[7,123,146] the

*[xyz] indices are used for cubic structures and [$hklm$] are used for hexagonal structures.

probability of nucleating wurtzite rather than zincblende therefore increases for smaller nucleus sizes.

Recent *in-situ* studies have observed a connection between the resulting crystal structure and the size of the droplet with respect to the nanowire. In particular, the angle between the solid top facet and the droplet, the so-called wetting angle, has been suggested as a parameter which determines which crystal phase that forms[34]. In addition, the formation of zincblende at high wetting angles has been observed in conjunction with a changed growth interface between the droplet and the nanowire, a so-called truncation of the top facet[29]. The connection between droplet wetting and crystal growth has been modeled from the perspective of nucleation as the truncation changes the surface at the droplet interface[155]. These findings are indicating that the droplet wetting may be controlling the growth, a principle that will be covered in greater detail in the following chapter.

We can thus conclude that the droplet has an important role for crystal growth. Its importance ranges from controlling the reaction rates through its chemical potential and composition, to the dynamics of truncation and wetting that have been observed during crystal growth. So far, this thesis has focused on the chemical potential and composition of the droplet showing that the droplet can not only assist growth, but also etching of a III-V semiconductor nanowire. By investigating the composition of the droplet during both etching and growth, we could evaluate the steady-state conditions of the droplet at different temperatures and partial pressures of gases. For reactions that do not reach a steady state, we instead validated the approach of using the change of projected droplet volume to estimate the droplet composition. This would allow us to estimate the droplet composition during imaging of dynamic processes, instead of relying entirely on spectroscopy. This enables us to study the limits of nanowire crystal growth, as in the case where the droplet is not stationary at the top nanowire facet or dynamically changes its interface to the nanowire. The following chapter introduces the concept of droplet migration and displacement and how it can be influenced by controlling the properties of the droplet, the crystal structure and the crystal surfaces.

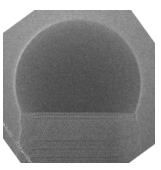

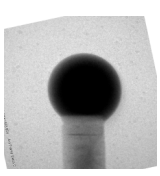

Droplet Positioning and Control on a Nanowire

Aside from assisting crystal growth, the droplet can be a determining factor for the resulting nanostructure shape. Since the idea of droplet-assisted nanowire growth is to form material in a pillar below the droplet; the principle is heavily reliant on the droplet being steady on top of the nanowire. If the droplet were to be displaced from the nanowire top facet, the assisted growth will no longer proceed from the same facet. *Ex-situ* studies of droplet-assisted nanowire growth have shown that the droplet can migrate from its position on the top of the nanowire as a result of annealing or cooling[36,39,55]. In doing so, both Kelrich *et al.*[36] and I have shown that the droplet leaves the top facet truncated in its wake (paper III).

Parallel to observations of droplet displacement, *in-situ* TEM observations of nanowire growth have shown that the droplet is dynamically wiggling to adjust during layer growth[78]. Other observations have shown that the edge of the interface between the nanowire and droplet can be truncated during crystal growth. This truncation of the interface, which can been seen in the image series in figure 4.1 (next page), has previously been observed in several material systems including II-VI[156], III-V[29,53] and group IV[57,58] materials. These observations have shown that the droplet is not stationary, but instead moves during the crystal growth.

The origin of the truncation has been addressed from a crystal growth point of view, relating the event to the energy difference between having a truncated facet or not[57]. In addition, the truncation has been observed to shrink during the growth of a crystal layer, and was suggested to be a measure of the difference in chemical potential between the liquid and the solid[58]. Furthermore, *in-situ* studies have observed the presence of a truncation, only when forming a zincblende crystal structure[29,34,155]. In this case, the droplet wetting was observed to be correlated to both the formation of a truncation and zincblende. The reports used the wetting angle of the droplet, the angle between the where the solid and liquid meets to form an interface, as a measure for the droplet wetting. If the measurement of the wetting angle is indeed a determining factor for the formation of a truncation and crystal growth, both would be influenced by the composition of the droplet and how the droplet wets the nanowire. In other words, the formation of a truncation would be dependent on the surface energies of the droplet and nanowire interfaces[157,158].

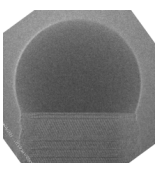

Interestingly, droplet migration and facet truncation are observed as a result of increased droplet size on top of the nanowire. Yet the connection between these two observations have not been experimentally shown until our *in-situ* studies relating truncation to droplet wetting and displacement. Drawing that connection has, as part of my studies, enabled fundamental investigations of the droplet and its dynamic behavior on top of a nanowire. Instead of relating the observations to nucleation and growth, we suggested the droplet wetting and displacement to be the cause for truncation formation.

By investigating a droplet that assists nanowire growth in real-time, we could observe the truncation of the top facet and droplet migration in sequence, as the droplet size is increased (figure 4.1a-e). The sequence shows a Au-Ga droplet on the top of the nanowire which expands with gallium to a point where a truncation is formed and eventually the droplet migrates to the side. With this type of observation, it is possible to analyze what would be happening during *ex-situ* MOCVD under conditions that swell the droplet with material. Such a growth condition would be a result of an insufficient supply of the group V precursor[28,36]. *In-situ* investigations of the conditions that result in droplet migration allow us to find and understand the ultimate limit for one-directional droplet-assisted nanowire growth. For this, it is important to know what determines the droplet wetting and what influences the droplet movement.

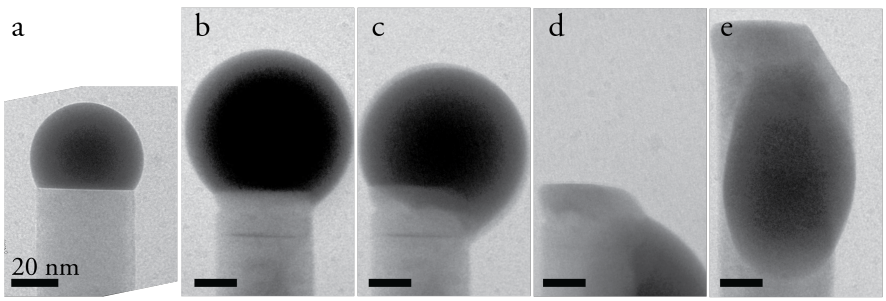

Figure 4.1: *In-situ* TEM observation of a Au-Ga droplet on top of a GaAs that increases its size starting from its regular nanowire growth volume (a). As the droplet incorporates more and more gallium, the droplet swells up and stabilizes itself by forming a truncation (b-c). Further volume increase results in the droplet migrating entirely from the top facet and onto the nanowire sidewall (d-e). The image sequence is also presented as a flip-book on the even-numbered pages from (p 2-64).

Droplet Wetting

To understand how and why a droplet moves on the top of a nanowire, we compare it to the situation when a droplet wets a planar surface. The droplet shape and surface wetting can be derived by minimization of the surface free energy. In the simplest case of a free-floating droplet, the minimum energy results in a spherical droplet shape as it minimizes the area. When in contact with a solid surface the droplet adapts and minimizes its free energy by controlling the wetted area. Figure 4.2a illustrates a droplet wetting a solid and the surface energies of each interface that separates two

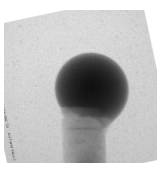

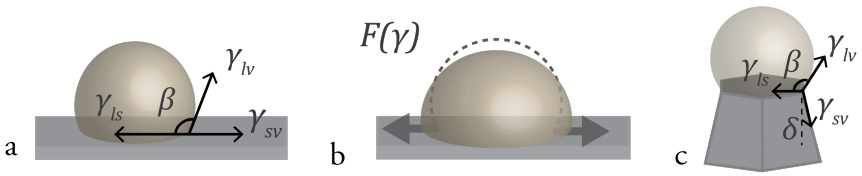

Figure 4.2: A droplet on a planar at mechanical equilibrium (according to equation 4.1), and its surface energies γ of the interfaces that separate the three phases; vapor (v), liquid (l) and solid (s). The surface energies are drawn as forces as a visual representation. The forces that pull on a droplet are oriented and related by the wetting angle β. If a force is exerted on the droplet as a result of changing any of the surface, the droplet changes its shape to obtain its new equilibrium shape (b). The wetting can be translated to a nanowire geometry by the addition of a tapering angle (δ) of the nanowire sidewall (c).

phases (γ_{sv}, γ_{ls}&γ_{lv}). The wetting property of the droplet is referred to as wetting angle* (β), which describes the angle between the solid-liquid and the liquid-vapor interface[157]. As a droplet finds its mechanical and thermodynamic equilibrium it obtains an equilibrium shape and wetting angle based on the surface energies[159,160]:

$$\gamma_{sv} = \gamma_{ls} + \gamma_{lv} \cos \beta \tag{4.1}$$

The equation is commonly known as Young's relation and is widely used to describe the droplet wetting on a surface[159,161].

The thermodynamic approach using energy minimization provides the same relationship as if you were to consider the force balance at the line where the three phases (solid, liquid and vapor) meet[157,160]. This mechanical equilibrium approach considers the surface tensions ([N/m]) rather than the surface energies ([J/m^2])[159,160,162,163]. Both approaches result in the same relation and the surface energy and surface tension has, during the last century, been used interchangeably to describe an interface[6,164–167].

If the droplet experiences a resulting surface force outwards, as if the surface energy of the liquid-solid interface suddenly decreased, the droplets strive to wet more of the surface. This results in droplet adjustments to decrease the wetting angle and thus the droplet spreads over a larger area, as illustrated in figure 4.2b. This type of wetting adjustment does not move the droplet's center of mass but instead changes the wetted area.

Wetting a Nanowire and the Origin of Truncated Facets

The principles of wetting can be transferred to a droplet residing on a pillar-shape geometry, to investigate how a droplet wets a nanowire. In contrast to the case of a planar surface, wetting a nanowire top facet confines the droplet by the edges. Introduction of edges has been shown to hinder the droplet from increasing its interface area to the solid[168]. As a result, the droplet can achieve an equilibrium shape with larger wetting angle if confined by edges than for the planar case[168,169]. However, the energy barrier related to the edges, so-called edge energies, are commonly neglected when discussing droplet wetting on a nanowire for simplicity[56,170,171].

*Commonly known as contact angle

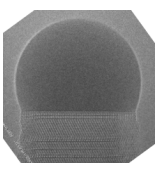

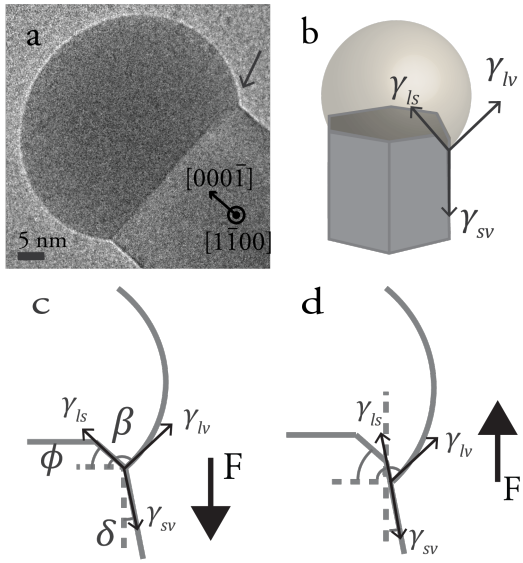

Figure 4.3: The wetting concept transferred to a droplet on a nanowire. The transmission electron micrograph shows the expanded droplet with a truncation formed (a). The illustration in (b) is meant as a three-dimensional guide to the image. The schematics of the droplet-nanowire interface are shown for a droplet that wets the top facet and the truncation (c) and partially wetting the sidewall (d). The schematics represent the cases which a droplet would dynamically shift back and forth between based on the resulting forces. The resulting force is evaluated based on the wetting (β), truncation (ϕ) and tapering (δ) angle.

The wetting concept was introduced for droplet-assisted nanowires by Nebol'sin and Shchetinin in 2003, where they evaluated the surface energies using Young's relation (equation 4.1)[170,172]. The resulting Nebolsin-Shchetinin model was used to estimate the probability of having a droplet on the top facet of a Si nanowire, as illustrated in figure 4.2c. The model gave a prediction for why some metals (*e.g.* Au, Ag, Cu) were able to assist the vertical nanowire growth while others (*e.g.* Pb, Sb) were not. By evaluating the surface energies at equilibrium, they derived a condition for the surface energy ratios which would allow a droplet on top of the nanowire.

$$\gamma_{sv}/\gamma_{lv} < \frac{\sin(\beta - 90°) + \cos(\beta - 90°)}{\cos\delta - \sin\delta} \tag{4.2}$$

where the tapering (δ) is the slope of the nanowire sidewall, and 0° tapering corresponds to a vertical nanowire sidewall. This has been used to illustrate and explain different growth modes, mostly with respect to the crystal nucleation rather than the droplet wetting and mobility[56,172,173].

However, the Nebolsin-Shchetinin model has a few potential blindspots where it can contradict the observed experimental outcomes. First, the model predicts a droplet of the self-assisted III-V nanowire growth (gallium and indium) to be unstable and therefore rejects gallium and indium as candidates to assist one-directional growth with vertical facets (based on surface energies from ref[146])[174]. This comes as a result of the surface energy ratios between liquid gallium and the solid GaAs being higher than the upper boundary set by relation 4.2. In contrast, both gallium and indium droplets have been experimentally shown to assist nanowire growth of GaAs and InAs,

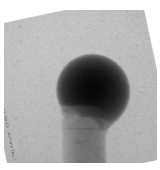

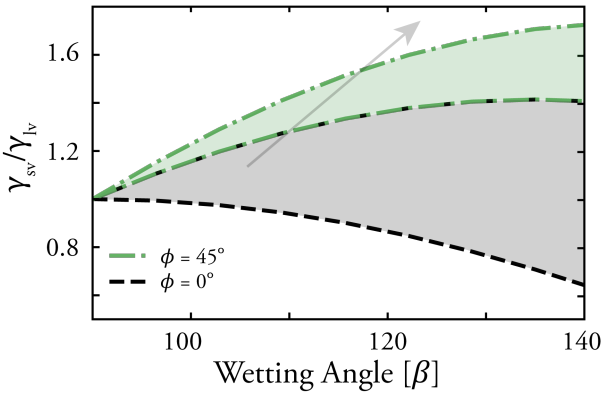

Figure 4.4: Graphic illustration of the intervals in which the droplet remains stable on an un-tapered nanowire top facet, both for the case of a flat interface (zero truncation) and 45° truncation. These are the most commonly observed case of the in-situ studies in paper IV. The faded arrow illustrates the hypothetical case for a droplet that can be lower its surface tension and increase its wetting angle, forming a truncated facet before exiting the truncated region and no longer be able to wet the top facet.

respectively[34,175–177]. This either means that the surface energies that were used for the evaluation are not true to the nature of Ga-assisted GaAs nanowire growth, or that the model is not universal.

The second potential blindspot is related to the geometry of the nanowire. *In-situ* observations have shown that the growth front can be truncated during nanowire formation[57,58,156]. The truncated corner, illustrated by figure 4.3a-b, affects the geometry for the surface energy balance which in turn would affect relation (4.2)[155]. To directly address the geometrical mismatch between experiments and model, we implemented the truncation into the surface energy balance through an angle (ϕ) in paper IV. This truncation angle represents the acute angular difference between the horizontal and the truncation plane. In other words, a flat interface would be represented by a 0° truncation, and the steeper truncation - the higher angle.

With the introduction of a truncation to the model, we considered the limits of droplet wetting on the top of a nanowire by applying Young's relation at the triple-phase line (where the arrows intersect in figure 4.3b). For a droplet to cross the edge, and become un-pinned, there has to be a resulting force downwards (figure 4.3c). By investigating which surface energies that would generate a downward force, we derived a lower limit of the surface energy ratio (γ_{sv}/γ_{lv}).

For a droplet that can partially wet the nanowire sidewall, as shown in figure 4.3d, there could still be a resulting force upward which would recover the droplet to the top facet. As a result, we could derive an upper limit for the surface energy ratio which allow the droplet to recover from a small dynamic displacement.

$$\gamma_{sv}/\gamma_{lv} < \frac{\sin\beta\cos\phi - \cos\beta\cos\delta}{\cos\delta\cos\phi - \sin\delta\cos\delta} \tag{4.3}$$

Each facet geometry (tapering and truncation), has an upper and lower surface energy ratio (γ_{sv}/γ_{lv}) for which a droplet is stable on the facet. The full derivation can be found in the supporting information of paper IV. As a note, our derived model provides the same result as equation 4.2 for no truncation and small nanowire tapering (below 15°).

The surface energy boundaries for a flat droplet-nanowire interface (gray) and an interface that has been truncated by a 45° cut (green) are shown in figure 4.4. The intervals presented provide a prediction for which interface 'geometries' that could have a droplet wetting the top facet based on the surface energy ratios. In the case of a droplet wetting both the top facet and a truncated corner, a higher surface energy ratio is allowed to avoid wetting of the sidewall. For comparison, Au-Ga droplets at growth temperatures of 400-500 °C have surface energies between 0.68 (pure Ga) and 1.2 J/m^2(Pure Au)[167,178,179]. And the GaAs nanowire sidewalls, *e.g.* {1 1 0}, have surface energies reported between 0.4 to 1.5 J/m^2 [7,146,180] depending on the environment. In the case of Ga-assisted GaAs the surface energy ratio γ_{vs}/γ_{lv} ranges from 0.6 to 2.25 based on the reported values. While a truncation of 45° is not enough to lift the surface energy ratio above 1.7, as can be seen in figure 4.4, larger truncation angles shift the interval to higher surface energy ratios which can be seen in detail in figure 2 of paper IV (page 116).

From Truncation to Displacement

Our model was experimentally tested by *in-situ* studies of Au-assisted GaAs nanowire growth by increasing the gallium content of the droplet during ETEM imaging. The nanowires studied were either nucleated inside the ETEM by supplying TMGa and AsH_3[*] to gold particles at 420°C, or by utilizing pre-grown MOCVD nanowires that are then introduced to the TEM. In the case of starting from pre-grown nanowires, the nanowires were annealed for 10 minutes in 1 Pa of AsH_3 at 420 °C to reduce the native oxide of the nanowires. The oxide otherwise encapsulates the droplet and the nanowire, as a result of transporting the nanowires in air, and makes one-directional crystal growth more difficult. From there, the nanowires were grown by continuously supplying growth precursors at 420 °C.

In paper IV we reported that increased droplet volume, or the wetting angle, by increasing the TMGa flow resulted in the formation of the truncated corner. This truncation disappeared and reoccurred at an edge of the hexagonal nanowire crossection during the nanowire growth. This can be seen from the side in the image sequence of figure 4.5a. In contrast to previous reports on the truncation being connected to each grown layer[29,58], the truncation was not necessarily appearing for each grown layer in our experiment. While not observing the truncation at repeated layers, there could still be a truncation of one of the edges in front or behind the droplet which is less apparent as for the truncated facets observed in the figure sequence 4.5b.

Increasing the droplet volume as a result of a higher TMGa flow resulted in a higher gallium concentration in the droplet (paper II). This in turn changes the surface tension of the droplet alloy, which is determined by the droplet composition. For higher concentrations of gallium, a Au-Ga droplet reduces its surface tension (γ_{lv}) due to gallium having a lower surface tension than gold. As a result of reduced surface tension, the surface energy ratio (γ_{vs}/γ_{lv}) is increased during our experiment.

Figure 4.4 shows two separate regions of wetting angles and surface energy ratios where wetting on a flat (gray) and truncated (green) growth interface is favored. Since they are separated, it should be possible to go from one wetting regime to another, *i.e.* from wetting a flat to truncated interface, by modifying the droplet-nanowire system. By increasing both wetting angle and surface energy ratio

[*] 4.4e-2 mmol/min AsH3 and 2.33e-7mmol/min TMGa

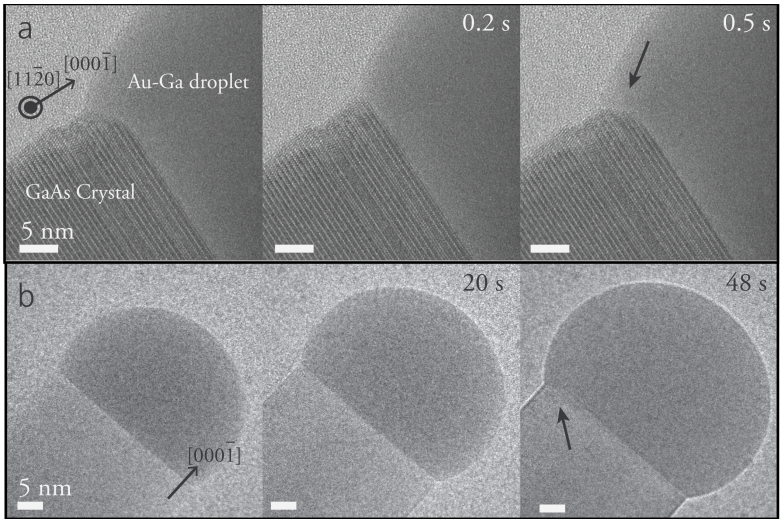

Figure 4.5: Two image sequences, showing the appearance of truncation at the interface between the droplet and the nanowire. The sequences show a truncation that appears in different angles to the viewing direction. Depending on the viewing direction the truncation will appear as a clean cut of the crystal (a), if the truncation plane is parallel to the viewing direction (arrow at 0.5 s), or as a shaded region (b) under the droplet (arrow at 48 s). The shaded region indicates that the truncation appears towards or away from the viewing direction. The truncation appears as the droplet volume and wetting angle increases (b), and is observed to disappear and reappear over the growth (a).

simultaneously, as the parameters are experimentally interdependent, we probe a line in the graph from the flat facet region into the truncated region. The combined affect of changing the droplet composition and volume allowed us to probe the wetting condition for a range of wetting angle-surface tension combinations. The model presented is in agreement with the previous observations of a truncated growth front at higher wetting angles and gallium concentrations[29]. But transition from flat to truncated growth-interface will be dependent on the surface energy of the nanowire sidewall.

In addition, we showed in paper III that expanding a Au-In droplet on top of an InAs nanowire would eventually cause the droplet to wet the sidewall. This *ex-situ* MOCVD study showed how the droplet wetting of a nanowire was influenced by reduction of the AsH_3 supply during growth, this while continuously supplying precursor for indium*. Starting from gold particles[181] on a $[\bar{1}\,\bar{1}\,\bar{1}]$-oriented InAs substrate, a wurtzite InAs nanowire stem was grown (figure 4.6a) to lift the droplet from the substrate. The stem enable studies of the droplet wetting rather than nucleation and crystal growth from a substrate. As a result, we could study the transition point where the droplet migrates and wets the nanowire sidewall, depending on the AsH_3 background.

Droplet migration to the nanowire sidewall has previously been observed for Au-assisted InP[36] and In-assisted InAs[39,55] nanowires as a result of annealing or cooling. These studies achieved droplet migration by annealing in either a low background pressure of group V precursor[36] or vacuum[39]. The resulting droplet migration was attributed to increased droplet volume and related to the previous reports on droplet un-pinning from the nanowire top edge[56]. Our approach in paper III was

* tri-methyl-indium [TMIn]

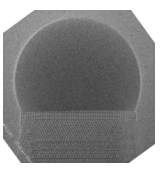

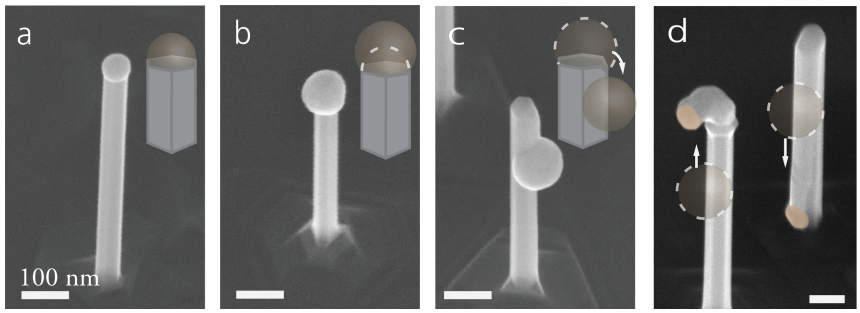

Figure 4.6: Scanning electron micrographs of Au-In assisted InAs where the droplet volume has been increased with indium, by reducing the supply of arsenic to the droplet. Starting from a droplet that represents the size during wurtzite growth (a), the droplet expands with more indium (b), and eventually migrates to the sidewall (c). At the sidewall the droplet can be moved as the droplet size is reduced, either by surface energy gradient or by the parasitic growth that can be seen behind the droplet in (d). Each sample is grown using a separate AsH_3 flow during the last five minutes prior to cooling the sample. The panels are modifications to the figures presented in paper III.

an adaptation of Madsen's work, where he observed indium droplets on the InAs nanowire sidewall as a result of cooling in an indium-rich and AsH_3-free environment[55]. Instead of modifying the cooling conditions, we modified AsH_3 supply during the last five minutes of growth, before cooling under AsH_3-free environment. This approach allowed us to study how the supply of growth species, rather than how temperature, affects the droplet wetting.

Decreasing the supply of arsenic effectively decreased the growth-rate while still supplying indium to the droplet. This resulted in an increased droplet volume as a due to accumulation of indium, shown in figure 4.6b. Increasing the droplet volume further resulted in droplet displacement and wetting of the nanowire sidewall (figure 4.6c). By analyzing the droplet and nanowire diameters using electron microscopy we were able to report that all droplets on the nanowire top-facet had a smaller spherical wetting angle than $141 \pm 3°$. This corresponds to a droplet diameter that is 1.7 times larger than the nanowire diameter.

The *ex-situ* displacement provided two observations which would help understanding the droplet wetting on a nanowire. First, closer electron microscopy analysis showed that the top facet of the nanowire had an inclined (or truncated) facet at the corner which the droplet appeared to have crossed during its displacement. This observation is in agreement with previous reports on Au-In-droplets migrating on InP nanowires, where the author suggested that the migration could be a result of truncation[36]. They suggested that the formation of a truncation would dissolve the material, that was once part of the nanowire, into the droplet and thus increase its volume enough to cause droplet migration. The suggestion was based on the observation of Gamalski *et al.*, who correlated that the missing volume related to the truncation with the supersaturation of the droplet $(\mu^s - \mu^l)$[58]. This assumes that the additional atoms dissolved in the droplet as a result of the truncated corner would be enough to cause a truncation and the following droplet displacement. However, it could, at the time, not be determined if the truncation preceded the displacement or the opposite way round. The observations of Kelrich *et al.*, and paper III in combination with our *in-situ* study (especially the image sequence of figure 4.1), indicates that the truncation was formed prior to the displacement.

Secondly, by resupplying AsH_3 to a droplet that wets the nanowire sidewall, the droplet was depleted of indium and returned to its smaller size (comparable to the droplet of in figure 4.6a). As the droplet

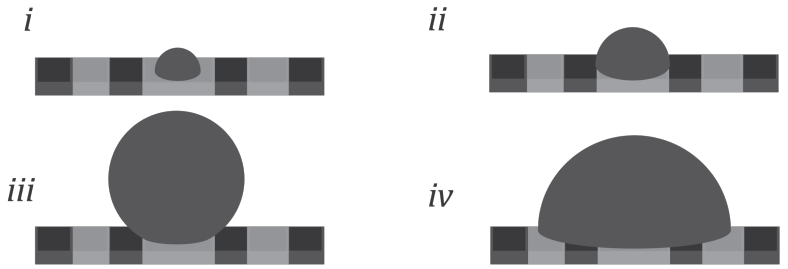

Figure 4.7: The droplet (i) increases its radius until it reaches transition to the dark hydrophobic surface (a surface that results in a larger wetting angle) where the droplet sticks (ii). When the volume increases it increases its wetting angle instead of spreading (iii) until it can wet the full dark area. The droplet then continues to increase its contact area to the surface (iv), until it reaches the next border. This is called a 'stick-and-slip'-method.

became depleted or rapidly thereafter, the droplet migrated towards one of the $[\bar{1}\,\bar{1}\,\bar{1}]$ facets. This is shown in figure 4.6d, where the droplet can be found either at the top of the nanowire or at the substrate. We can therefore state that wetting the sidewall is not favorable as the droplet size and/or its indium content decreases. In the process of indium-depletion and migration of the droplet, the excess indium was used for growth along the nanowire sidewall (figure 4.6d). If the growth initiates the migration or the migration controls the growth could not be determined from on the *ex-situ* studies. Similarly, observations of droplet migration have been reported for planar surfaces where droplet migration was shown as an effect of an energy gradient of the surface energies[182–185]. If an energy gradient exists, the droplet would experience an uneven wetting angle and migrate towards the surface that results in the lowest wetting angle.[182,183]

These two observations connect the events of truncation of droplet-nanowire interface and droplet displacement. This indicates that the connection may be result of the wetting properties of the droplet. The possible relation between truncation and wetting was introduced in paper IV and demonstrated that wetting could be the cause for the truncation.

Intentional Barriers for the Droplet

Previous studies[36] and Paper V observed that planar stacking faults within the nanowire can hinder droplet migration, or even pin the droplet at the nanowire sidewall. In the case of a planar stacking fault in a wurtzite nanowire, misplacing an atomic plane would lead to an un-intentional zincblende segment. As discussed at the end of chapter 3, misplacing an atomic layer after a BAB stacking (wurtzite) would result in a B-ABC stacking (zincblende). Changing the crystal structure also changes the surface energy, which can result in a barrier for the droplet wetting and migration. More specifically, the border separating the segments of a chemical[186–188] or topological[168,189,190] heterostructured surface have been shown to act as a barrier.

The concept can be illustrated by evaporation or condensation studies where the droplet size is intentionally changed on a chemically heterogeneous surface[186,187]. As the droplet volume increases, the droplet spreads evenly until reaching the border between the surfaces. During this phase, the droplet keeps its wetting angle constant, which can be seen as part of the illustration series of figure 4.7. Increasing the volume further instead causes the droplet wetting angle to increase and the

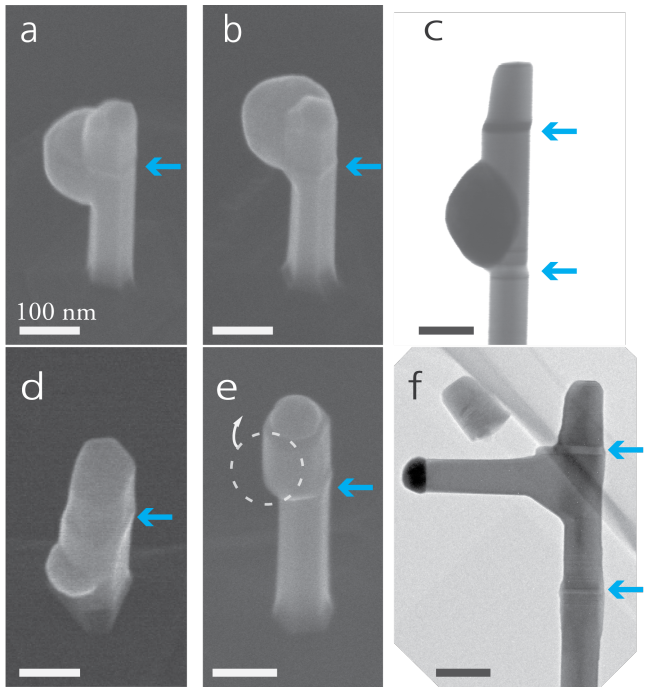

Figure 4.8: The barrier effect of a zincblende segment is here seen for droplets that are pinned below (a), above (b) or between (c) the segments. But also how the barrier hinders the movement of the droplet for the case of one barrier (d-e) and when the droplet are between tow barriers (f). The Scanning electron micrographs of a,b,d and e are viewing the structure at an 30° angle, while the Transmission electron micrographs of figure (c) (transmission-SEM) and (f) (c-TEM mode) are side views of the structure.

droplet swells up until the energy barrier of the surface border is exceeded. When this happens, the droplet quickly spreads out in order to recover a low wetting angle. This principle is well documented and referred to as the stick-and-slip method[186–188], where the droplet fixates its position at a pinning point rather than wetting the adjacent surface.

Combining the observations of droplet pinning at stacking faults with the idea of wetting a heterogeneous surface, we controlled the droplet migration on the nanowire sidewall. This control was achieved in paper V by intentionally introducing zincblende segments as barriers in our wurtzite nanowires. For these segments to act as barriers during displacement, they have to allow the droplet to fit on the nanowire sidewall above the barrier. As shown in figure 4.8a-b, the droplet either pins above or below the small segment (indicated by an arrow). If the droplet migrates past or gets pinned above the barrier was shown in paper V to be related to how close the barrier was introduced to the top of the nanowire. Introducing two zincblende segments enables the droplet to be enclosed between the barriers as a result of droplet migration, if the topmost segment is introduced close to the top of the nanowire. The droplet positioning between the barriers is shown in the transmission scanning electron micrograph of figure 4.8c.

The effect of the barrier is more prominent when returning to conditions for the vertical nanowire growth, for the case when the droplet wets the sidewall. The zincblende segment was shown in

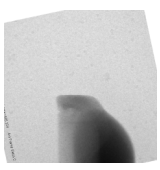

paper V to favor crystal growth directed away from the barrier. In other words, if the droplet was limited by one barrier it grew towards the 'free' $[\bar{1}\,\bar{1}\,\bar{1}]$-facet (up- or downward). This effect is shown in figure 4.8d-e, where thickening of the nanowire can be seen either above or below the zincblende segment.

If, on the other hand, the droplet was enclosed between two barriers, the droplet was not observed to migrate to an $[\bar{1}\,\bar{1}\,\bar{1}]$ facet. Instead, the droplet assisted crystal growth at the interface between wurtzite and zincblende before continuing growth in an alternative direction, vertical to the original growth direction (*i.e.* $\langle 1\,0\,\bar{1}\,0\rangle$). The resulting T-shaped nanowire is shown in the transmission electron micrograph of figure 4.8f. In contrast to previous reports of T-shaped structures and intersection of nanowires[42,43,191], this structure was grown using a single assisting droplet and the same precursor flows for growth in both directions. This crystal growth using crystal structure as barriers provides the conclusion that controlling the droplet positioning is essential for controlling nanowire growth.

Since the discussion of crystal growth, droplet wetting and migration are all concepts based on surface energy ratios, knowing the actual surface energies becomes necessary for making predictions based on these concepts. While calculations of surface energies have been made for several compounds and crystal structures, limited experimental works have addressed them with respect to their absolute values. The presented studies of this chapter, on understanding the truncation formation and droplet displacement, has been designed in order to highlight the importance of knowing the surface energies. In addition, these results have, as will be covered below, provided an experimental design to estimate the surface energy of the nanowire sidewall as a result of the droplet wetting behavior.

Surface Energies - Theory vs Experiment

This thesis has covered the basic concepts of crystal growth and etching, as well as how the droplet-nanowire interface can be truncated and assist droplet displacement. The common denominator for these four topics is surface energy. The surface energy is a parameter which, as briefly discussed with respect to crystal growth in chapter 3, describes the interaction energy between the atoms at an interface. In the case of a liquid, the surface energy can refer to the cohesive forces of its components and is commonly measured as surface tension. The surface tension depends on the composition and temperature of the droplet[167,179]. To a first approximation, the surface tension of a droplet can be estimated by linear interpolation between the pure species in the droplet. If the droplet contains equal quantities of gold and indium, the droplet surface tension could be approximated as the average of the surface tensions of gold and indium.

Experimental measurements and calculations of the surface tensions have been reported for micro-droplets of selected material systems of interest, *e.g.* the Au-In system has been studied at 550 °C[179]. The report by Novakovic *et al.* showed that a higher concentration of indium is predicted at the surface as a result of having lower surface tension as a pure element, in comparison to gold[179]. By interpreting their experimental surface tension as a function of indium concentration, we can evaluate the accuracy of the above suggested approximation by linear interpolation. In the case of Au-In droplets, we note that this approximation would be an overestimation of the droplet sur-

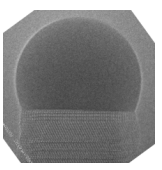

Table 1: Surface energies for GaAs facets that are common sidewalls for nanowires grown in $\langle\bar{1}\bar{1}\bar{1}\rangle$-direction. All energies are given in J/m^2.

Method	Surface	$\{1\bar{1}0\}$	$\{11\bar{2}\}$	$\{11\bar{2}0\}$	$\{1\bar{1}00\}$	
Broken Bonds	un-reconstructed	1.54	1.79	1.54	1.3	Ref[146]
Free Energy	reconstructed	0.82	1.07	0.73	0.69	Ref[196]
Free Energy	H2-passivated	0.43	0.37	0.53	0.4	Ref[195]

face tension (less than 15%). On the other hand, there are no reports on surface tension of Au-Ga droplets, one of the most common model systems for droplet-assisted III-V semiconductor growth. For that reason we have assumed that the approximation of interpolation holds for Au-Ga as well. This approach is commonly used for estimating the surface tension of a droplet in nanowire growth modeling[30,123,154,192,193].

Compared to the surface tension, the solid-vapor surface energies have been calculated for many of the III-V semiconductors, *e.g.* GaAs, InAs, GaSb[6,146,194]. These calculations of surface energies have been made using either the broken bonds of the surface[146], or by calculating the total free energy of the both bulk and surface material using iterative calculations[*] [6,7,180]. In the case of GaAs and InAs, the surface energies for low index facets[†] of both zincblende and wurtzite structures have been calculated for several types of surface reconstructions, passivations and environments[6,146,180,195]. For a GaAs $\{1\bar{1}0\}$ sidewall, the predicted surface energy varies with more than a factor 3 (from 0.43[195] to 1.54 J/m^2 [146]) depending on arsenic environment, reconstructions of the surface atoms or H_2 passivation. Similarly, reports on the wurtzite counterpart during growth ($\{11\bar{2}0\}$) have calculated values between 0.4 and 1.35 J/m^2 [146,195]. Table 1 shows a few reported values for the atomic planes that could be associated with $\langle\bar{1}\bar{1}\bar{1}\rangle$-oriented GaAs nanowire sidewalls. A more extensive table containing a collection of reported calculations for different materials, crystal orientations, reconstructions and passivation is provided as an external link at the bottom of the page[‡].

As a reference to the variations, the full graph of surface energy ratios and wetting angles for a droplet on top of a nanowire (figure 4.4) was ranging from 0.5 to 1.7. Multiply any given value within that range by 3 and the ratio is outside the range for having a droplet wetting the top facet of a nanowire. When compared to the variations presented in table 1, we note that the surrounding environment and/or the reconstruction at the surface are important for any modeling that requires the surface energies. Apart from influencing the droplet wetting, the surface energies also affect the nucleation, as presented in chapter 3. Yet the surface energies are common fitting parameters for the theoretical models instead of arguing for which environment or which reconstruction the surface has adopted[30,121,192,197]. This opens for the question, how are the atoms arranged at the surface during growth? Despite the fact that there are no direct answers in this thesis for that question, the surface energies of the droplet-nanowire system here have been investigated from the wetting perspective using a few assumptions regarding the droplet (papers III and IV).

First, we assume that the droplet surface tension can be estimated by interpolation of the pure species. Second, the droplet volume can be used to estimate its composition. And third, the edge

[*] Density Functional Theory

[†] $\{1\bar{1}0\}/\{11\bar{2}0\}$,$\{11\bar{2}\}/\{10\bar{1}0\}$, and $\{111\}/\{0001\}$

[‡] https://bit.ly/32kst9E

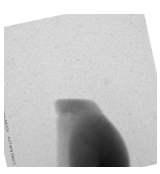

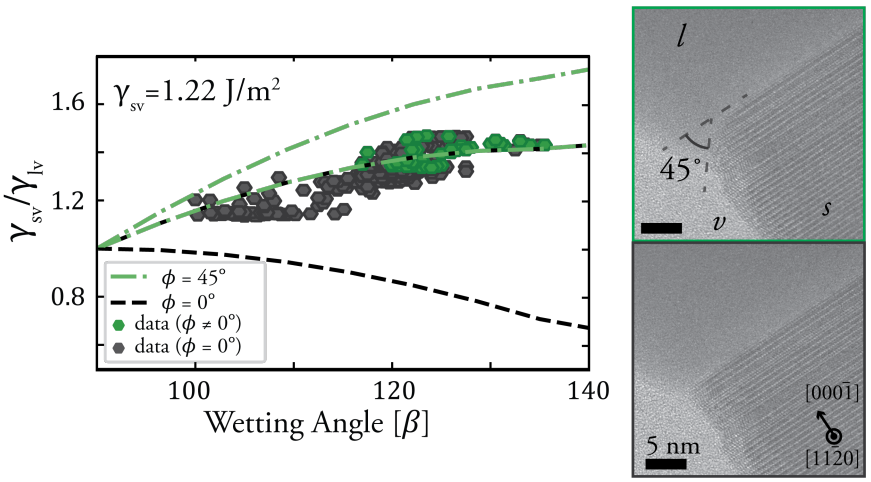

Figure 4.9: Modeled intervals of a stable droplet on the top facet of a non-tapered nanowire for both 0 and 45° truncation. The experimentally estimated surface energy ratios are then superimposed and colored based on interface shape, either flat interface (gray) or truncated interface (green). Here, the solid-vapor surface energy is fixed to 1.22 J/m^2 to optimize the observed interface shape with the model behavior. The model and data are presented and discussed further in paper IV.

energy of the nanowire top facet can be neglected, which is justified by the fact that the truncation is formed. If a truncation is formed, *i.e.* the corner dissolves, the edge energy is not likely the limiting factor for the droplet wetting the sidewall.

While there are several reports on surface energy calculations of III-V semiconductors, especially for arsenides, the experimental reports on the subject are limited. This is even more so when considering the surface energies during conditions for crystal growth, *e.g.* 400-600°C with H_2, AsH_3 and TMGa present in the vapor. The droplet wetting on the top of the nanowire was used in papers III and IV as a way of estimating the surface energies.

In our case, *in-situ* studies of nanowire growth in a TEM have enabled measurements of droplet composition and wetting angle (paper IV). These measurements were conducted using imaging of the droplet projection and reference X-ray EDS analysis, as described in chapter 3. This enabled us to estimate the surface energy of the nanowire sidewall, by combining direct observations of a droplet during nanowire growth with the surface modeling presented in figure 4.4 (paper IV). Using measurements of the droplet volume and converting it to composition provides and an estimation of the surface tension of the Au-Ga droplet on the top of a GaAs nanowire. By correlating the surface tension, wetting angle and interface shape (truncation angle) the method provided a way of fitting the surface energy of the sidewall based on the intervals of truncation. When visualizing the data, the surface energy of the sidewall was used as a fitting parameter to match data with its interface geometry (truncated or not). The result is presented in figure 4.6 using a sidewall surface energy of 1.22 J/m^2, where the data from instances of truncated and flat facets are displayed in green and gray, respectively. From the result that both truncation and flat interfaces are present for the same conditions, we suggest that the truncation formation is a result of the droplet wetting. This is in contrast to the earlier reports and observations of truncated growth fronts, where the truncation

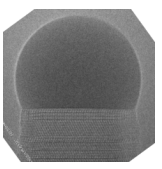

formation was suggested to result from low supersaturation in the droplet which would trigger dissolution of the corner[58].

Based on the fitting, the surface energy of the $\{1\,0\,\bar{1}\,0\}$ sidewall facet was estimated as 1.22 ± 0.1 J/m^2. The surface energy was attributed to the wurtzite $\{1\,0\,\bar{1}\,0\}$ facet, as this was the original facet of the nanowire. When taking into account that the surface tension can be slightly overestimated, it would result in a slightly lower 'true value' of the surface energy from the experiment.

Nevertheless, the surface energy estimation suggests that the surface of the sidewall is close to unreconstructed (1.30 J/m^2)[146]. A similar conclusion was found when investigating the volume of Au-In droplets after growth of the displaced droplets (paper III). Based on the surface tension and assuming that no truncation and tapering occurs, the experimental data was shown to agree well with theory if the solid surface was unreconstructed. The droplet analysis for this *ex-situ* study was made at room temperature after the droplet has been solidified during cooling in H_2.

Papers III and IV, and the reported estimations of the surface energies within, highlight the gap between theory and experiment, even though the concepts are frequently used. While it is possible to predict growth based on surface energy fittings, finding the surface energies for the system would benefit the understanding of crystal growth. Ideally, to reach a global description for growth, independent on being droplet-assisted or deposited directly from the vapor. The presented reports on surface energies can be used to provide support for argumentation when choosing the surface energy for the next calculation.

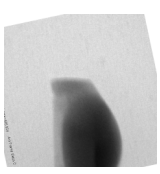

Outlook

The focus of this thesis has been to enable and study droplet-assisted nanowire growth inside an ETEM. By facilitating the nanowire growth, the observation is compared with basic scientific modeling to understand the significance of having a droplet to assist growth. One of the main points that separates this thesis from other nanowire growth studies is that it does not focus on the grown nanowire itself. Instead, it focuses on the droplet. I have in this thesis shown how the droplet wets the top facet of a nanowire and how to displace it from its original position. But perhaps more important, this was shown to happen by a truncation of the growth front, an observation which was previously connected to crystal growth and supersaturation. Instead of being connected to the crystal growth, the occurrence of a growth front truncation could be explained based on droplet wetting, an effect of that fact that we have more material in the droplet, larger wetting angle and lower surface tension.

One of the more basic findings of the thesis is the measured **droplet compositions** during growth of Au-assisted GaAs nanowires at temperatures between 400 and 500 °C. We showed that the thermodynamic phase diagram of the Au-Ga system is a good estimation of the droplet composition during MOCVD, especially if a small fraction of arsenic is included for calculation of the phase diagram. Instead of using the results from *ex-situ* measurements which represents the stable phase at room temperature, the data presented here can be used as a translation for growth of Au-assisted GaAs nanowires. Using a better estimation of the composition would increase the accuracy of the theoretical predictions for crystal growth. This as the droplet chemical potential is dependent on the composition, which in turn affects the change in free energy as a result of crystal growth.

My studies are based in the maze of **surface energies** as droplet wetting and migration is controlled by surface energy gradients and abrupt changes of the energies due to sharp crystal interfaces. This thesis aims to address the surfaces present during nanowire growth in order to further understand the requirements for the droplet to assist growth. Surface energies are key parameters in determining the nucleation and crystal growth. Unfortunately, the complex environment during MOCVD makes it difficult to assess the surfaces of a growing nanowire. And the fact that nanowires form an otherwise metastable phase (wurtzite) means that we know very little about how its surface atoms behave in environments containing for example AsH_3 or TMGa. From the observations of the droplet movement and wetting during growth in comparison to theoretical calculations of surface energies, we suggested that the surface of the nanowire sidewall is close to unreconstructed during growth. While this is based on fitting experimental data to a model, rather than a more direct observation, it is a step towards understanding the surface conditions during growth. For a more direct observation

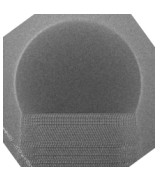

of the surface energy, we could study the growth or decomposition rate of a surface that is limited by nucleation to use the rate presented by Frenkel in 1939[108].

Addressing the Surface Energies

I think that if we want to fully understand why gold is an ideal metal to assist nanowire growth, or understand the subtle differences between the formation of different crystal structures of polymorphic materials, we have to know the real environment at which we perform crystal growth. How are the surfaces of the droplet and nanowire constructed? Do these surfaces affect the material supply? Which surfaces are formed as a result of the droplet assisted growth? And which surfaces are formed as a result of vapor deposition?

Notably, the main scientific finding of this thesis is the **droplet dynamics and displacement** from the top of the nanowire by a **truncation** of the growth front. This does not only include the displacement of the droplet, but also the ability to favor re-positioning at the nanowire top facet. To understand the droplet behavior during its migration on a nanowire, it would therefore be of interest to investigate the surface energy gradient that affects the process. How large would the barriers need to be to hinder migration? And how would a droplet move on a nanowire that is patterned with alternating segments of different crystal structure, not just a mixed crystal structure? If it would be possible to evaporate a droplet while still positioned at a patterned nanowire sidewall, it could provide access to experimentally investigating relative surface energies of the crystal sidewalls at the 'growth' conditions.

Alternatively, by addressing the vapor-solid growth or decomposition, not using a droplet, the surface energies could be extracted from the temperature-dependent reaction rate. If the growth rate is limited by the nucleation, the reaction rate has been suggested to be proportional to $e^{-\Delta G/k_B T}$ [equation (3.3)]. As the growth rate would be related to the binding energy of the atoms, it would be possible to extract the surface energy from such an experiment as long as we can estimate the chemical potentials of the system. A similar approach was utilized to estimate the surface energy of a CuO surface during vapor-solid etching of the surface of interest[198].

The truncation formation and droplet displacement have been addressed from the perspective of surface energies. However, the surface energy modeling presented as part of this thesis includes a few assumptions which could limit the conclusions. First, the assumption that the liquid tension of a Au-Ga droplet is linearly dependent on the composition, is most likely an overestimation. In the case of a 15% overestimation, the resulting vapor-solid surface energy would be equally overestimated. The equal overestimation is a consequence of using the surface energy ratio for the fitting our data to the geometry based interval presented in figure 4.9. Since the surface tension partly governs the droplet wetting it would be beneficial to know how its tension is dependent on temperature and composition. In the case of this thesis, the surface tension is used to fit the surface energy of the nanowire sidewall. Providing a more accurate estimation of the surface tension of the pure species at growth temperatures and relevant precursor pressures, would in turn be more representative of the real droplet. This type of study would improve the investigation of the surface energies of the solid, which is a crucial part of the nucleation theory when considering nucleation at the edge of the top facet of the nanowire.

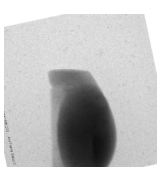

The second assumption made for the surface energy discussion is the fact that we are neglecting the droplet pinning point at the edge of the top facet. This effect could in principle result in an additional term to the calculation. However, it would be interesting to experimentally assess the droplet pinning for the purpose of understanding its influence on the droplet wetting. It could, for instance, be addressed by using a droplet alloy that we know the surface tension of, either pure gallium or Au-In, and change the droplet volume or composition in order to make the droplet unpin. If this could be realized without changing the nanowire diameter or without forming a truncation, it would give insight to the influence of the edges of the nanowire top facet on the droplet. In turn, it would provide insight into the droplet dynamics at the nanowire tip and possibly improve the presented method in chapter 4.

Droplet Controlled Crystal Growth

The ability to control the droplet and its positioning by tailoring the nanowire sidewall before displacement opens up the possibility for design of more complicated structures. The dynamics of the droplet on top of a nanowire are, to me, interesting just for the fact that there is a possibility to control where the droplet should be. When the droplet has been 'placed' on the desired spot, growth can be initiated. This would utilize the two concepts of growth and droplet dynamic separately, creating flexibility of the growth and nanostructure design.

The conclusion that the droplet wetting results in a truncation is similar to finding a piece of the puzzle that you did not think you needed. Instead of being discussed in relation to the crystal growth, the truncation observed shown to occur in a growth regime for both wurtzite and zincblende. This leads to the possibility that the correlation between the truncation/wetting angle and crystal structure control could be a coincidence and not a causation. Since the crystal structure formation has been experimentally investigated by varying the external precursor flows, the vapor and droplet are significantly different during growth. Such changes may effectively change more than the droplet size and shape, *e.g.* the supply of growth species. It would therefore be interesting to study the crystal growth in a 'mixed' regime where growth of both crystal structures, zincblende and wurtzite, are probable. With the intention of keeping the precursor supply and temperature as constant as we experimentally can, we would be able to study the subtle, but perhaps fundamental, differences between the formation of the crystal structures.

Finally, we seem to have entered a new era of material science, where *in-situ* experiments enable imaging and investigations of chemical reactions with high spatial and temporal resolution. Imaging during crystal growth provides the possibility to confirm or reject the current theories of nanowire growth and nucleation, which have been developed from *ex-situ* studies. The technique of *in-situ* microscopy also provides the ability to uncover new phenomena and dynamics of crystal growth, as was the case for the truncation in 2010 or the resulting displacement. While there are practical challenges with these *in-situ* experiments, such studies can provide insight which would help us create the artificial environment needed to control the crystal growth at the nanoscale.

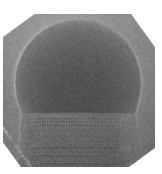

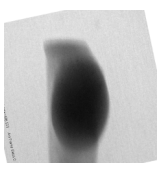

References

[1] L. Royer, *Bull. Soc. Fr. Minéral. Cristallogr.* **1928**, 51.

[2] U. W. Pohl, *Epitaxy of Semiconductors: Introduction to Physical Principles* (Springer-Verlag, 2013).

[3] G. Wulff, *Z. Kristallogr.* **1901**, 34, 449.

[4] W. Burton, N. Cabrera, F. C. Frank, *Philos. Trans. R. Soc. London. Ser. A, Math. Phys. Sci.* **1951**, 243, 299.

[5] J. S. Lee, S. Choi, M. Pendharkar, D. J. Pennachio, B. Markman, M. Seas, S. Koelling, M. A. Verheijen, L. Casparis, K. D. Petersson, I. Petkovic, V. Schaller, M. J. W. Rodwell, C. M. Marcus, P. Krogstrup, L. P. Kouwenhoven, E. P. A. M. Bakkers, *Phys. Rev. Mater.* **2019**, 084606, 1.

[6] N. Moll, A. Kley, E. Pehlke, M. Scheffler, *Phys. Rev. B* **1996**, 54, 8844.

[7] R. Leitsmann, F. Bechstedt, *J. Appl. Phys.* **2007**, 102, 1.

[8] N. Shin, M. A. Filler, *Nano Lett.* **2012**, 12, 2865.

[9] F. Oehler, P. Gentile, T. Baron, P. Ferret, *Nanotechnology* **2009**, 20, 475307.

[10] A. D. Gamalski, J. Tersoff, S. Kodambaka, D. N. Zakharov, F. M. Ross, E. A. Stach, *Nano Lett.* **2015**, 15, 8211.

[11] R. S. Wagner W. C. Ellis, *Appl. Phys. Lett.* **1964**, 4, 89.

[12] E. I. Givargizov, *J. Cryst. Growth* **1975**, 31, 20.

[13] E. Givargizov, *Krist. und Tech.* **1975**, 10, 473.

[14] M. Yazawa, M. Koguchi, A. Muto, M. Ozawa, K. Hiruma, *Appl. Phys. Lett.* **1992**, 61, 2051.

[15] M. Yamaguchi, T. Takamoto, K. Araki, N. Ekins-Daukes, *Sol. Energy* **2005**, 79, 78.

[16] M. Yao, N. Huang, S. Cong, C. Y. Chi, M. A. Seyedi, Y. T. Lin, Y. Cao, M. L. Povinelli, P. D. Dapkus, C. Zhou, *Nano Lett.* **2014**, 14, 3293.

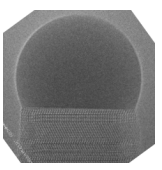

[17] A. W. Dey, C. Thelander, E. Lind, K. A. Dick, B. M. Borg, M. Borgström, P. Nilsson, L. E. Wernersson, *IEEE Electron Device Lett.* **2012**, 33, 791.

[18] Y. Cui, Q. Wei, H. Park, C. M. Lieber, *Science* **2001**, 293, 1289.

[19] R. S. Wagner, W. C. Ellis, K. A. Jackson, S. M. Arnold, *J. Appl. Phys.* **1964**, 35, 2993.

[20] K. Hiruma, M. Yazawa, T. Katsuyama, K. Ogawa, K. Haraguchi, M. Koguchi, H. Kakibayashi, *J. Appl. Phys.* **1995**, 77, 447.

[21] M. T. Björk, B. J. Ohlsson, T. Sass, A. I. Persson, C. Thelander, M. H. Magnusson, K. Deppert, L. R. Wallenberg, L. Samuelson, *Appl. Phys. Lett.* **2002**, 80, 1058.

[22] J. Creighton, *Surf Sci.* **1990**, 234, 287.

[23] J. Butler, N. Bottka, R. Sillmon, D. Gaskill, *J. Cryst. Growth* **1986**, 11, 163.

[24] D. Gaskill, V. Kolubayev, N. Bottka, R. Sillmon, J. Butler, *J. Cryst. Growth* **1988**, 93, 127.

[25] C. A. Larsen, N. I. Buchan, , G. B. Stringfellow, *Appl. Phys. Lett.* **1988**, 52, 480.

[26] P. W. Lee, T. R. Omstead, D. R. McKenna, K. F. Jensen, *J. Cryst. Growth* **1988**, 93, 134.

[27] N. I. Buchan, C. A. Larsen, , G. B. Stringfellow, *J. Cryst. Growth* **1988**, 92, 591.

[28] S. Lehmann, D. Jacobsson, , K. a. Dick, *Nanotechnology* **2015**, 26, 301001.

[29] D. Jacobsson, F. Panciera, J. Tersoff, M. C. Reuter, S. Lehmann, S. Hofmann, K. A. Dick, F. M. Ross, *Nature* **2016**, 531, 317.

[30] S. Assali, L. Gagliano, D. S. Oliveira, M. A. Verheijen, S. R. Plissard, L. F. Feiner, E. P. A. M. Bakkers, *Nano Lett.* **2015**, 15, 8062.

[31] D. Jacobsson, S. Lehmann, , K. A. Dick, *Phys. Status Solidi - Rapid Res. Lett.* **2013**, 7, 855.

[32] K. Takahashi T. Morizumi, *Jpn. J. Appl. Phys.* **1966**, 5, 657.

[33] S. Lehmann, J. Wallentin, D. Jacobsson, K. Deppert, K. A. Dick, *Nano Lett.* **2013**, 13, 4099.

[34] F. Panciera, Z. Baraissov, G. Patriarche, V. G. Dubrovskii, F. Glas, L. Travers, U. Mirsaidov, J.-C. Harmand, *Nano Lett.* **2020**, Just Accep.

[35] K. A. Dick, K. Deppert, M. W. Larsson, T. Mårtensson, W. Seifert, L. R. Wallenberg, L. Samuelson, *Nat. Mater.* **2004**, 3, 380.

[36] A. Kelrich, O. Sorias, Y. Calahorra, Y. Kauffmann, R. Gladstone, S. Cohen, M. Orenstein, D. Ritter, *Nano Lett.* **2016**, 16, 2837.

[37] R. S. Wagner, C. J. Ooherty, *J. Electrochem. Soc.* **1968**, 115, 93.

[38] P. Krogstrup, J. Yamasaki, C. B. Sørensen, E. Johnson, J. B. Wagner, R. Pennington, M. Aagesen, N. Tanaka, J. Nygård, *Nano Lett.* **2009**, 9, 3689.

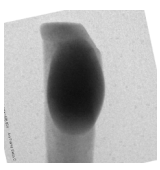

[39] H. Potts, N. P. Morgan, G. Tütüncüoglu, M. Friedl, A. F. i. Morral, *Nanotechnology* **2017**, 28, 054001.

[40] J. Wang, S. Plissard, M. Hocevar, T. T. T. Vu, T. Zehender, G. G. W. Immink, M. A. Verheijen, J. Haverkort, E. P. A. M. Bakkers, *Appl. Phys. Lett.* **2012**, 100, 053107.

[41] B. Tian, P. Xie, T. J. Kempa, D. C. Bell, C. M. Lieber, *Nat. Nanotechnol.* **2009**, 4, 824.

[42] F. Krizek, T. Kanne, D. Razmadze, E. Johnson, J. Nygård, C. M. Marcus, P. Krogstrup, *Nano Lett.* **2017**, 17, 6090.

[43] D. Dalacu, A. Kam, D. G. Austing, P. J. Poole, *Nano Lett.* **2013**, 13, 2676.

[44] J. C. Harmand, G. Patriarche, N. Péré-Laperne, M.-N. Mérat-Combes, L. Travers, F. Glas, *Appl. Phys. Lett.* **2005**, 87, 203101.

[45] R. I. Walton, F. Millange, D. O. Hare, A. T. Davies, G. Sankar, C. R. A. Catlow, *J. Phys. Chem. B* **2001**, 105, 83.

[46] P. Nørby, S. Johnsen, , B. B. Iversen, *ACS Nano* **2014**, 8, 4295.

[47] D. Sharp, Jeff W; Eres, *J. Cryst. Growth* **2016**, 125, 553.

[48] T. Vystavel, M. Kolíbal, L. Novák, J. Mach, P. Wandrol, T. Šikola, *Microsc. Microanal.* **2012**, 18, 1082.

[49] F. M. Ross, J. Tersoff, M. C. Reuter, *Phys. Rev. Lett.* **2005**, 95, 1.

[50] C. Hetherington, R. Wallenberg, D. Jacobsson, K. Dick, *Semiconductor Science and Technology* **2020**, 35.

[51] C. B. Maliakkal, E. K. Mårtensson, M. Tornberg, D. Jacobsson, A. R. Persson, J. Johansson, R. Wallenberg, K. A. Dick, *ACS Nano* **2020**, JustAccepted.

[52] C. Chatillon, F. Hodaj, , A. Pisch, *J. Cryst. Growth* **2009**, 311, 3598.

[53] K. Hillerich, K. A. Dick, C. Y. Wen, M. C. Reuter, S. Kodambaka, F. M. Ross, *Nano Lett.* **2013**, 13, 903.

[54] K. W. Schwarz J. Tersoff, *Phys. Rev. Lett.* **2009**, 102, 1.

[55] M. H. Madsen, *Indium Arsenide Nanowires*, Ph.D. thesis, University of Copenhagen, Denmark, **2012**.

[56] S. M. Roper, A. M. Anderson, S. H. Davis, P. W. Voorhees, S. M. Roper, A. M. Anderson, S. H. Davis, P. W. Voorhees, *J. Appl. Phys.* **2010**, 107, 114320.

[57] C. Y. Wen, J. Tersoff, K. Hillerich, M. C. Reuter, J. H. Park, S. Kodambaka, E. A. Stach, F. M. Ross, *Phys. Rev. Lett.* **2011**, 107, 1.

[58] A. D. Gamalski, C. Ducati, , S. Hofmann, *J. Phys. Chem. C* **2011**, 115, 4413.

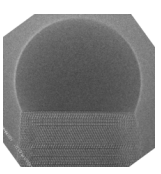

[59] L. Liggieri, A. Passerone, *High Temp. Technol.* **1989**, May, 82.

[60] C. T. Foxon, J. A. Harvey, , B. A. Joyce, *J. Phys. Chem. Solids* **1973**, 34, 1693.

[61] B. Goldstein, D. J. Szostak, V. S. Ban, *Surf. Sci.* **1976**, 57, 733.

[62] M. Heurlin, N. Anttu, C. Camus, L. Samuelson, M. T. Borgström, *Nano Lett.* **2015**, 15, 3597.

[63] J.-I. Chikawa, *J. Cryst. Growth* , **1974**, 24/25, 61.

[64] T. Kobayashi, Tatsumasa; Imura, *Jpn. J. Appl. Phys.* **1984**, 23, 632.

[65] L. Aucott, H. Dong, W. Mirihanage, R. Atwood, A. Kidess, S. Gao, S. Wen, J. Marsden, S. Feng, M. Tong, T. Connolley, M. Drakopoulos, C. R. Kleijn, I. M. Richardson, D. J. Browne, R. H. Mathiesen, H. V. Atkinson, *Nat. Commun.* **2018**, 9, 1.

[66] B. Jenichen, W. Braun, V. M. Kaganer, A. G. Shtukenberg, L. Däweritz, G. Schulz, K. H. Ploog, A. Erko, A. Erko, *Rev. Sci. Instrum.* **2003**, 74, 1267.

[67] A. Senyshyn, M. J. Mühlbauer, K. Nikolowski, T. Pirling, H. Ehrenberg, *J. Power Sources* **2012**, 203, 126.

[68] H. Hashimoto, T. Naiki, T. Eto, K. Fujuwara, *Jpn. J. Appl. Phys.* **1968**, 7, 946.

[69] E. J. Gallegos, *Rev. Sci. Instrum.* **1964**, 35, 1123.

[70] M. Hammar, F. K. LeGoues, J. Tersoff, M. C. Reuter, R. M. Tromp, *Surf. Sci.* **1996**, 349, 129.

[71] E. Sutter, P. Sutter, *Nano Lett.* **2008**, 8, 411.

[72] S. Chikawa, Jun-ichi; Shirai, *J. Cryst. Growth* **1977**, 39, 328.

[73] J. Riikonen, T. Tuomi, A. Lankinen, J. Sormunen, A. Säynätjoki, L. Knuuttila, H. Lipsanen, P. J. McNally, L. O'Reilly, A. Danilewsky, H. Sipilä, S. Vaijärvi, D. Lumb, A. Owens, *J. Mater. Sci. Mater. Electron.* **2005**, 16, 449.

[74] H. Chung, M. Dudley, D. J. Larson, D. T. J. Hurle, D. F. Bliss, V. Prasad, **1998**, 187, 9.

[75] M. O'Keefe, C. Hetherington, Y. Wang, E. Nelson, J. Turner, C. Kisielowski, J.-O. Malm, R. Mueller, J. Ringnalda, M. Pan, A. Thust, *Ultramicroscopy* **2001**, 89, 215 .

[76] J. Orloff, *Ultramicroscopy* **1989**, 28, 88 .

[77] M. Haider, H. Rose, S. Uhlemann, E. Schwan, B. Kabius, K. Urban, *Ultramicroscopy* **1998**, 75, 53.

[78] J. C. Harmand, G. Patriarche, F. Glas, F. Panciera, I. Florea, J. L. Maurice, L. Travers, Y. Ollivier, *Phys. Rev. Lett.* **2018**, 121, 166101.

[79] D. B. Williams C. B. Carter, *Transm. Electron Microsc.* (Springer-Verlag, 2009).

[80] L. Marton, *Bull. Acad. r. Belg. Cl. Sci.* **1935**, 21, 553.

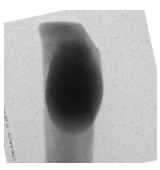

[81] T. Hansen J. Wagner, *Controlled Atmosphere Transmission Electron Microscopy: Principles and Practice* (Springer, London, 2016).

[82] I. M. Abrams J. W. McBain, *J. Appl. Phys.* **1944**, 15.

[83] H. Fujita, T. Tabata, Y. Abe, H. Arakawa, K. Hayashi, K. Yoshino, Y. Inuishi, F. Wu, N. Yao, *Jpn. J. Appl. Phys.* **1976**, 15, 2221.

[84] N. D. Jonge, D. B. Peckys, G. J. Kremers, D. W. Piston, *PNAS* **2009**, 106, 2159.

[85] M. J. Williamson, R. M. Tromp, P. M. Vereecken, R. Hull, F. M. Ross, *Nature* **2003**, 2, 532.

[86] J. F. Creemer, S. Helveg, G. H. Hoveling, S. Ullmann, A. M. Molenbroek, P. M. Sarro, H. W. Zandbergen, *Ultramicroscopy* **2008**, 108, 993.

[87] H. Heide, *J. Cell Biol.* **1962**, 13, 147.

[88] R. Straubinger, A. Beyer, T. Ochs, W. Stolz, K. Volz, *Microsc. Microanal.* **2017**, 23, 751.

[89] E. D. Boyes, P. L. Gai, *Ultramicroscopy* **1997**, 67, 219.

[90] G. Cliff, G. Lorimer, *J. Microsc.* **1975**, 103, 203.

[91] J. E. Wood, D. B. Williams, , J. I. Goldstein, *J. Microsc.* **1984**, 133, 255.

[92] T. Kamino, K. Sasaki, H. Saka, *Microsc. Microanal.* **1997**, 3, 393.

[93] J. T. V. Omme, M. Zakhozheva, R. G. Spruit, M. Sholkina, , H. H. Pérez, *Ultramicroscopy* **2018**, 192, 14.

[94] S. K. Eswaramoorthy, J. M. Howe, G. Muralidharan, *Science* **2007**, 318, 1437.

[95] Oxford Instruments, *SDD Explained* **2012**, OINA/SDDExplained/0212.

[96] H. Shtrikman, R. Popovitz-Biro, A. Kretinin, L. Houben, M. Heiblum, M. Bukala, M. Galicka, R. Buczko, P. Kacman, *Nano Lett.* **2009**, 9, 1506.

[97] J. Wang, Y. J. Liu, L. B. Liu, H. Y. Zhou, Z. P. Jin, *Calphad Comput. Coupling Phase Diagrams Thermochem.* **2011**, 35, 242.

[98] H. J. Joyce, J. Wong-Leung, Q. Gao, H. H. Tan, C. Jagadish, *Nano Lett.* **2010**, 10, 908.

[99] L. Namazi, S. G. Ghalamestani, S. Lehmann, R. R. Zamani, K. A. Dick, *Nanotechnology* **2017**, 28, 165601.

[100] S. H. Oh, Y. Kauffmann, C. Scheu, W. D. Kaplan, M. Rühle, *Science* **2005**, 310, 661.

[101] F. Lenrick, M. Ek, K. Deppert, L. Samuelson, L. Reine Wallenberg, *Nano Res.* **2014**, 7, 1188.

[102] S. Kodambaka, J. Tersoff, M. C. Reuter, F. M. Ross, *Science* **2007**, 316, 729.

[103] T. Altantzis, Y. Zhang, S. Basak, I. Lobato, A. D. Backer, A. Be, M. Porcu, Q. Xu, A. Sa, *Nano Lett.* **2019**, 19, 477.

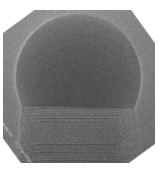

[104] W. Steckelmacher, *Reports on Progress in Physics* **1986**, 49.

[105] DensSolution, *https://denssolutions.com/products/climate/gas-supply-system/* **2020-03-16**, Climate.

[106] Protochips, *https://www.protochips.com/products/atmosphere/* **2020-03-16**, Atmosphere.

[107] Hummingbird, *http://hummingbirdscientific.com/multichannel-gas-flow-gas-delivery/* **2020-03-16**, Single/Multi channel gas delivery.

[108] J. Frenkel, *J. Chem. Phys.* **1939**, 538.

[109] K. A. Jackson, *Mater. Sci. Eng.* **1984**, 65, 7.

[110] G. B. Stringfellow, *Organic Metal Vapor Phase Epitaxy*, 2nd ed. (Academic Press, 1999).

[111] M. Knudsen, *Ann. Phys. (Leipzig)* **1909**, 29, 179.

[112] R. T. DeHoff, *Thermodynamics in Materials Science*, 2nd ed. (Chapman and Hall/CRC, Boca Raton, Florida, 2006).

[113] C. L. Bauer, *Surf. Sci.* **1986**, 168, 395.

[114] H. Y. Hui M. A. Filler, *Nano Lett.* **2015**, 15, 6939.

[115] V. T. Fauske, J. Huh, G. Divitini, D. L. Dheeraj, A. M. Munshi, C. Ducati, H. Weman, B. O. Fimland, A. T. J. Van Helvoort, *Nano Lett.* **2016**, 16, 3051.

[116] A. I. Persson, M. W. Larsson, S. Stenstrom, B. J. Ohlsson, L. Samuelson, L. R. Wallenberg, *Nat Mater* **2004**, 3, 677.

[117] M. Tornberg, K. A. Dick, , S. Lehmann, *J. Phys. Chem C* **2017**, 121, 21678.

[118] R. Pennington, J. R. Jinschek, J. B. Wagner, C. Boothroyd, , R. E. Dunin-Borkowski, *J. Phys. Conf. Ser.* **2010**, 209, 012013.

[119] B. M. Hudak, Y.-J. Chang, L. Yu, G. Li, D. N. Edwards, B. S. Guiton, *ACS Nano* **2014**, 8, 5441.

[120] E. Kinsbron, P. K. Gallagher, A. T. English, *Solid. State. Electron.* **1979**, 22, 517.

[121] F. Glas, *J. Appl. Phys.* **2010**, 108, 073506.

[122] Y. Calahorra, A. Kelrich, S. Cohen, D. Ritter, *Sci. Rep.* **2017**, 7, 40891.

[123] F. Glas, J. C. Harmand, , G. Patriarche, *Phys. Rev. Lett.* **2007**, 99, 146101.

[124] E.K Mårtensson, A. M., Withicar, M. De La Mata, R.R Zamani, J. Nygård, J., Johansson, K.A Dick, J. Bolinsson, *Cryst. Growth Des.* **2018**, 18, 6702.

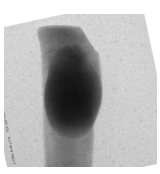

[125] S. Karthika, T. K. Radhakrishnan, P. Kalaichelvi, *Cryst. Growth Des.* **2016**, 16, 6663.

[126] J. W. Gibbs, *Am. J. Sci.* **1878**, s3-16, 441.

[127] R. Jothilingam, R. Dhanasekaran, P. Ramasamy, *Il Nuovo Cimento* **1995**, 17.

[128] V. G. Dubrovskii, N. V. Sibirev, J. C. Harmand, F. Glas, *Phys. Rev. B - Condens. Matter Mater. Phys.* **2008**, 78, 235301.

[129] J. Johansson, K. A. Dick, P. Caroff, M. E. Messing, J. Bolinsson, K. Deppert, L. Samuelson, *J. Phys. Chem. C* **2010**, 114, 3837.

[130] J. Grecenkov, V. G. Dubrovskii, M. Ghasemi, J. Johansson, *Cryst. Growth Des.* **2016**, 16, 4529.

[131] G. Priante, S. Ambrosini, V. G. Dubrovskii, A. Franciosi, S. Rubini, *Cryst. Growth Des.* **2013**, 13, 3976.

[132] R. T. Hallberg, M. E. Messing, K. A. Dick, *Nanotechnology* **2019**, 30, 055005.

[133] Y.-C. Chou, K. Hillerich, J. Tersoff, M. C. Reuter, K. A. Dick, F. M. Ross, *Science* **2014**, 343, 281.

[134] M. Ghasemi J. Johansson, *J. Phys. D. Appl. Phys.* **2017**, 50, 134002.

[135] C. Y. Wen, J. Tersoff, M. C. Reuter, E. A. Stach, F. M. Ross, *Phys. Rev. Lett.* **2010**, 105, 195502.

[136] V. C. Holmberg, M. G. Panthani, B. A. Korgel, *Science* **2009**, 326, 405.

[137] S. Andric, L. Ohlsson Fhager, F. Lindelöw, O.-P. Kilpi, L.-E. Wernersson, *J. Vac. Sci Techol. B* **2019**, 37, 061204.

[138] C. Chatillon D. Chatain, *J. Cryst. Growth* **1995**, 151, 91.

[139] C. B. Alcock, V. Itkin, M. K. Horrigan, *Canadian Metallurgical Quartely* **1984**, 23, 309.

[140] E. R. Hemesath, D. K. Schreiber, E. B. Gulsoy, C. F. Kisielowski, A. K. Petford-Long, P. W. Voorhees, L. J. Lauhon, *Nano Lett.* **2012**, 12, 167.

[141] S. Kodambaka, J. Tersoff, M. C. Reuter, F. M. Ross, *Phys. Rev. Lett.* **2006**, 96.

[142] P. Krogstrup, S. Curiotto, E. Johnson, M. Aagesen, J. Nygård, D. Chatain, *Phys. Rev. Lett.* **2011**, 106, 1.

[143] C. Panse, D. Kriegner, F. Bechstedt, *Phys. Rev. B* **2011**, 84, 075217.

[144] F. Bechstedt, A. Belabbes, *Journal of Physics: Condensed Matter* **2013**, 25, 273201.

[145] J. Johansson, Z. Zanolli, , K. A. Dick, *Cryst. Growth Des.* **2016**, 16, 371.

[146] N. V. Sibirev, M. a. Timofeeva, a. D. Bol'shakov, M. V. Nazarenko, V. G. Dubrovskii, *Phys. Solid State* **2010**, 52, 1531.

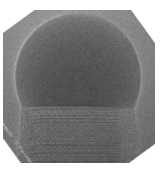

[147] V. Pankoke, P. Kratzer, , S. Sakong, *Phys. Rev. B - Condens. Matter Mater. Phys.* **2011**, 84, 075455.

[148] R. R. Zamani, F. S. Hage, S. Lehmann, Q. M. Ramasse, K. A. Dick, *Nano Lett.* **2018**, 18.

[149] X. Yuan, P. Caroff, J. Wong-Leung, L. Fu, H. H. Tan, C. Jagadish, *Adv. Mater.* **2015**, 27, 6096.

[150] M. De La Mata, C. Magen, J. Gazquez, M. I. B. Utama, M. Heiss, S. Lopatin, F. Furtmayr, C. J. Fernández-Rojas, B. Peng, J. R. Morante, R. Rurali, M. Eickhoff, A. Fontcuberta I Morral, Q. Xiong, J. Arbiol, *Nano Lett.* **2012**, 12, 2579.

[151] P. Krogstrup, R. Popovitz-Biro, E. Johnson, M. H. Madsen, J. Nygård, H. Shtrikman, *Nano Lett.* **2010**, 10, 4475.

[152] A. Kelrich, V. G. Dubrovskii, Y. Calahorra, S. Cohen, , D. Ritter, *Nanotechnology* **2015**, 26, 085303.

[153] M. Koguchi, H. Kakibayashi, M. Yazawa, K. Hiruma, T. Katsuyama, *Jpn. J. Appl. Phys.* **1992**, 31, 2061.

[154] E. K. Mårtensson, S. Lehmann, K. A. Dick, , J. Johansson, *Nano Lett.* **2019**, 19, 1197.

[155] V. G. Dubrovskii, *Cryst. Growth Des.* **2017**, 17, 2544.

[156] S. H. Oh, M. F. Chisholm, Y. Kauffmann, W. D. Kaplan, W. Luo, M. Rühle, C. Scheu, M. Ruhle, C. Scheu, *Science* **2010**, 330, 489.

[157] T. Young, *Philos. Trans. R. Soc. London* **1805**, 95, 65.

[158] L. Makkonen, *J. Phys. Condens. Matter* **2016**, 28.

[159] R. N. Wenzel, *Ind. Eng. Chem.* **1936**, 28, 988.

[160] P. Roura, *Am. J. Phys.* **2005**, 73, 1139.

[161] D. Gennes, *Rev. Mod. Phys.* **1985**, 57, 827.

[162] L. Gao, T. J. Mccarthy, *Langmuir* **2007**, 23, 3762.

[163] G. McHale, *Langmuir* **2007**, 23, 8200.

[164] D. J. Woodland, E. Mack, *J. Am. Chem. Soc.* **1933**, 55, 3149.

[165] S. Kaufman, T. Whalen, *Acta Metall.* **1965**, 13, 797.

[166] M. E. Schrader, *Langmuir* **1995**, 11, 3585.

[167] U. Konig, W. Keck, *J. Less-Common Met.* **1983**, 90, 299.

[168] G. Fang, A. Amirfazli, *Langmuir* **2012**, 28, 9421.

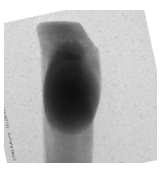

[169] L. Ghisalberti, H. Potts, M. Friedl, M. Zamani, L. Güniat, G. Tütüncüoglu, W. C. Carter, A. Fontcuberta, *Nanotechnology* **2019**, 30, 285604.

[170] V. A. Nebol'sin, A. A. Shchetinin, *Inorg. Mater.* **2003**, 39, 899.

[171] K. W. Schwarz, J. Tersoff, *Nano Lett.* **2012**, 12, 1329.

[172] V. A. Nebol'sin, A. I. Dunaev, A. F. Tatarenkov, S. S. Shmakova, *J. Cryst. Growth* **2016**, 450, 207.

[173] V. G. Dubrovskii, T. Xu, A. D. Álvarez, S. R. Plissard, P. Caroff, F. Glas, B. Grandidier, *Nano Lett.* **2015**, 15, 5580.

[174] V. G. Dubrovskii, *Nucleation theory and growth of nanostructures* (Springer-Verlag, Berlin Heidelberg, 2014).

[175] M. H. Madsen, M. Aagesen, P. Krogstrup, C. Sørensen, J. Nygård, *Nanoscale Res. Lett.* **2011**, 6, 516.

[176] T. Grap, T. Rieger, C. Blömers, T. Schäpers, D. Grützmacher, M. I. Lepsa, *Nanotechnology* **2013**, 24, 335601.

[177] T. Rieger, S. Heiderich, S. Lenk, M. I. Lepsa, D. Grützmacher, *J. Cryst. Growth* **2012**, 353, 39.

[178] S. C. Hardy, *J. Cryst. Growth* **1985**, 71, 602.

[179] R. Novakovic, E. Ricci, , F. Gnecco, *Surf. Sci.* **2006**, 600, 5051.

[180] M. Galicka, M. Bukała, R. Buczko, P. Kacman, *J. Phys. Condens. Matter* **2008**, 20, 454226.

[181] M. H. Magnusson, K. Deppert, J.-O. Malm, J.-O. Bovin, L. Samuelson, *Nanostructured Mater.* **1999**, 12, 45.

[182] M. K. Chaudhury, G. M. Whitesides, N. F. Drive, N. Q. Street, *Science* **1992**, 256, 1539.

[183] M. K. Chaudhury, A. Chakrabarti, S. Daniel, *Langmuir* **2015**, 31, 9266.

[184] J. S. Lee, J. Y. Moon, J. S. Lee, *Appl. Therm. Eng.* **2014**, 72, 104.

[185] R. S. Subramanian, N. Moumen, J. B. Mclaughlin, *Langmuir* **2005**, 21, 11844.

[186] M. Shanahan, E.R., *Langmuir* **1995**, 11, 1041.

[187] Q. Li, P. Zhou, H. J. Yan, *Langmuir* **2016**, 32, 9389.

[188] J. Zhang, F. Müller-Plathe, F. Leroy, *Langmuir* **2015**, 31, 7544.

[189] T. Ondarcuhu, A. Piednoir, *Nano Lett.* **2005**, 5, 1744.

[190] Y. V. Kalinin, V. Berejnov, , R. E. Thorne, *Langmuir* **2009**, 25, 5391.

[191] J.-H. Kang, M. Galicka, P. Kacman, H. Shtrikman, *Nano Lett.* **2017**, 17, 531.

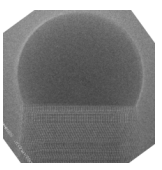

[192] G. E. Cirlin, V. G. Dubrovskii, Y. B. Samsonenko, A. D. Bouravleuv, K. Durose, Y. Y. Proskuryakov, B. Mendes, L. Bowen, M. A. Kaliteevski, R. A. Abram, D. Zeze, *Phys. Rev. B - Condens. Matter Mater. Phys.* **2010**, 82.

[193] R. E. Algra, M. A. Verheijen, L.-F. Feiner, G. G. W. Immink, W. J. P. van Enckevort, E. Vlieg, E. P. A. M. Bakkers, *Nano Lett.* **2011**, 11, 1259.

[194] J. Cahn R. Hanneman, *Surf. Sci.* **1964**, 1, 387.

[195] R. Leitsmann, F. Bechstedt, *J. Appl. Phys.* **2007**, 102.

[196] M. Rosini R. Magri, *ACS Nano* **2010**, 4, 6021.

[197] L. Lugani, D. Ercolani, L. Sorba, N. V. Sibirev, M. a. Timofeeva, V. G. Dubrovskii, *Nanotechnology* **2012**, 23, 095602.

[198] S. Rackauskas, S. D. Shandakov, H. Jiang, J. B. Wagner, A. G. Nasibulin, *Sci. Rep.* **2017**, 7, 12310.